Electronic Supplementary Material (ESI) for ChemComm.

Supplementary Information For:

Heating Activated Isomeric All-hydrocarbon Molecular Receptors for Fullerene Separation

Yu-Dong Yang, Han-Yuan Gong*.

College of Chemistry, Beijing Normal University, No. 19, XinJieKouWai St, HaiDian District, Beijing 100875, P. R. China

Author e-mail address: hanyuangong@bnu.edu.cn

Table of Contents

Section S1: *General considerations*

Section S2: *Synthesis, characterization, and theoretical calculation*

Section S3: *Fullerene (C_{60} or C_{70}) receptor property studies of* ***C_s-CDMB-8*** *or* ***D_{4d}-CDMB-8*** *both in solution and solid state*

Section S4: *Fullerene (C_{60} and/or C_{70}) purification from mixed C_{60}/C_{70} or carbon soot via* ***D_{4d}-CDMB-8*** complexation

Section S1: *General considerations*

Deuterated solvents were purchased from Cambridge Isotope Laboratory (Andover, MA). All other solvents and reagents were purchased commercially (Aldrich, Acros, or Fisher) and used without further purification.

NMR spectra, including ^{1}H, ^{13}C, tempreture-dependent ^{1}H, high temperature (373 K) ^{13}C, heteronuclear singular quantum correlation (HSQC), heteronuclear multiple quantum correlation (HMBC), or nuclear Överhauser effect (NOESY) NMR spectroscopies were recorded on Bruker AVANCE III 500WB or AVANCE 600 spectrometer. The ^{1}H and ^{13}C NMR chemical shifts are referenced to residual solvent signals ($CDCl_3$: δ_H = 7.26 ppm, δ_C = 77.16 ppm; tetrachloroethane-d_2 (TCE-d_2): δ_H = 5.95 ppm, δ_C = δ 74.10 ppm; *o*-dichlorobenzene-d_2 (*o*-DCB-d_2): δ_C = 131.68 ppm, 129.30 ppm and 126.44 ppm).

High resolution mass spectra (HMRS) were detected on Bruker autoflex speed MALDI-TOF or AB SCIX TripleTOF 5600. High-performance liquid chromatography (HPLC) analysis was performed using an Agilent 1260. UV-vis spectra were collected on a Shimadzu UV-2450. X-ray photoelectron spectroscopy (XPS) data were characterized on a Thermofisher ESCALAB 250Xi.

Unless otherwise noted, single crystals used to obtain the X-ray diffraction structures reported in the text grew as colourless prisms, blocks, or red-brown prisms. The .cif documents, available as the separate supporting information files, provide details regarding the specific crystals used for the analysis, along with the structures in question. The data crystals used for single crystal analyses were cut from clusters of the corresponding crystals and had the approximate dimensions given in the .cif documents. The data were collected on a Saturn724+ (2x2 bin mode) or SuperNova, Dual, Cu at home/near, AtlasS2. Data reduction was performed using CrystalClear (Rigaku Inc., 2007), CrysAlisPro 1.171.39.6a (Rigaku OD, 2015) or CrysAlisPro 1.171.39.32a (Rigaku OD, 2017). The structures were refined by full–matrix least–squares on F^2 with anisotropic displacement parameters for the non–H atoms using SHELXL–97 or SHELXL-2014[1-3]. The hydrogen atoms were calculated in idealized positions with isotropic displacement parameters set to 1.2 x Ueq of the attached atom (1.5 x Ueq for methyl hydrogen atoms). Definitions used for calculating R(F), Rw(F2) and the goodness of fit, S, are given below and in the .cif documents[4]. Neutral atom scattering factors and values used to calculate the linear absorption coefficient are from the International Tables for X-ray Crystallography (1992)[5]. All ellipsoid figures were generated using SHELXTL/PC[6]. Tables of positional and thermal

parameters, bond lengths and angles, torsion angles, figures and lists of observed and calculated structure factors are located in the .cif documents available from the Cambridge Crystallographic Centre and may be obtained by quoting ref. numbers 1820645, 1820646, 1820647, 1820648, 1820649, 1820651, 1820652, and 1859997. The documents also contain details of the crystal data, data collection, and structure refinement for each structure.

DFT calculations were performed using the Gaussian 09 program[7]. The geometry optimizations of minima and the intermediates were carried out in the gas phase with the Becke three-parameter hybrid density functional (B3LYP)[8] with the D3 empirical dispersion correction by Grimme[9] *et al.* and the 6-31G(d) basis set[10,11] for C, H and P atoms and the LanL2DZ basis set[12,13] was used for transition metals Pd and Fe. Frequency analyses were carried out at the same level to verify all of the stationary points as minima (zero imaginary frequencies) or transition states (one imaginary frequency) and to evaluate the zero-point vibrational energy and thermal corrections at 298 K. The detail information of optimized geometries are shown in .mol documents.

Section S2: *Synthesis, characterization, and theoretical calculation*

Synthesis of 1,5-bis(4,4,5,5-tetramethyl-1,3,2-dioxaborolan-2-yl)-2,4-dimethylbenzene 2

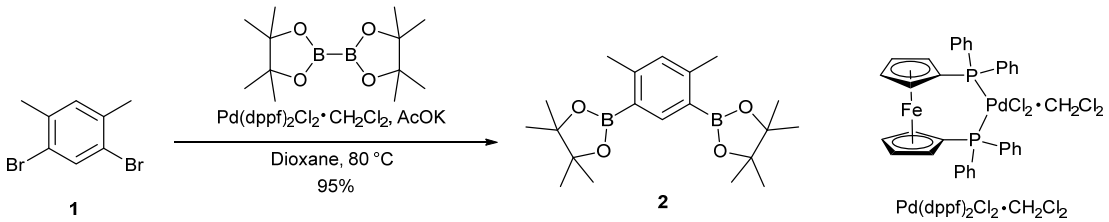

1,5-dibromo-2,4-dimethylbenzene **1** (5.6 g, 21 mmol), bis(pinacolato)diboron (12 g, 47 mmol), $Pd(dppf)_2Cl_2 \cdot CH_2Cl_2$ (0.87 g, 1.1 mmol), AcOK (14 g, 0.14 mol), and 40 mL of 1,4-dioxane were added in 100 mL flask. The reaction mixture was degassed with argon for 30 min and then heated to 80 °C under argon for 24 hours. The reaction mixture was filtered and the filter residue was washed with 50 mL CH_2Cl_2, the filtrate was dried *via* rotary evaporation, and the obtained residue was dissolved in 100 mL CH_2Cl_2, then washed with water (3 × 50 mL) and brine (3 × 50 mL). The extract was dried over sodium sulfate, filtered, and concentrated. The residue was purified by a silica gel column with *n*-hexanes/CH_2Cl_2 (60:1, *v*/*v*) as the eluent, which give out

product **2** as white solid (7.2 g, 95%). ^{1}H NMR (600 MHz, $CDCl_3$, 298 K) δ (ppm): 8.14 (s, 1H), 6.99 (s, 1H), 2.52 (s, 6H), 1.35 (s, 24H); ^{13}C NMR (150 MHz, $CDCl_3$, 298 K) δ (ppm): 147.9, 143.9, 131.7, 83.3, 25.0, 22.5; ESI HRMS (*m*/*z*): $[M+H]^{+\bullet}$ calcd. for $C_{20}H_{33}B_2O_4$, 359.2567; found, 359.2564.

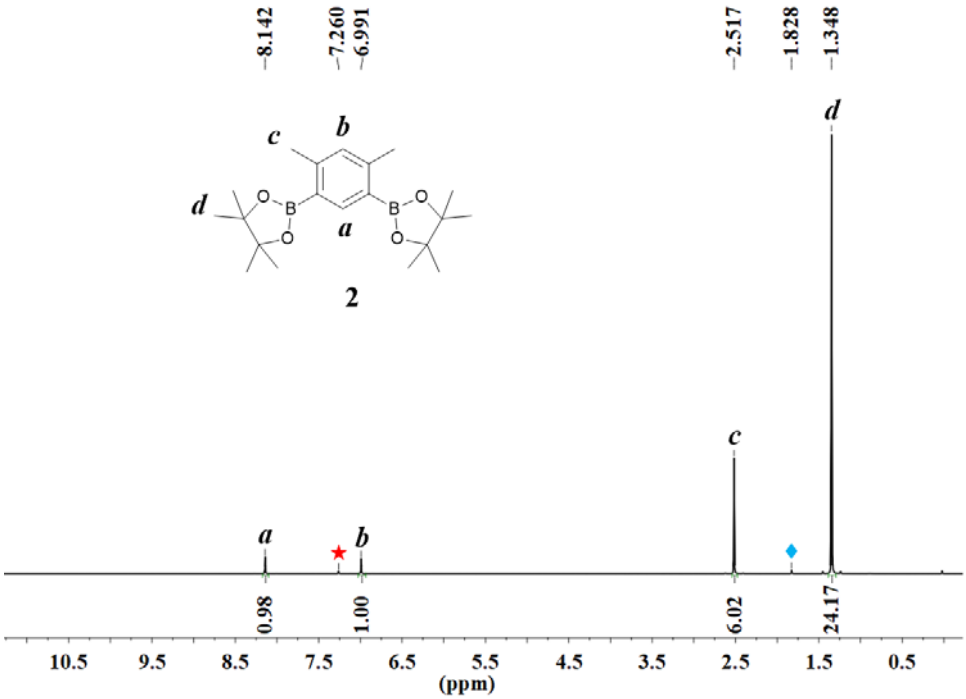

Figure S1. ^{1}H NMR spectrum of **2** (2.00×10^{-2} M) in $CDCl_3$ at 298 K (600 MHz) (red "★" represents residual $CHCl_3$; blue "♦" represents H_2O).

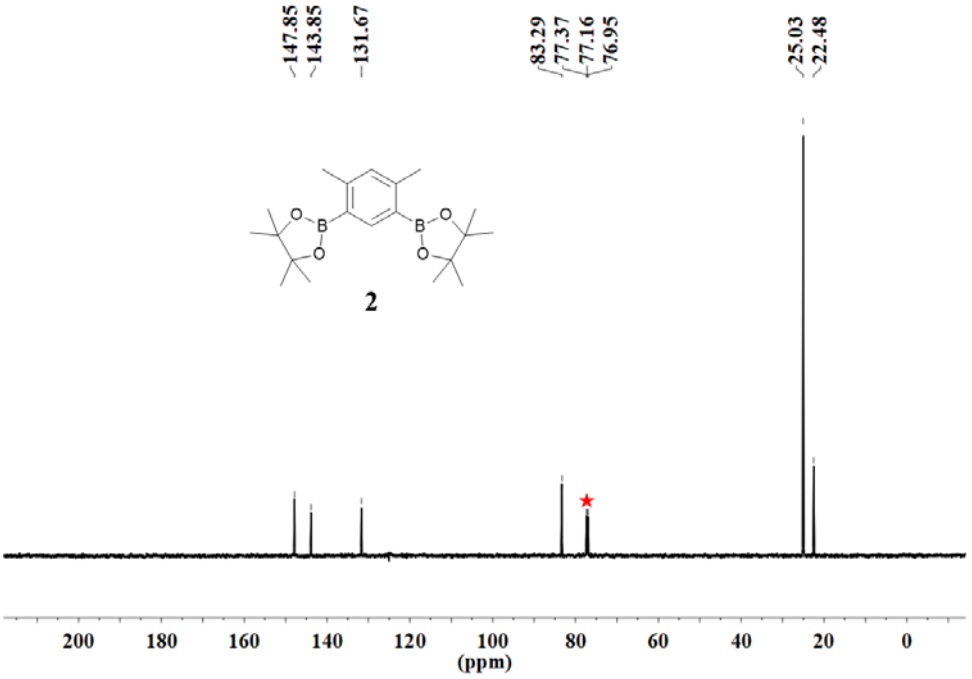

Figure S2. ^{13}C NMR spectrum of **2** (2.00×10^{-2} M) in $CDCl_3$ at 298 K (150 MHz) (red "★" represents residual $CHCl_3$).

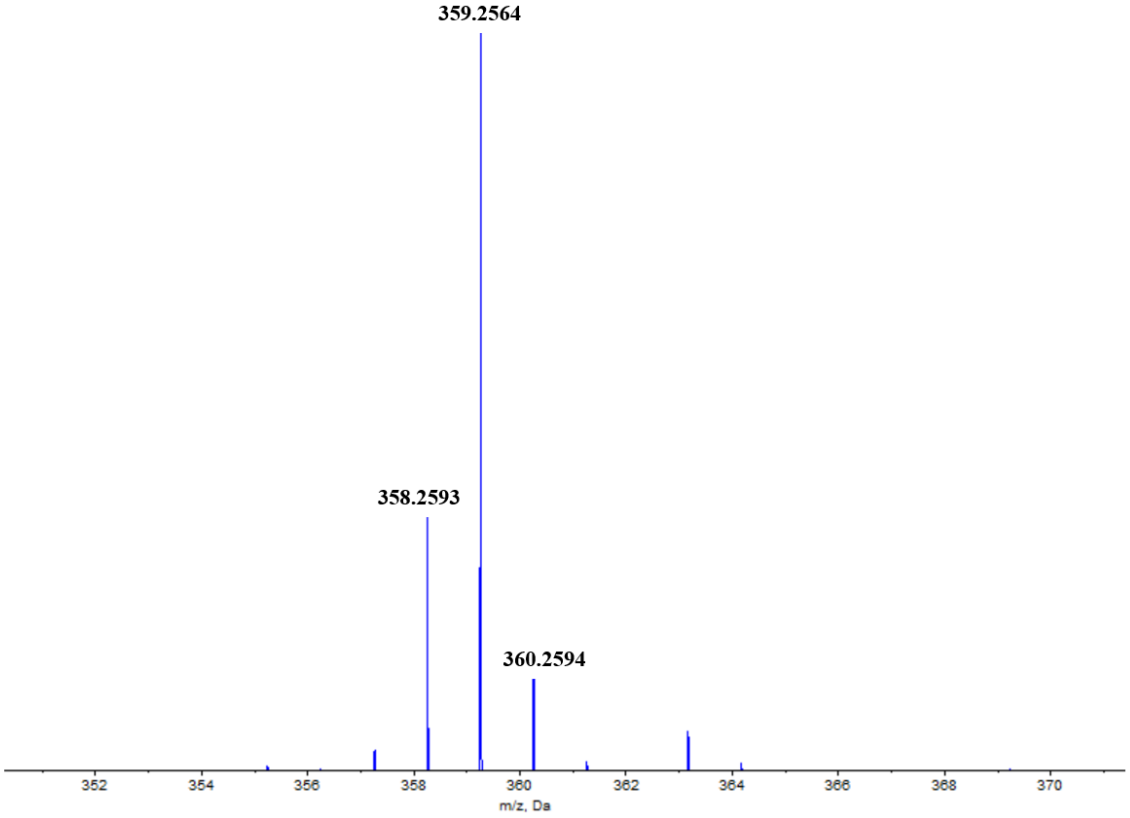

Figure S3. Positive ESI HRMS spectrum of **2**.

Synthesis of trimer 3 and pentamer 4 (*i.e.*, compound 2 in main text).

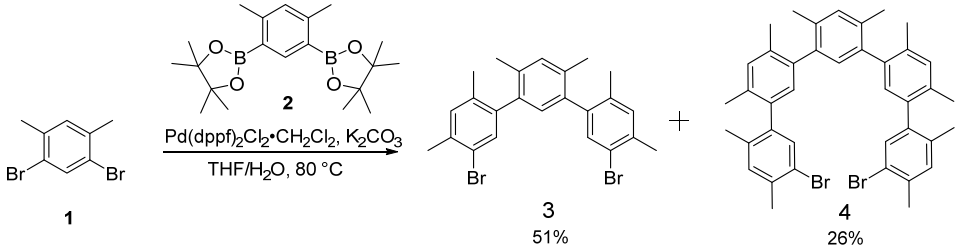

Under the protection of argon, a mixture of **1** (18 g, 68 mmol), $Pd(dppf)_2Cl_2 \cdot CH_2Cl_2$ (0.29 g, 0.35 mmol), K_2CO_3 (5.0 g, 46 mmol) and 15 mL deaerated water were added in 100 mL three-necked round-bottomed flask. After the mixture was heated to 80 ℃, a solution of **2** (2.5 g, 7.0 mmol) in deaerated THF (30 mL) was slowly added dropwise to the mixture over a period of 8 h. The reaction mixture was heated under 80 ℃ for 16 h. After cooling to room temperature, the solvent was removed *via* rotary evaporation, the resulting residue was dissolved in 200 mL CH_2Cl_2, then washed with water (3 × 100 mL) and brine (3 × 100 mL). The residue solution was dried over sodium sulfate and purified by a silica gel column with *n*-hexane as the eluent to recycle **1** (14 g, 53 mmol) and obtain pure trimer **3** (1.7 g, 51%) and pentamer **4** (0.62 g, 26%). Trimer **3**: ^{1}H NMR (500 MHz, TCE-d_2, 373 K) δ (ppm): 7.32 (s, 2H), 7.15 (s, 1H), 7.12 (s, 2H), 6.80 (s, 1H), 2.41 (s, 6H), 2.09 (s, 6H), 2.02 (s, 6H); ^{13}C NMR (125 MHz, TCE-d_2, 373 K) δ (ppm): 140.9, 137.6, 136.3, 135.4, 135.0, 133.1, 132.3, 131.7, 130.4, 121.5, 22.3, 19.4, 19.2; MALDI-TOF HRMS (*m*/*z*): $[M-H]^{+\bullet}$ calcd. for $C_{24}H_{23}Br_2$, 471.0146; found, 471.0319. Pentamer **4**: ^{1}H NMR (500 MHz, TCE-d_2, 373 K) δ (ppm): 7.32 (s, 2H), 7.13 (s, 3H), 7.11 (s, 2H), 6.91 (s, 1H), 6.86 (s, 2H), 2.41 (s, 6H), 2.11 (s, 12H), 2.08 (s, 6H), 2.02 (s, 6H); ^{13}C NMR (125 MHz, TCE-d_2, 373 K) δ (ppm): 141.2, 139.1, 138.6, 137.4, 136.2, 135.5, 135.1, 134.5, 134.3, 133.2, 132.3, 131.5, 131.4, 130.6, 121.5, 22.3, 19.50, 19.47, 19.38, 19.2; MALDI-TOF HRMS (*m*/*z*): $[M-H]^{+\bullet}$ calcd. for $C_{40}H_{39}Br_2$, 679.1398; found, 679.1567.

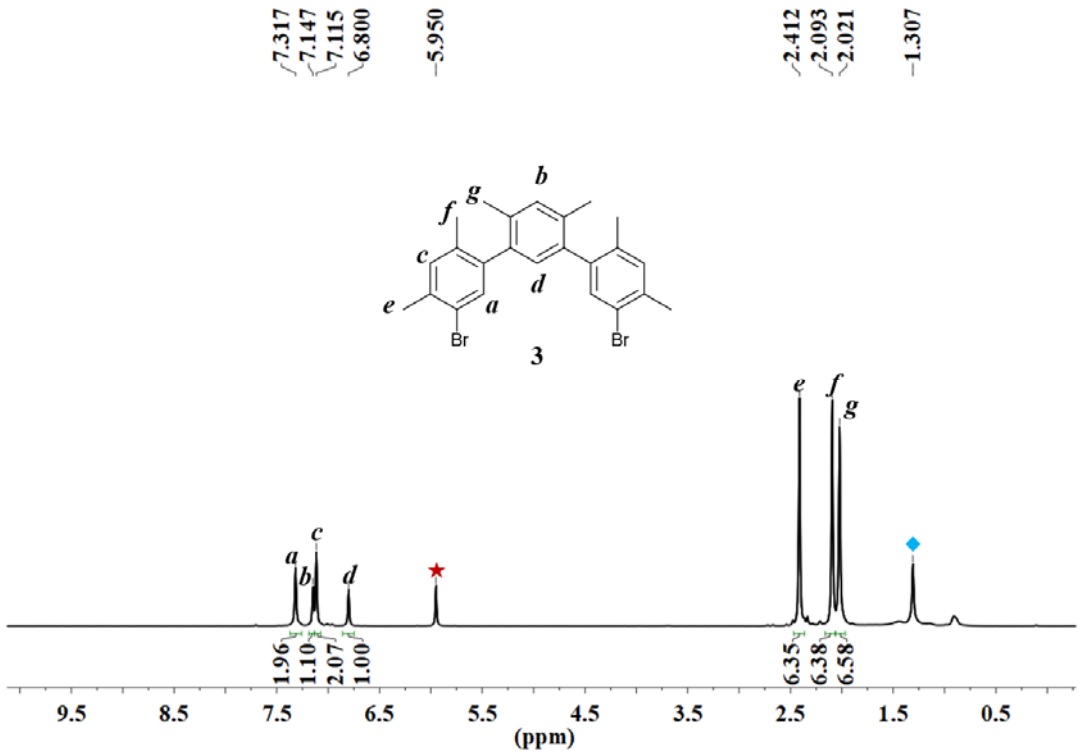

Figure S4. ^{1}H NMR spectrum of trimer **3** (2.00×10^{-2} M) in TCE-d_2 at 373 K (500 MHz) (red "★" represents residual TCE; blue "♦" represents H_2O).

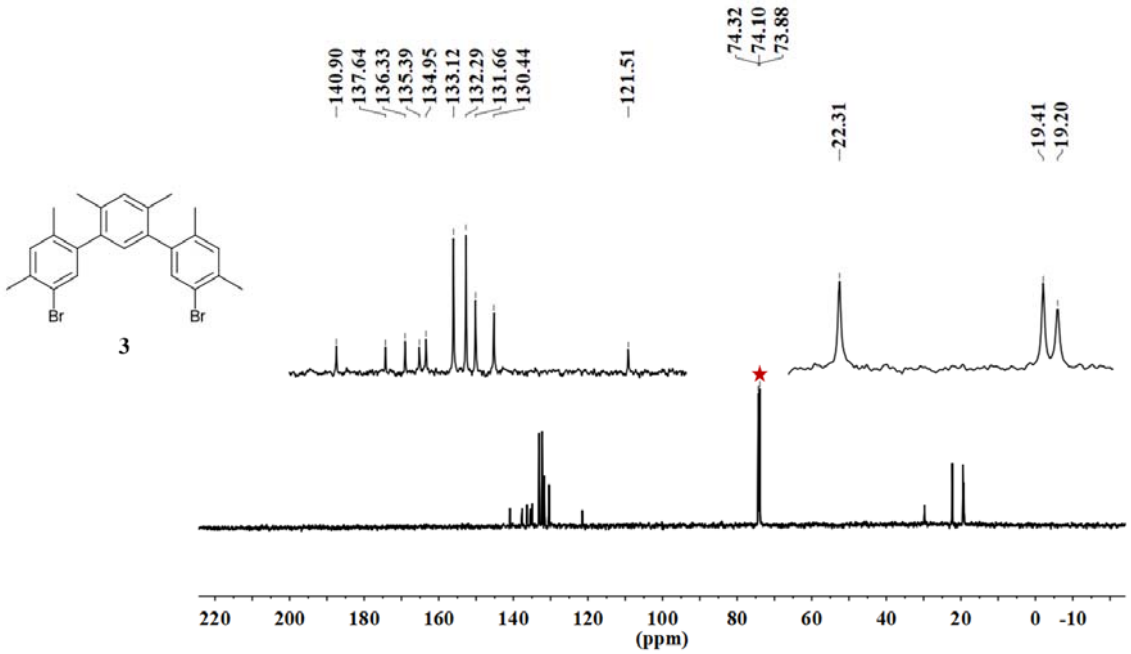

Figure S5. Expanded view (top) and full view (bottom) of the ^{13}C NMR spectrum of trimer **3** (2.00×10^{-2} M) in TCE-d_2 at 373 K (125 MHz) (red "★" represents residual TCE).

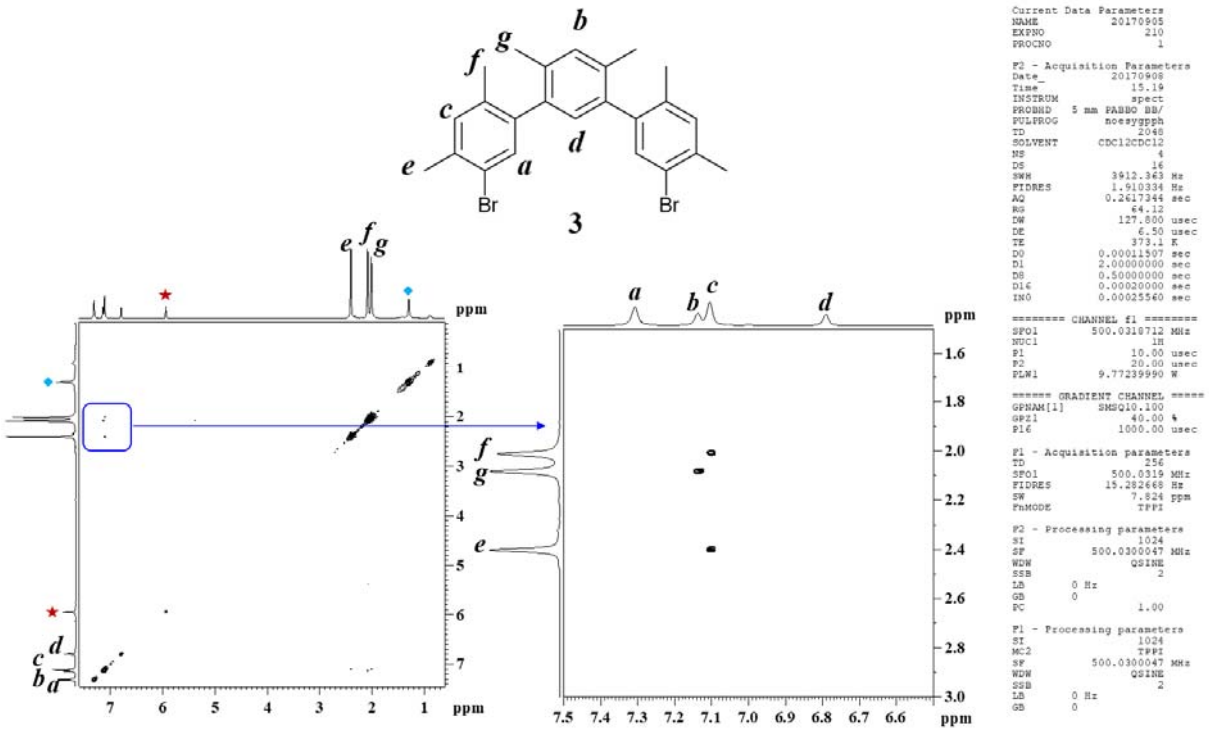

Figure S6. Full view (left) and expanded view (right) of the NOESY spectrum of trimer **3** (2.00 × 10^{-2} M) in TCE-d_2 at 373 K (500 MHz) (red "★" represents residual TCE; blue "♦" represents H_2O).

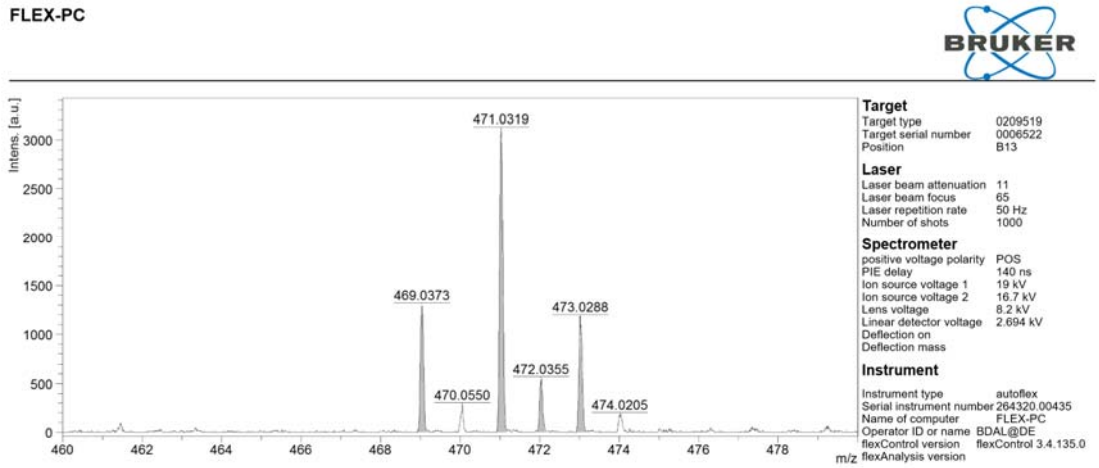

Figure S7. Positive MALDI-TOF HRMS spectrum of trimer **3**.

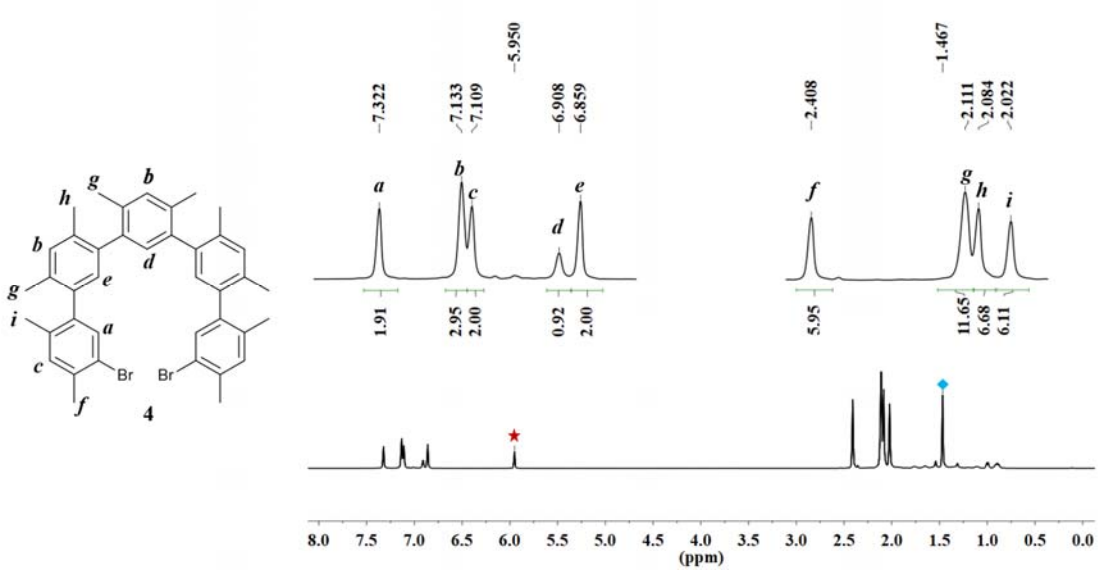

Figure S8. Expanded view (top) and full view (bottom) of the ^{1}H NMR spectrum of pentamer **4** (2.00×10^{-2} M) in TCE-d_2 at 373 K (500 MHz) (red "★" represents residual TCE; blue "♦" represents H_2O).

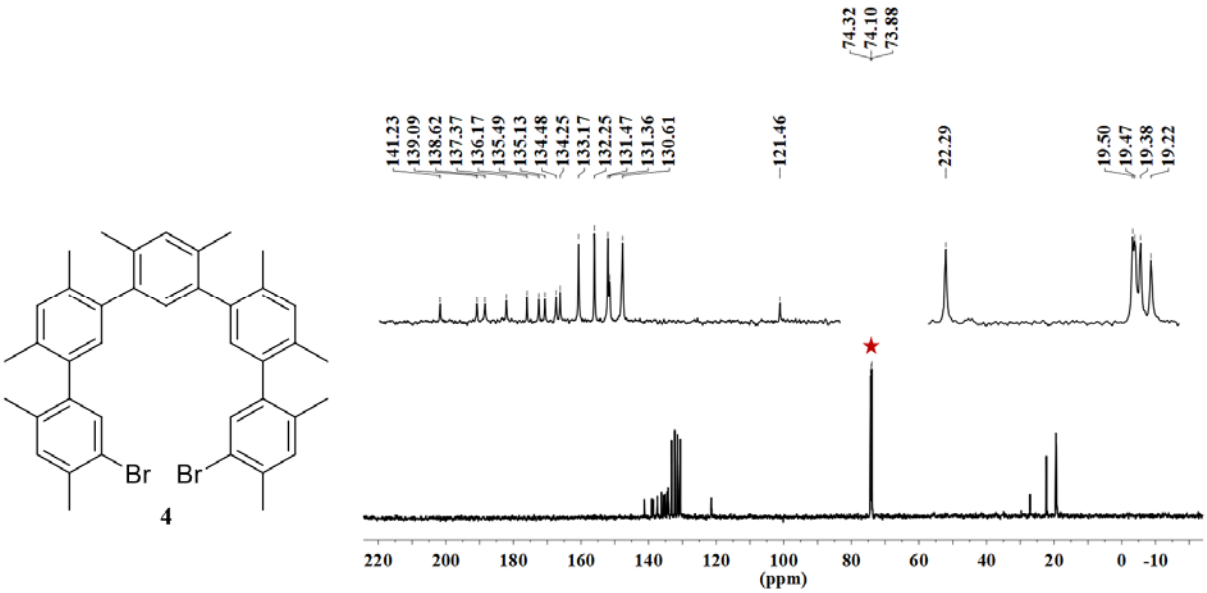

Figure S9. Expanded view (top) and full view (bottom) of the ^{13}C NMR spectrum of pentamer **4** (2.00×10^{-2} M) in TCE-d_2 at 373 K (125 MHz) (red "★" represents residual TCE).

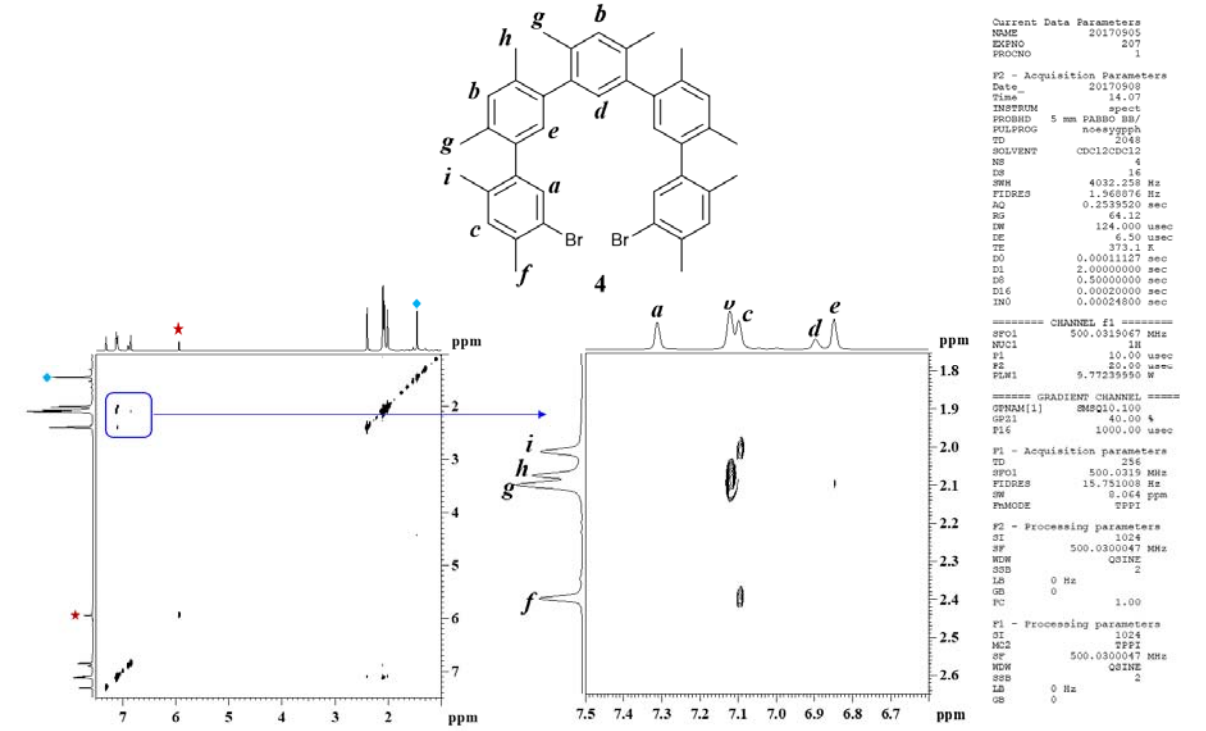

Figure S10. Full view (left) and expanded view (right) of the NOESY spectrum of pentamer **4** (2.00×10^{-2} M) in TCE-d_2 at 373 K (500 MHz) (red "★" represents residual TCE; blue "♦" represents H_2O).

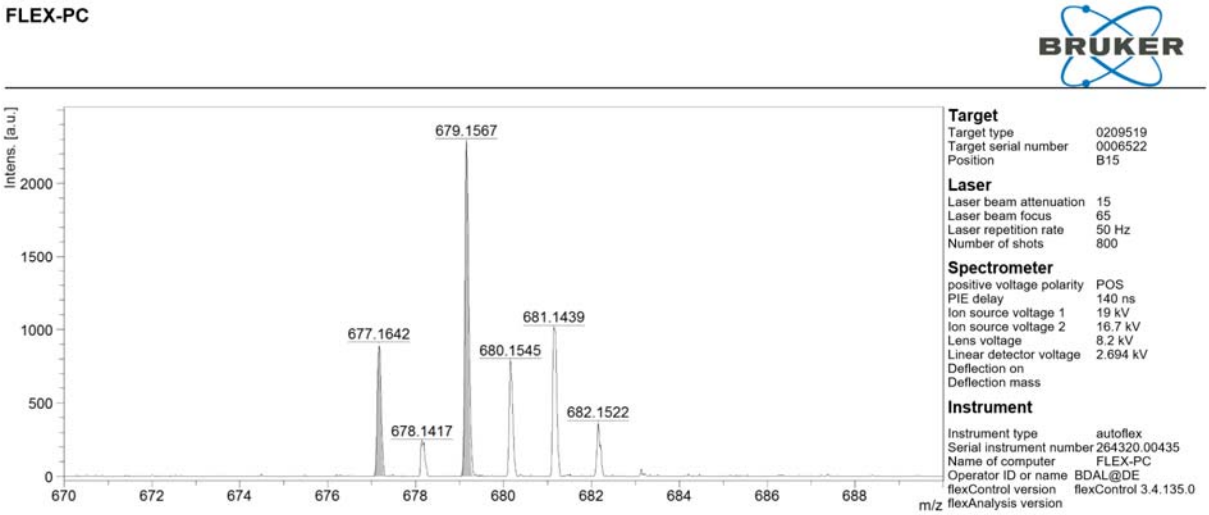

Figure S11. Positive MALDI-TOF HRMS spectrum of pentamer **4**.

Synthesis of boronylated trimer 5 (*i.e.*, compound 1 in main text).

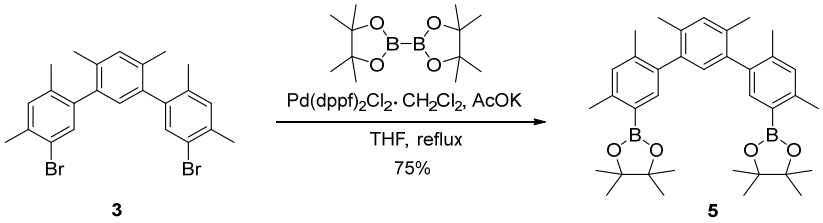

Under the protection of argon, **3** (1.0 g, 2.1 mmol), bis(pinacolato)diboron (1.1 g, 4.3 mmol), $Pd(dppf)_2Cl_2 \cdot CH_2Cl_2$ (0.09 g, 0.11 mmol), AcOK (1.5 g, 15 mmol) and 20 mL of THF were added into 50 mL flask for refluxing under argon. After 24 hours, the reaction mixture was cooled and filtered. The filter residue was washed with 50 mL CH_2Cl_2. The solvent of filtrate was removed *via* rotary evaporation, and the obtained residue was dissolved in 100 mL CH_2Cl_2, then washed with water (3 × 100 mL) and brine (3 × 100 mL). The extract was dried over sodium sulfate and purified by a silica gel column with mixed solvent (*n*-hexane: CH_2Cl_2: ethyl acetate = 80:6:1) as the eluent. The product was recrystallized from ethyl acetate to obtain product **5** as white solid (0.90 g, 75%). Boronylated trimer **5**: ^{1}H NMR (500 MHz, TCE-d_2, 373 K) δ (ppm): 7.51 (s, 2H), 7.15 (s, 1H), 7.05 (s, 2H), 6.86 (s, 1H), 2.54 (s, 6H), 2.10 (s, 12H), 1.34 (s, 24H); ^{13}C NMR (125 MHz, TCE-d_2, 373 K) δ (ppm): 143.3, 138.8, 138.7, 138.0, 137.2, 134.6, 131.4, 131.2, 83.4, 25.0, 21.8, 19.9, 19.6; ESI HRMS (*m*/*z*): $[M+H]^{+\bullet}$ calcd. for $C_{36}H_{49}B_2O_4$, 567.3824; found, 567.3829.

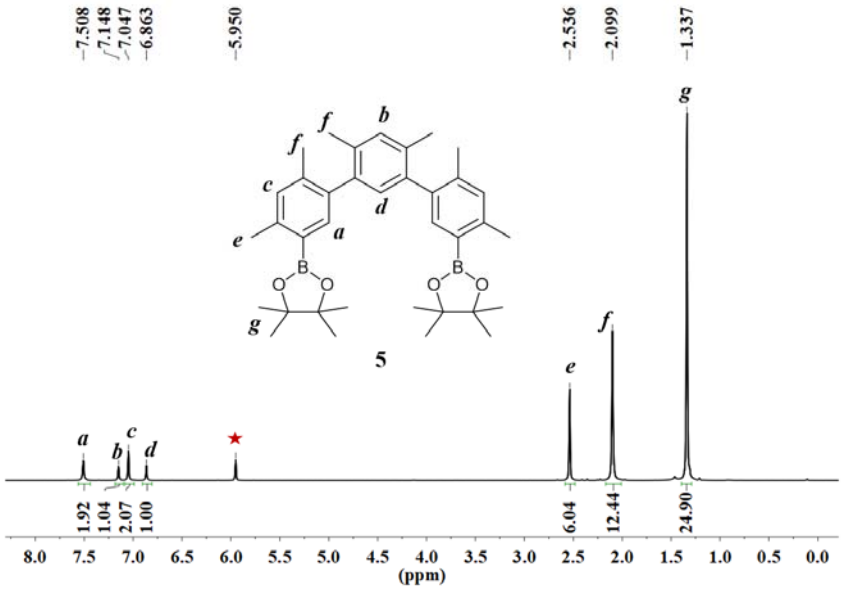

Figure S12. ^{1}H NMR spectrum of **5** (2.00×10^{-2} M) in TCE-d_2 at 373 K (500 MHz) (red "★" represents residual TCE).

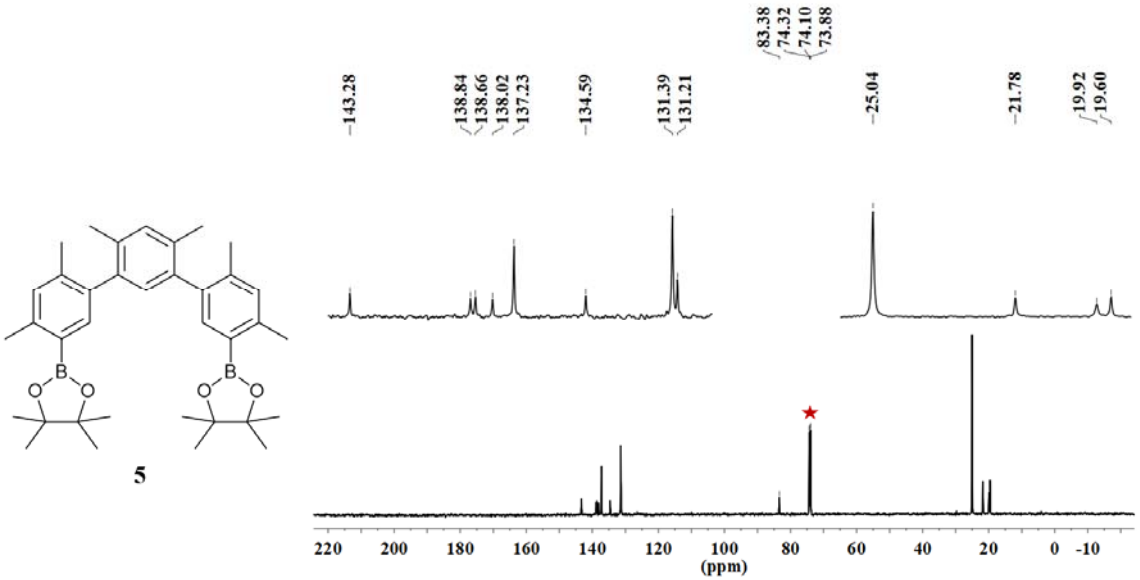

Figure S13. Expanded view (top) and full view (bottom) of the ^{13}C NMR spectrum of **5** (2.00×10^{-2} M) in TCE-d_2 at 373 K (125 MHz) (red "★" represents residual TCE).

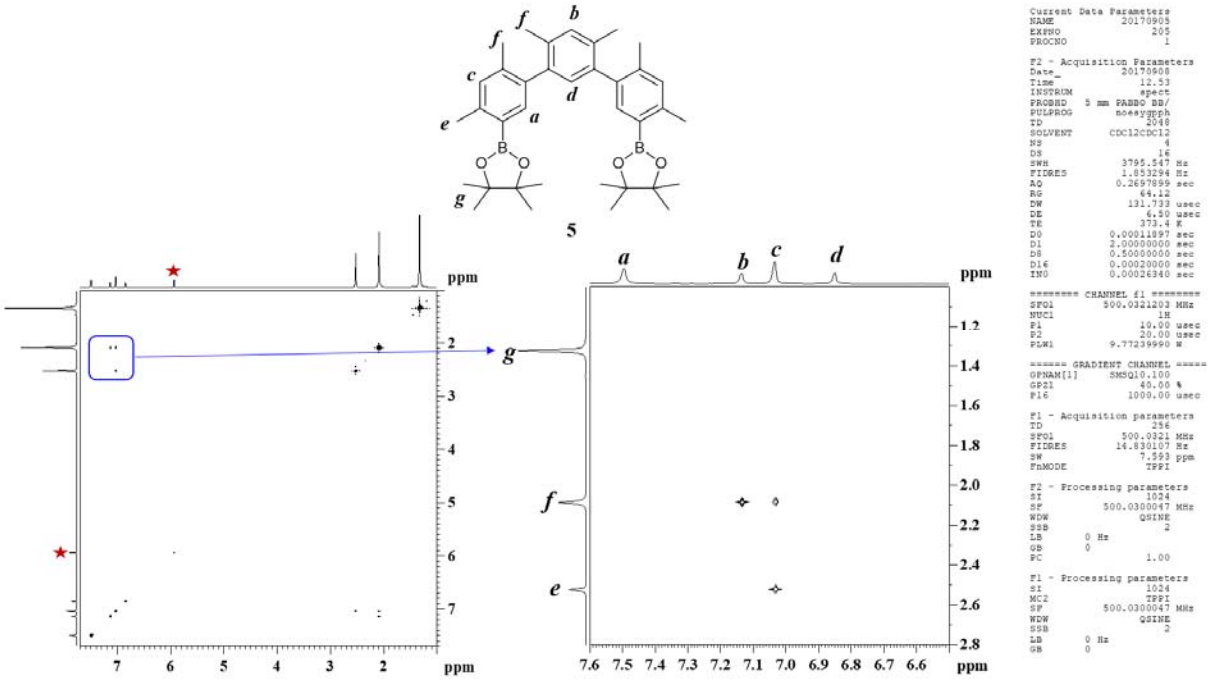

Figure S14. Full view (left) and expanded view (right) of the NOESY spectrum of **5** (2.00×10^{-2} M) in TCE-d_2 at 373K (500 MHz) (red "★" represents residual TCE).

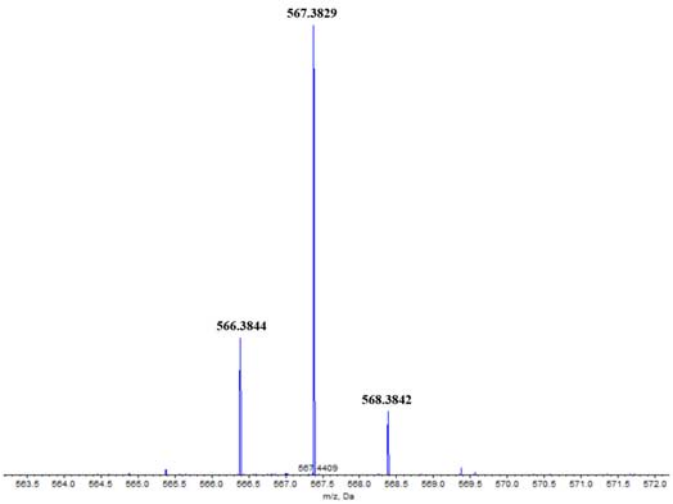

Figure S15. Positive ESI HRMS spectrum of **5**.

Temperature dependent ^{1}H NMR spectroscopic studies of compound 3, 4, 5, C_s-CDMB-8 or D_{4d}-CDMB-8 in tetrachloroethane-d_2

The ^{1}H NMR spectra of **3**, **4** or **5** in TCE-d_2 at 393 K showed a set of high resolution signals. Their ^{1}H NMR spectra become complex with decreasing temperature. This finding suggest us to speculate a variety of conformations of compounds **3**, **4** or **5** are interchangeable. All the three compounds contain a trimer fragment as show in Figure S16. For the compounds **3** and **5**, four possible conformations "*C*", "*W*", "S_1" and "S_2" probably exist in the solution state, and more complicated conformations will exist in the solution state of **4**.

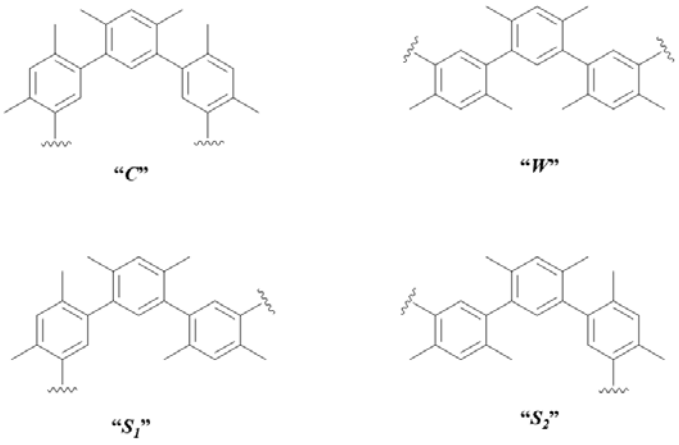

Figure S16. Four possible conformations "*C*", "*W*", "S_1" and "S_2" for the trimer fragment in **3**, **4** and **5**. Note that conformers "S_1" and "S_2" are symmetry related.

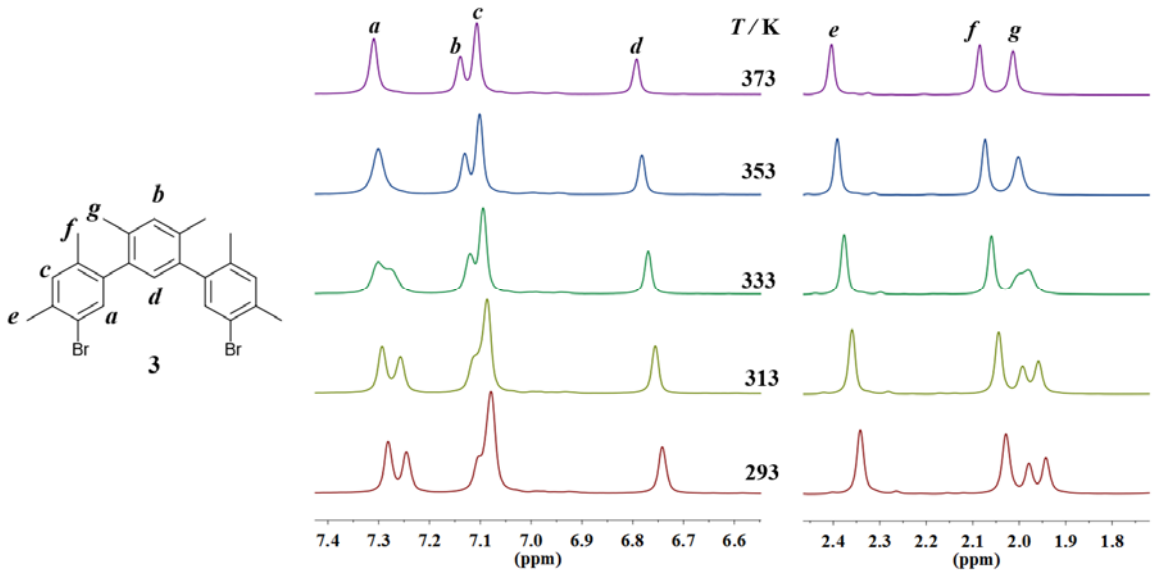

Figure S17. Expansion of the temperature dependent ^{1}H NMR spectra of trimer **3** (2.00×10^{-2} M) in TCE-d_2 (500 MHz).

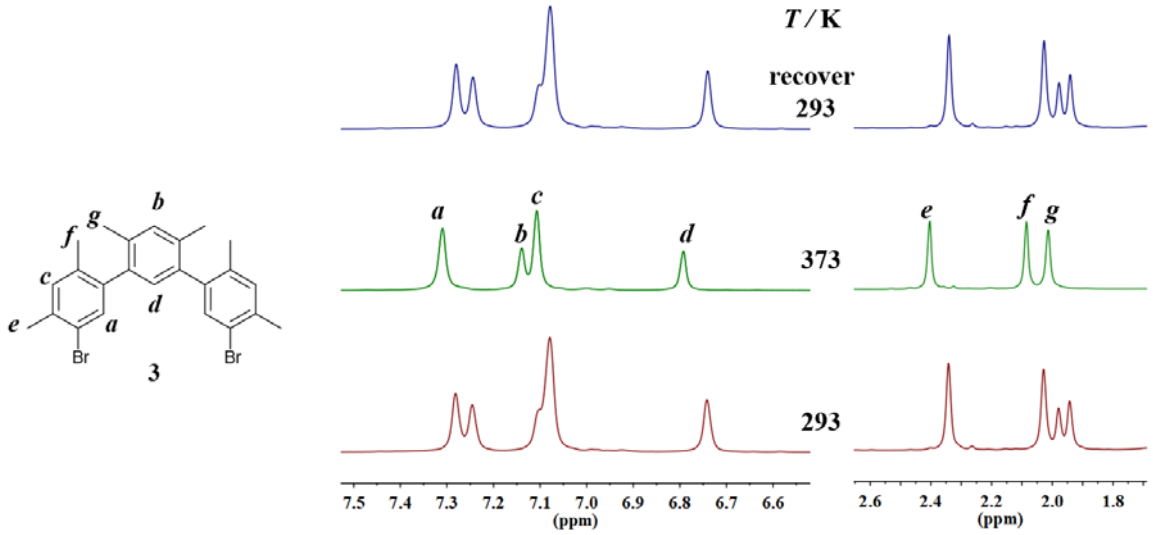

Figure S18. Expansion of ^{1}H NMR spectra of trimer **3** (2.00×10^{-2} M), which is recorded at 293 K, heating to 373 K and cooling back to 293 K in TCE-d_2 (500 MHz).

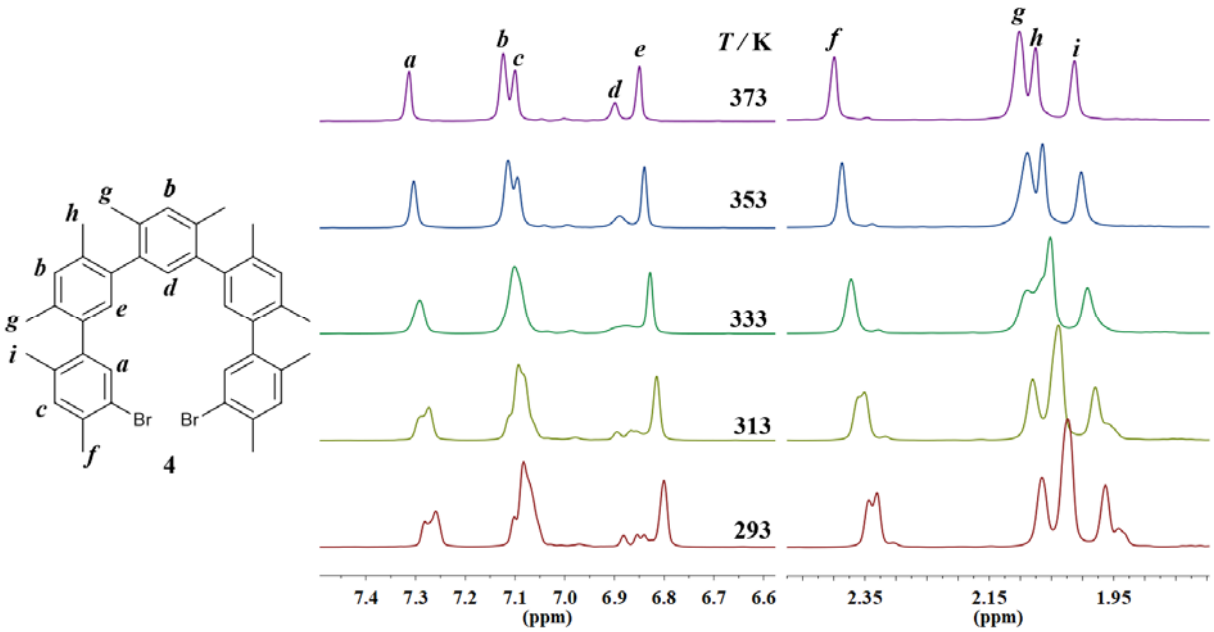

Figure S19. Expansion of the temperature dependent ^{1}H NMR spectra of pentamer **4** (2.00×10^{-2} M) in TCE-d_2 (500 MHz).

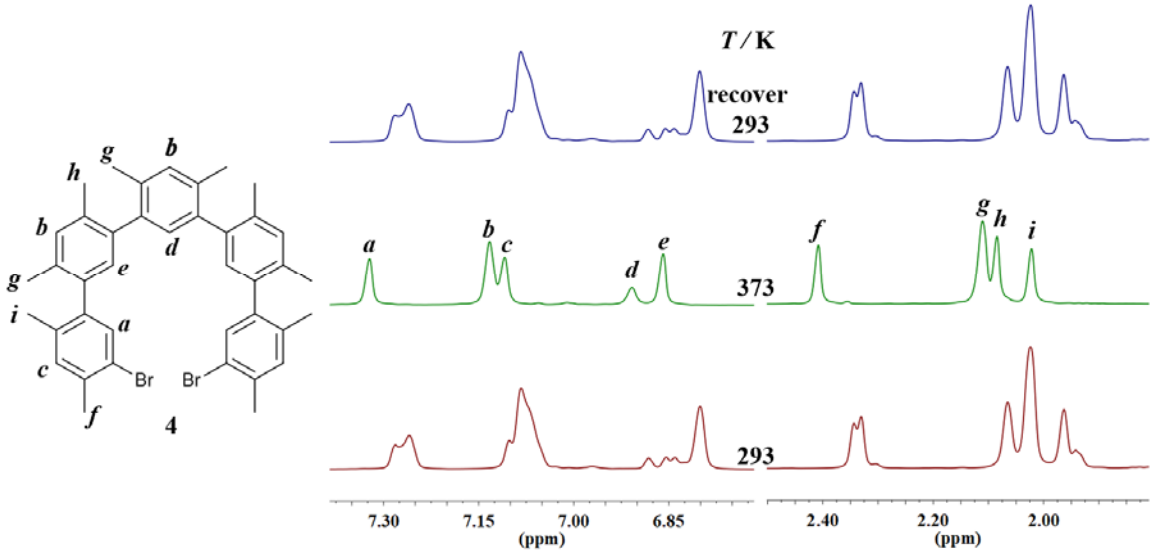

Figure S20. Expansion of ^{1}H NMR spectra of pentamer **4** (2.00×10^{-2} M), which is recorded at 293 K, heating to 373 K and cooling back to 293 K in TCE-d_2 (500 MHz).

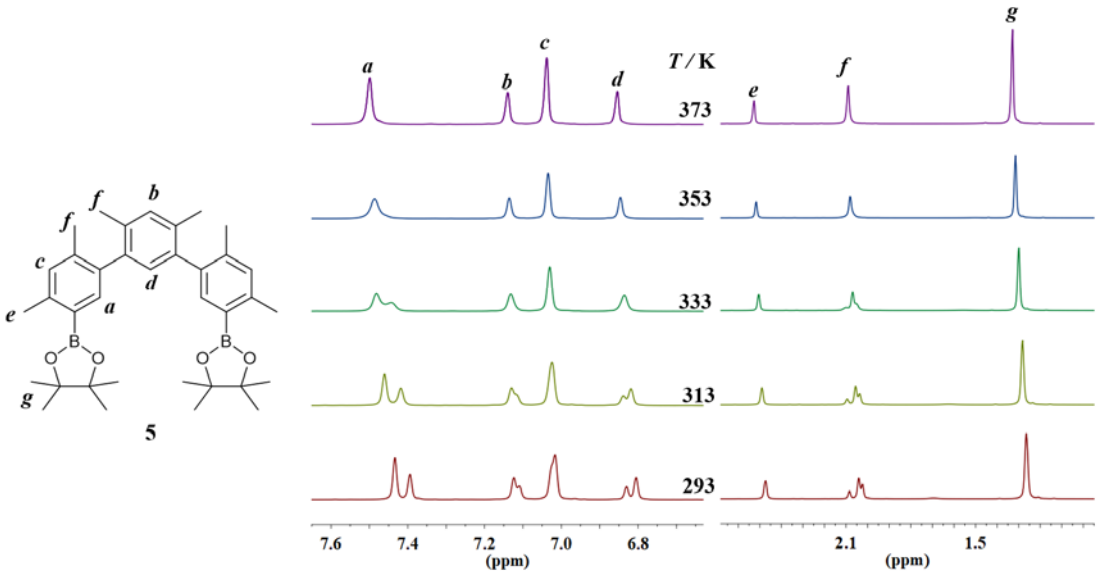

Figure S21. Expansion of the temperature dependent ^{1}H NMR spectra of **5** (2.00×10^{-2} M) in TCE-d_2 (500 MHz).

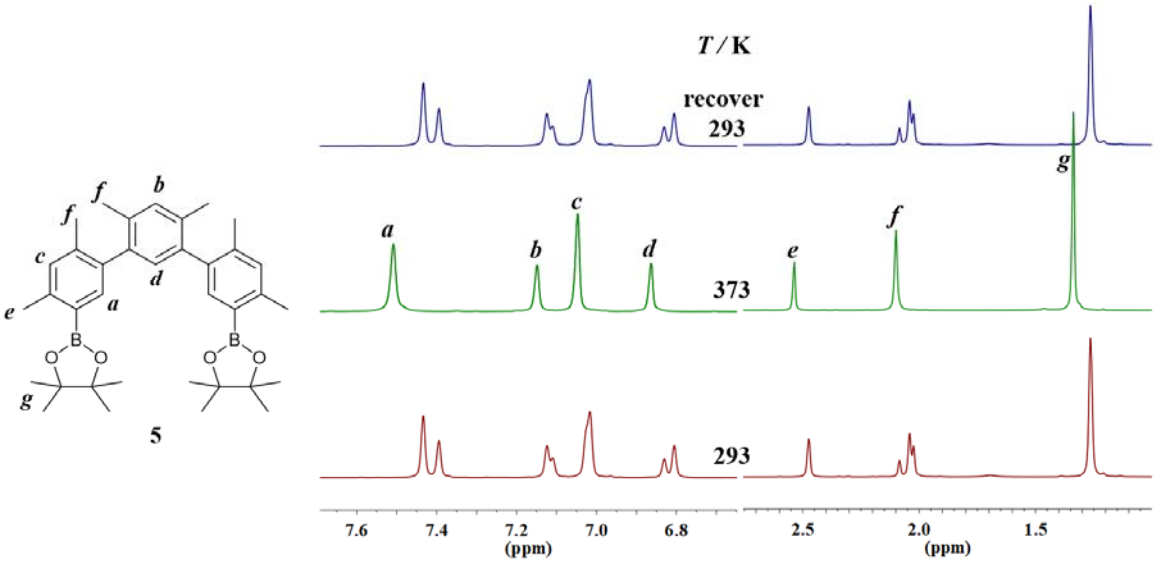

Figure S22. Expansion of ^{1}H NMR spectra of pentamer **5** (2.00×10^{-2} M) which is recorded at 293 K, heating to 373 K and cooling back to 293 K in TCE-d_2 (500 MHz).

Table S1. X-ray crystallographic data comparison of [**2**], [**3**•*n*-hexane], [**4**• CH_2Cl_2], and [**5**].

	[**2**]	[**3**•*n*-hexane]	[**4**• CH_2Cl_2]	[**5**]
CCDC No.	1820645	1820646	1820647	1820648
description	prism	prism	plate	prism
colour	colourless	colourless	colourless	colourless
from solution	CH_2Cl_2/CH_3CN	*n*-hexane/ CH_2Cl_2/DMF	CH_2Cl_2/CH_3CN	ethyl acetate
empirical formula	$C_{20}H_{32}B_2O_4$	$C_{30}H_{38}Br_2$	$C_{41}H_{42}Br_2Cl_2$	$C_{36}H_{48}B_2O_4$
Mr	358.07	558.42	765.46	566.36
crystal size (mm^3)	0.08 × 0.04 × 0.02	0.12 × 0.04 × 0.02	0.07 × 0.03 × 0.01	0.21 × 0.03 × 0.02
crystal system	triclinic	triclinic	orthorhombic	triclinic
space group	P-1	P-1	Pnma	P-1
a [Å]	10.476(2)	9.1118(18)	16.531(3)	7.3128(3)
b [Å]	10.781(2)	10.930(2)	32.295(7)	15.1938(6)
c [Å]	11.171(2)	12.902(3)	7.0758(14)	16.3540(7)
α [deg]	69.04(3)	101.36(3)	90.00	109.425(4)
β [deg]	63.35(3)	97.45(3)	90.00	91.690(3)
γ [deg]	88.53(3)	96.46(3)	90.00	97.061(3)
V / [$Å^3$]	1039.2(5)	1236.5(5)	3777.6(13)	1695.84(13)
d / [g/cm^3]	1.144	1.500	1.542	1.358
Z	2	2	4	2
T [K]	173(2)	173(2)	100.00(10)	100.00(10)
R1, wR2 $I > 2\acute{o}(I)$	0.0798, 0.1679	0.0948, 0.1980	0.0995, 0.2649	0.0934, 0.3174
R1, wR2 (all data)	0.0861, 0.1722	0.1343, 0.2188	0.1338, 0.2957	0.1186, 0.3268
quality of fit	1.009	1.035	1.061	1.028

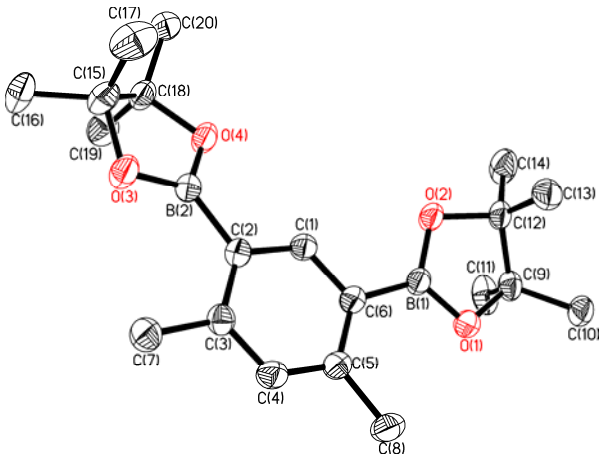

Figure S23. Ellipsoid form showing **2** in the single crystal structure of [**2**]. Displacement ellipsoids are scaled to the 50% probability level. All the other atoms have been omitted for clarity.

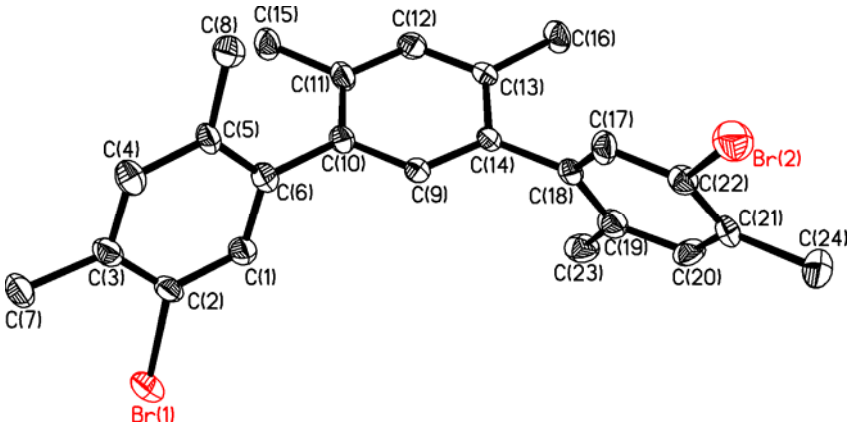

Figure S24. Ellipsoid form showing **3** in the single crystal structure of [**3**•*n*-hexane]. Displacement ellipsoids are scaled to the 25% probability level. All the other molecules and atoms have been omitted for clarity.

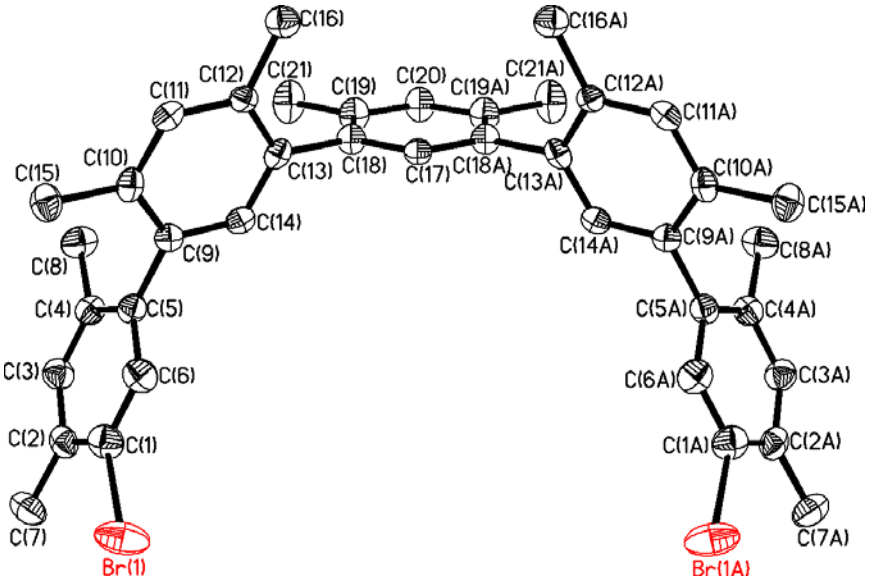

Figure S25. Ellipsoid form showing **4** in the single crystal structure of [**4**•CH_2Cl_2]. Displacement ellipsoids are scaled to the 50% probability level. All the other molecules and atoms have been omitted for clarity.

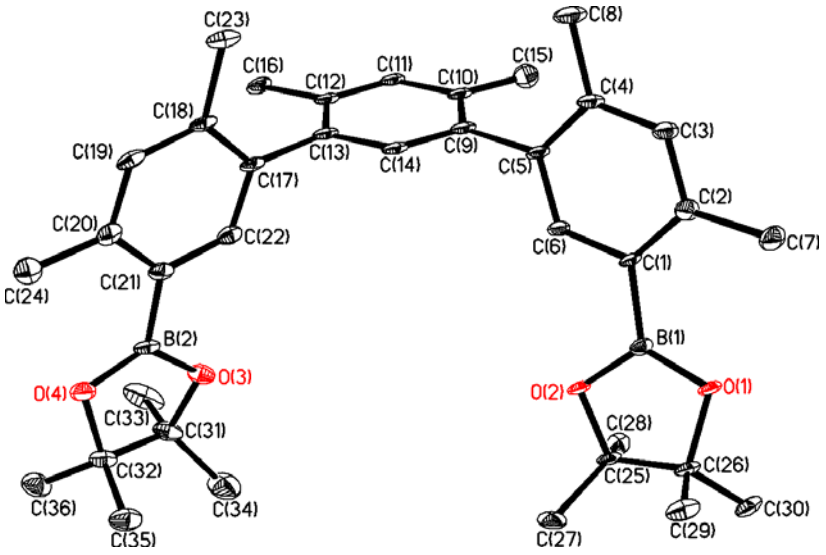

Figure S26. Ellipsoid form showing **5** in the single crystal structure of [**5**]. Displacement ellipsoids are scaled to the 50% probability level. All the other atoms have been omitted for clarity.

Synthesis of cyclo[8](1,3-(4,6-dimethyl)benzene (C_s-CDMB-8)

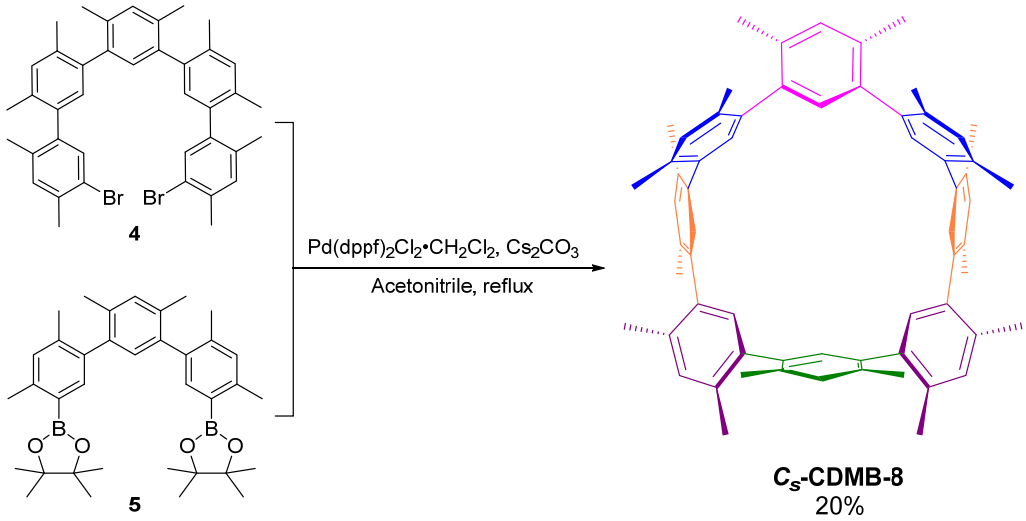

Under the protection of argon, a mixture of **4** (0.30 g, 0.44 mmol), **5** (0.25 g, 0.44 mmol) $Pd(dppf)_2Cl_2 \cdot CH_2Cl_2$ (74 mg, 0.09 mmol), Cs_2CO_3 (7.2 g, 22 mmol) and 250 mL deaerated acetonitrile were added in 500 mL three-necked round-bottomed flask. The reaction mixture was heated under reflux for 12 h. After cooling to room temperature, the solvent was removed *via* rotary evaporation, the resulting residue was dissolved in 50 mL CH_2Cl_2, then filter through a short neutral alumina column and washed with CH_2Cl_2 (50 mL). Remove CH_2Cl_2 from the

filtrate *via* rotary evaporation, the residue was dissolved in 50 mL cyclohexane and purified by a neutral alumina column with cyclohexane as the eluent to give pure ***C*$_s$-CDMB-8** as a white solid (73 mg, 20%). ***C*$_s$-CDMB-8**: ^{1}H NMR (500 MHz, TCE-d_2, 278 K) δ (ppm): 7.08 (s, 2H), 7.04 (s, 2H), 7.02 (s, 2H), 7.01 (s, 1H), 6.96 (s, 1H), 6.91 (s, 1H), 6.89 (s, 2H), 6.86 (s, 2H), 6.83 (s, 2H), 6.81 (s, 2H), 2.16 (s, 6H), 2.12(s, 6H), 2.11 (s, 6H), 2.09 (s, 6H), 2.08 (s, 6H), 2.07 (s, 12H), 2.02 (s, 6H); ^{13}C NMR (125 MHz, TCE-d_2, 278 K) δ (ppm): 139.2, 139.0, 138.7, 138.65, 138.63, 137.8, 134.5, 134.40, 134.36, 134.3, 133.8, 133.3, 133.1, 132.5, 131.5, 131.4, 131.2, 131.1, 130.5, 20.2, 20.0, 19.8, 19.7, 19.60, 19.57; MALDI-TOF HRMS (*m*/*z*): $[M]^{+\bullet}$ calcd. for $C_{64}H_{64}$, 832.5008; found, 832.5019.

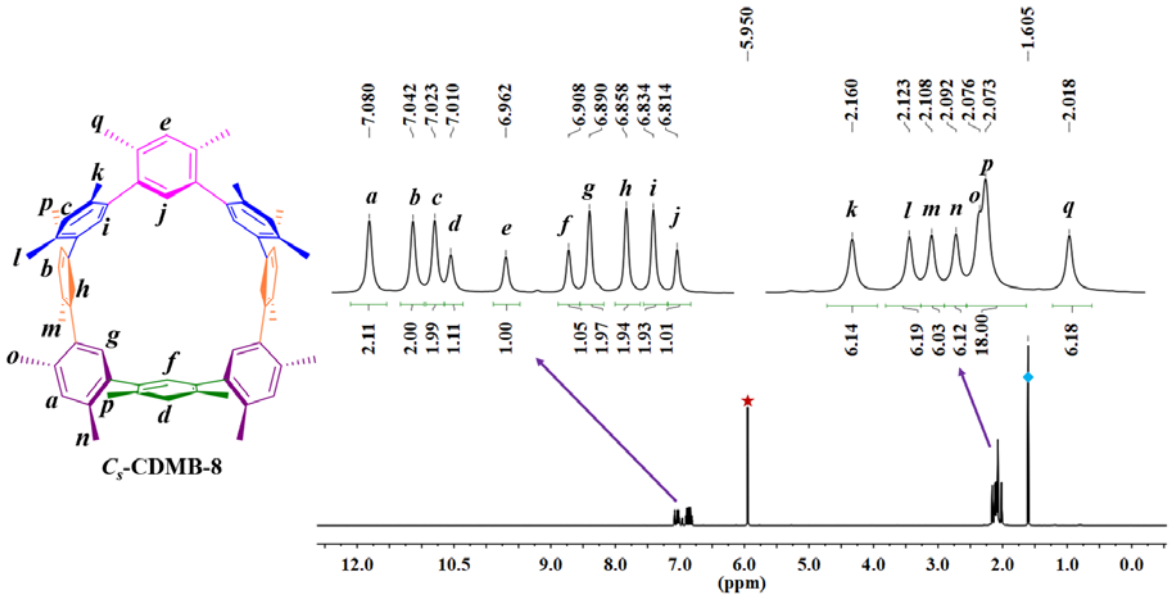

Figure S27. Expanded view (top) and full view (bottom) of the ^{1}H NMR spectrum of ***C*$_s$-CDMB-8** (5.00×10^{-3} M) in TCE-d_2 at 278 K (500 MHz) (red "★" represents residual TCE; blue "♦" represents H_2O).

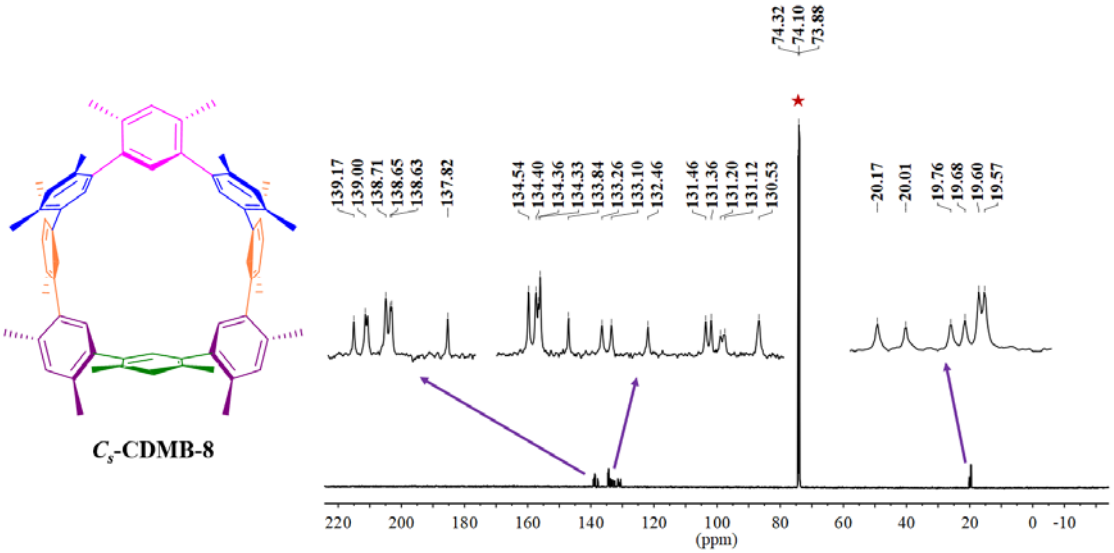

Figure S28. Expanded view (top) and full view (bottom) of the ^{13}C NMR spectrum of ***C*$_s$-CDMB-8** (5.00×10^{-3} M) in TCE-d_2 at 278 K (125 MHz) (red "★" represents residual TCE).

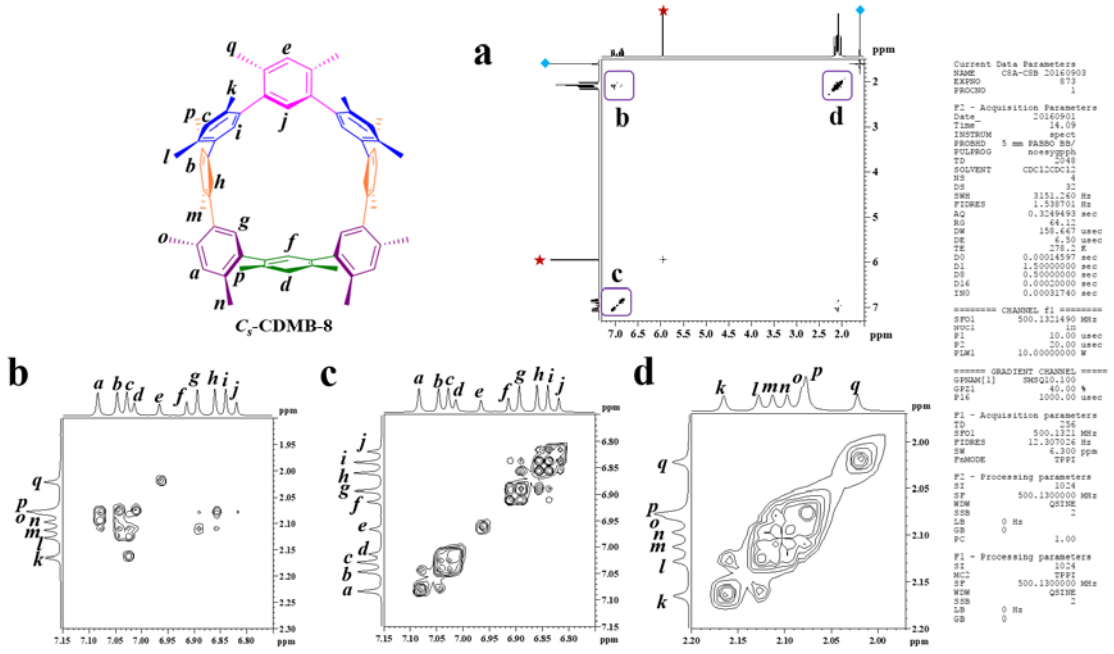

Figure S29. Full view (a) and expanded views (b, c, d) of the NOESY spectrum of ***C*$_s$-CDMB-8** (5.00×10^{-3} M) in TCE-d_2 at 278 K (500 MHz) (red "★" represents residual TCE; blue "♦" represents H_2O).

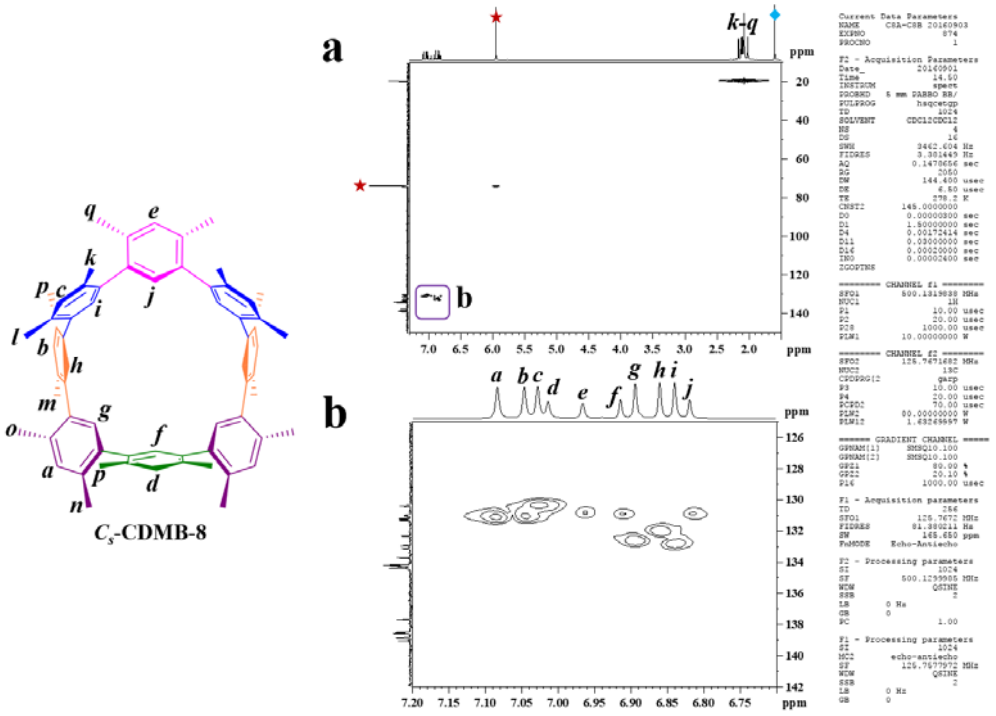

Figure S30. Full view (a) and expanded view (b) of the HSQC spectrum of ***C*$_s$-CDMB-8** (5.00 × 10^{-3} M) in TCE-d_2 at 278 K (500 MHz) (red "★" represents residual TCE; blue "♦" represents H_2O).

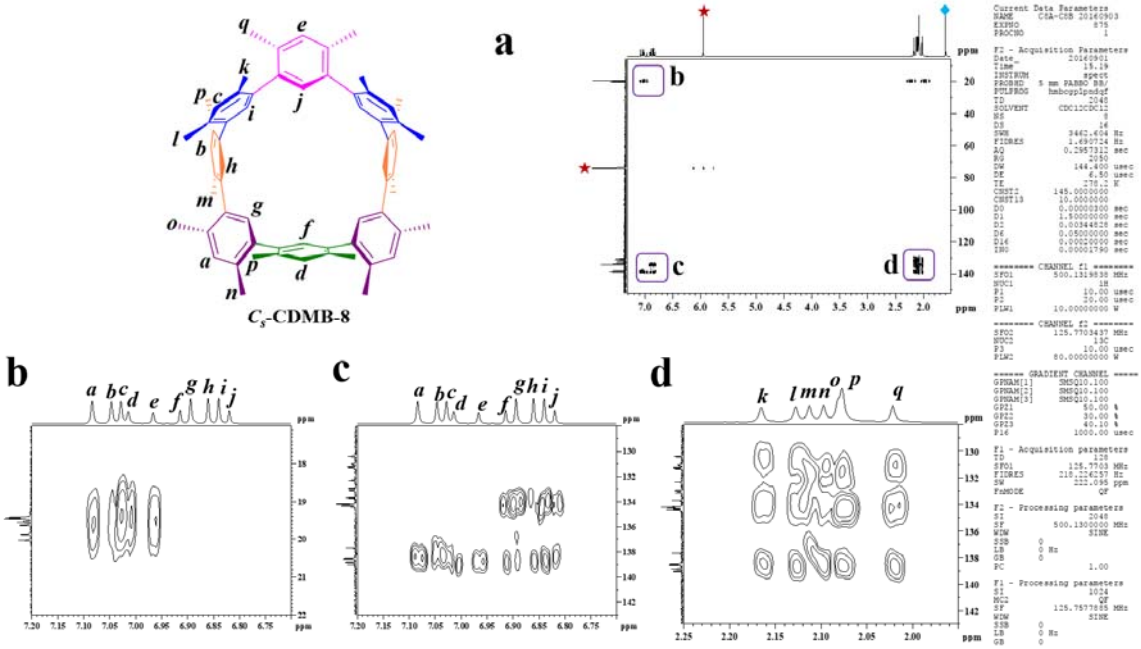

Figure S31. Full view (a) and expanded views (b, c, d) of the HMBC spectrum of ***C*$_s$-CDMB-8** (5.00 × 10^{-3} M) in TCE-d_2 at 278 K (500 MHz) (red "★" represents residual TCE; blue "♦" represents H_2O).

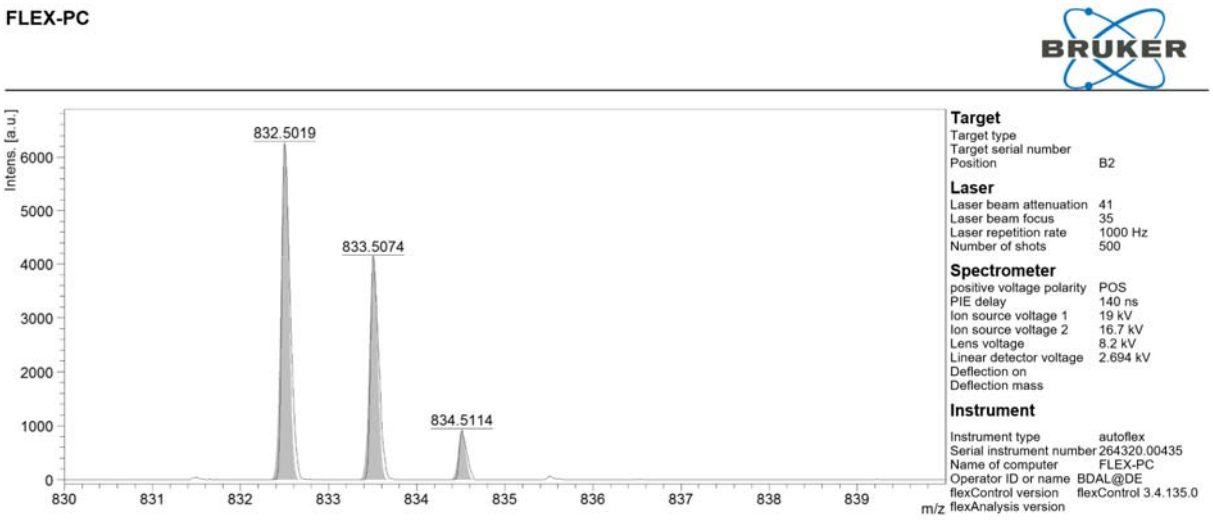

Figure S32. Positive MALDI-TOF HRMS spectrum of ***C*$_s$-CDMB-8**.

In the temperature dependent ^{1}H NMR spectrum of ***C*$_s$-CDMB-8** or ***D*$_{4d}$-CDMB-8**, only one set of high resolution signals was observed over the 233–398 K temperature range. Furthermore, the spectra were restored after heating to 398 K then cooling to 298 K. These findings are consistent with the fixed conformations of ***C*$_s$-CDMB-8** and ***D*$_{4d}$-CDMB-8**.

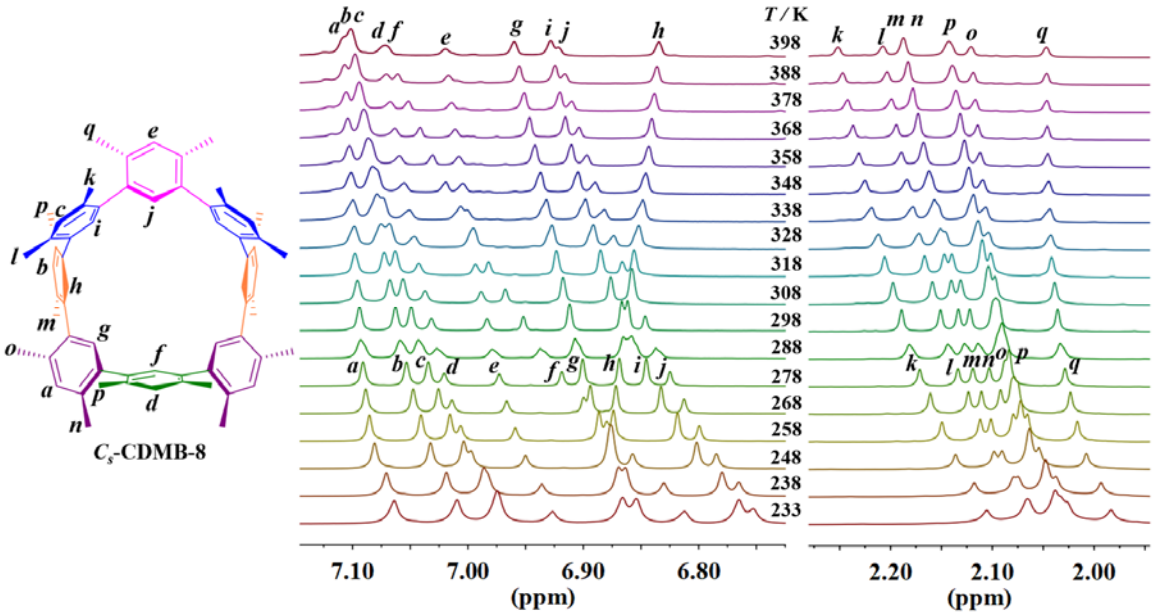

Figure S33. Expansion of the temperature dependent ^{1}H NMR spectra of ***C*$_s$-CDMB-8** (5.00×10^{-3} M) in TCE-d_2 (500 MHz).

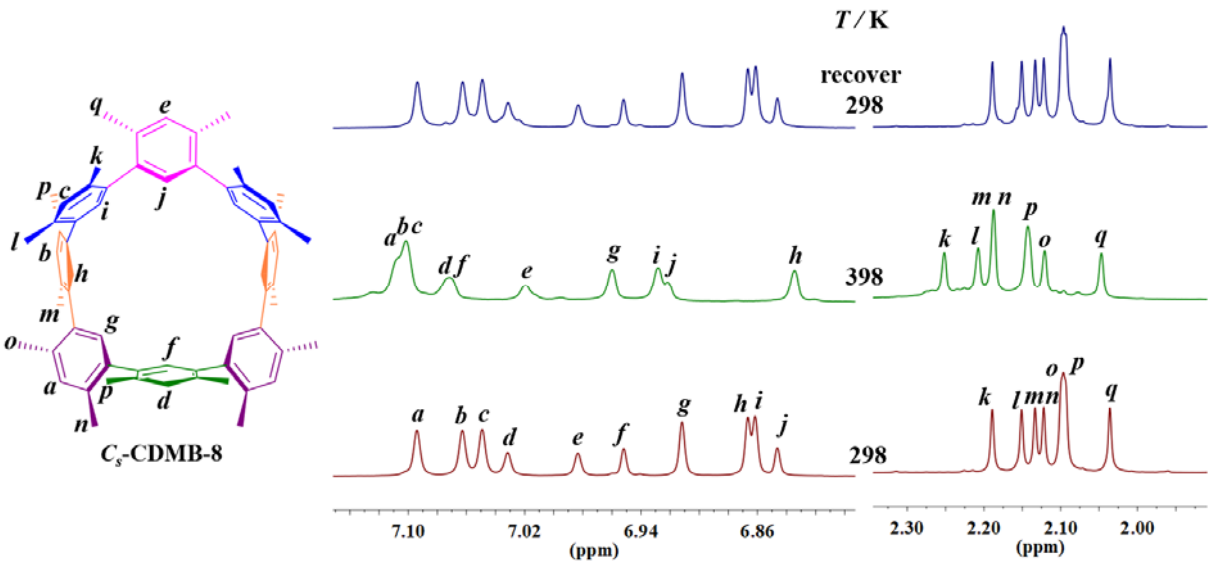

Figure S34. Expansion of ^{1}H NMR spectra of ***C*$_s$-CDMB-8** (5.00×10^{-3} M) which is recorded at 298 K, heating to 398 K and cooling back to 298 K in TCE-*d*$_2$ (500 MHz).

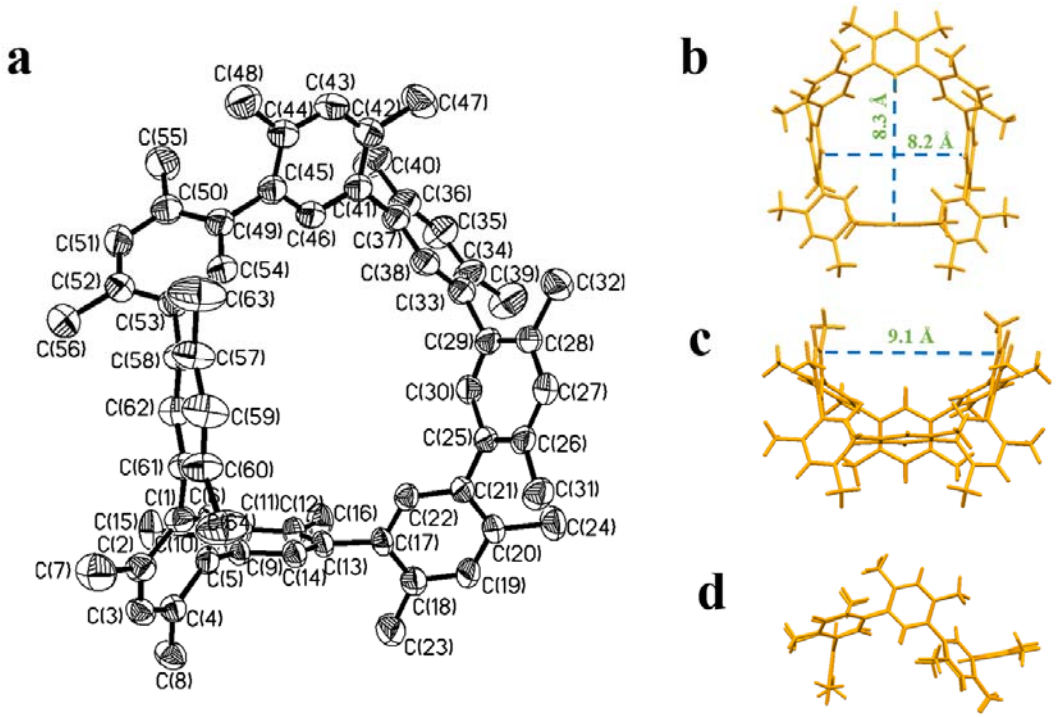

Figure S35. Ellipsoid form (a) showing the ***C*$_s$-CDMB-8** in the single crystal structure of [***C*$_s$-CDMB-8**•10.5H$_2$O]. Also shown as a top view (b) and side views (c, d) is the structure in stick form. Displacement ellipsoids are scaled to the 25% probability level. All the other molecules and atoms have been omitted for clarity.

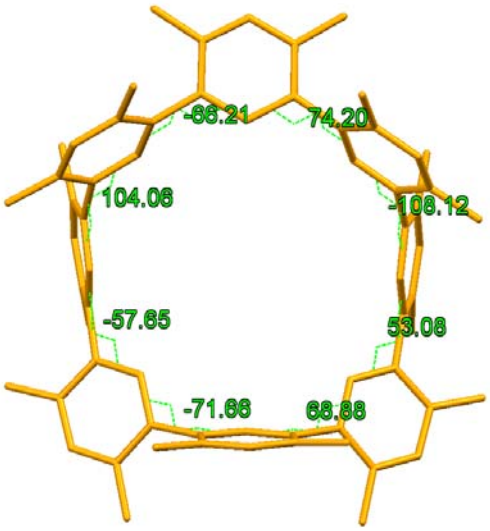

Figure S36. The torsion angles between the neighboring *meso*-dimethyl benzene units range on ***C*$_s$-CDMB-8** in the single crystal structure of [***C*$_s$-CDMB-8**•10.5H_2O].

Section S5: *Theoretical calculation*

The optimized geometries of ***C*$_s$-CDMB-8** and ***D*$_{4d}$-CDMB-8** are listed in Figure S37. The calculation results suggested that the energy of ***C*$_s$-CDMB-8** is 4.04 kcal•mol^{-1} higher than ***D*$_{4d}$-CDMB-8**.

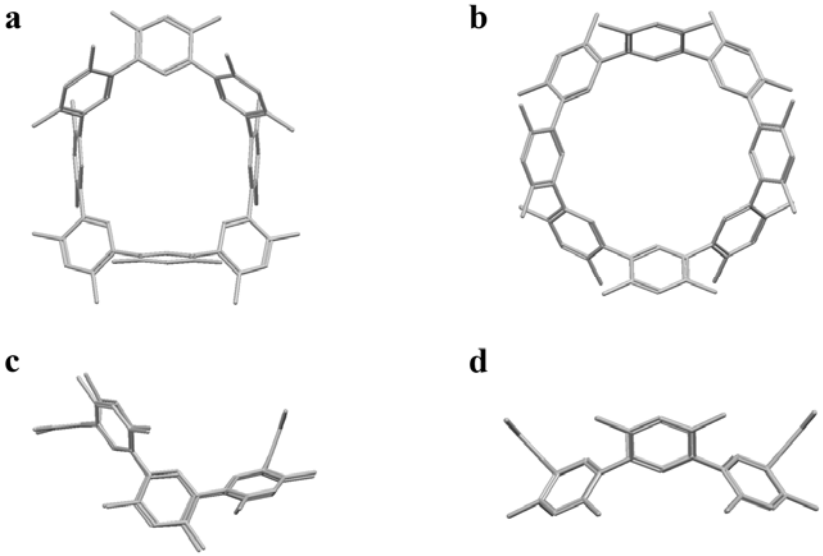

Figure S37. Optimized geometries of ***C*$_s$-CDMB-8** (a, top view; c, side view) and ***D*$_{4d}$-CDMB-8** (b, top view; c, side view) obtained by DFT (B3LYP-D3/6-31G(d)). All the hydrogen atoms have been omitted for clarity.

Synthesis of cyclo[8](1,3-(4,6-dimethyl)benzene (*D*$_{4d}$-CDMB-8)

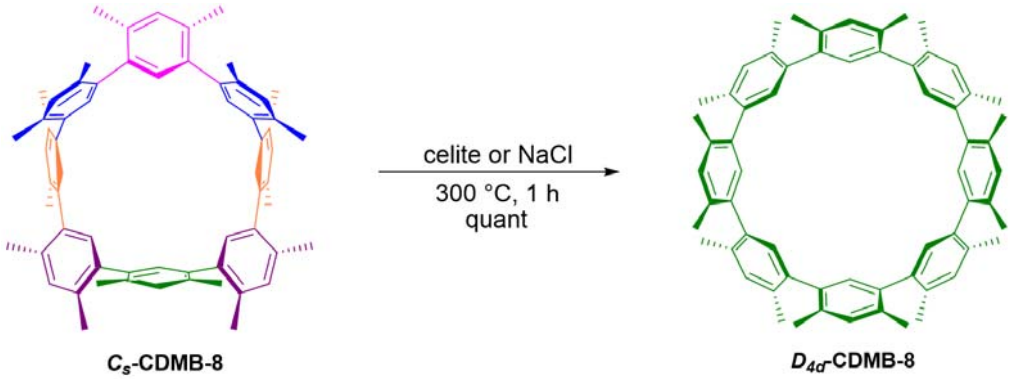

***C*$_s$-CDMB-8** (0.50 g, 0.60 mol) and 3.0 g celite or NaCl were fully grinded and mixed in 50 mL flask, the mixture was heated to 300 °C under argon for 1 hours. The reaction mixture was cooled to room temperature and washed with 50 mL CH_2Cl_2, the solvent was removed *via* rotary evaporation, and the obtained residue was recrystallized from CH_2Cl_2/CH_3CN (1:1, *v*/*v*) to obtain pure ***D*$_{4d}$-CDMB-8**, as a white solid in quantitative yield. ***D*$_{4d}$-CDMB-8**: ^{1}H NMR (500 MHz, TCE-*d*$_2$, 278 K) δ (ppm): 7.03 (s, 8H), 6.75 (s, 8H), 2.01 (s, 48H); ^{13}C NMR (125 MHz, TCE-*d*$_2$, 278 K) δ (ppm): 138.6, 134.3, 130.9, 130.6, 19.8; MALDI-TOF HRMS (*m*/*z*): $[M]^{+\bullet}$ calcd. for $C_{64}H_{64}$, 832.5008; found, 832.5000.

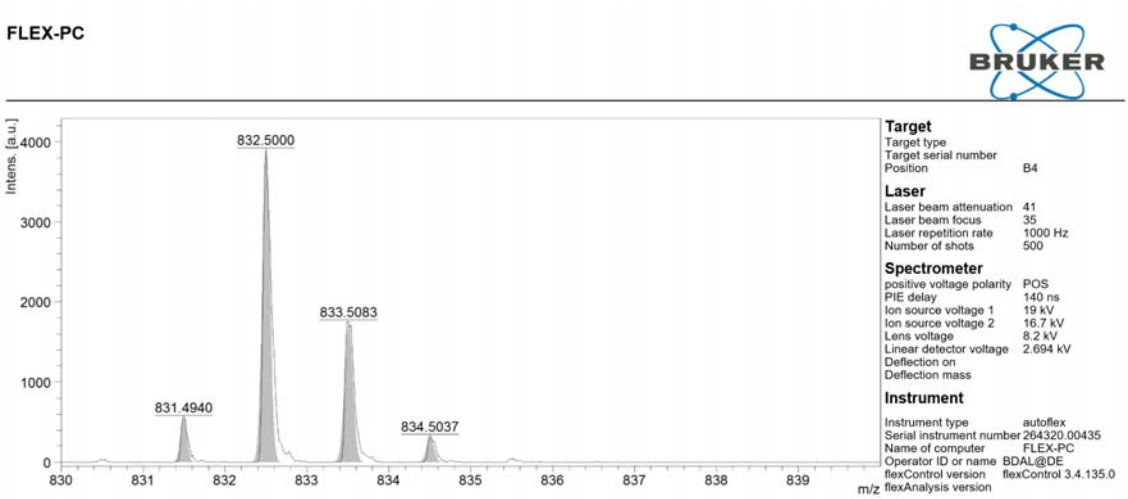

Figure S38. Positive MALDI-TOF HRMS spectrum of ***D*$_{4d}$-CDMB-8**.

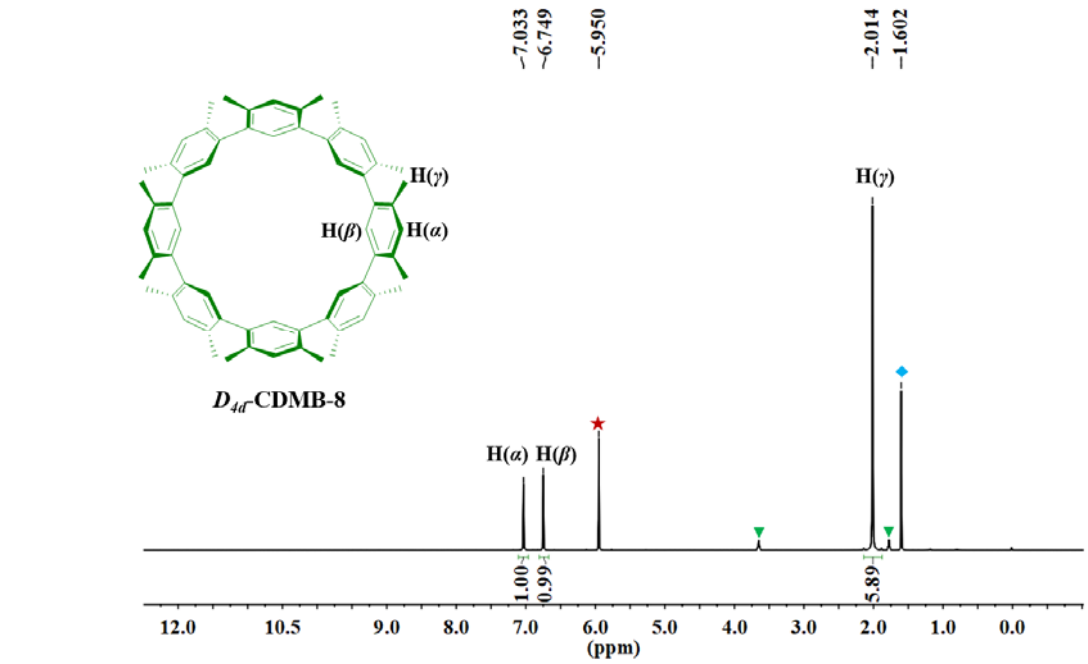

Figure S39. ^{1}H NMR spectrum of ***D*$_{4d}$-CDMB-8** (5.00 × 10^{-3} M) in TCE-*d*$_2$ at 278 K (500 MHz) (red "★" represents residual TCE; green "▼" represents residual THF; blue "♦" represents H_2O).

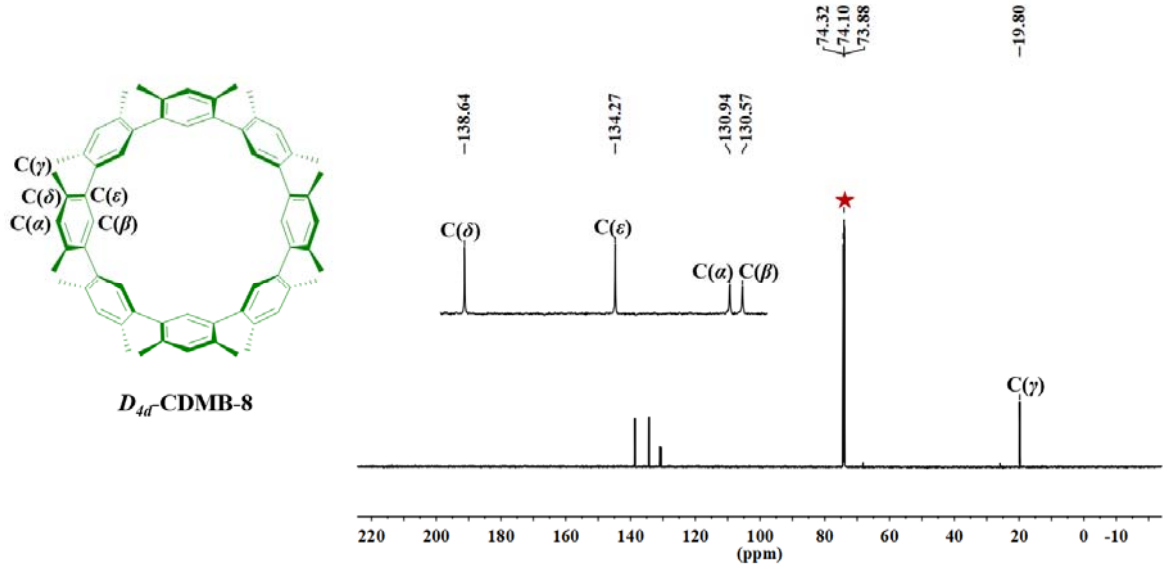

Figure S40. Expanded view (insert figure) and full view of the ^{13}C NMR spectrum of ***D*$_{4d}$-CDMB-8** (5.00 × 10^{-3} M) in TCE-*d*$_2$ at 278 K (125 MHz) (red "★" represents residual TCE).

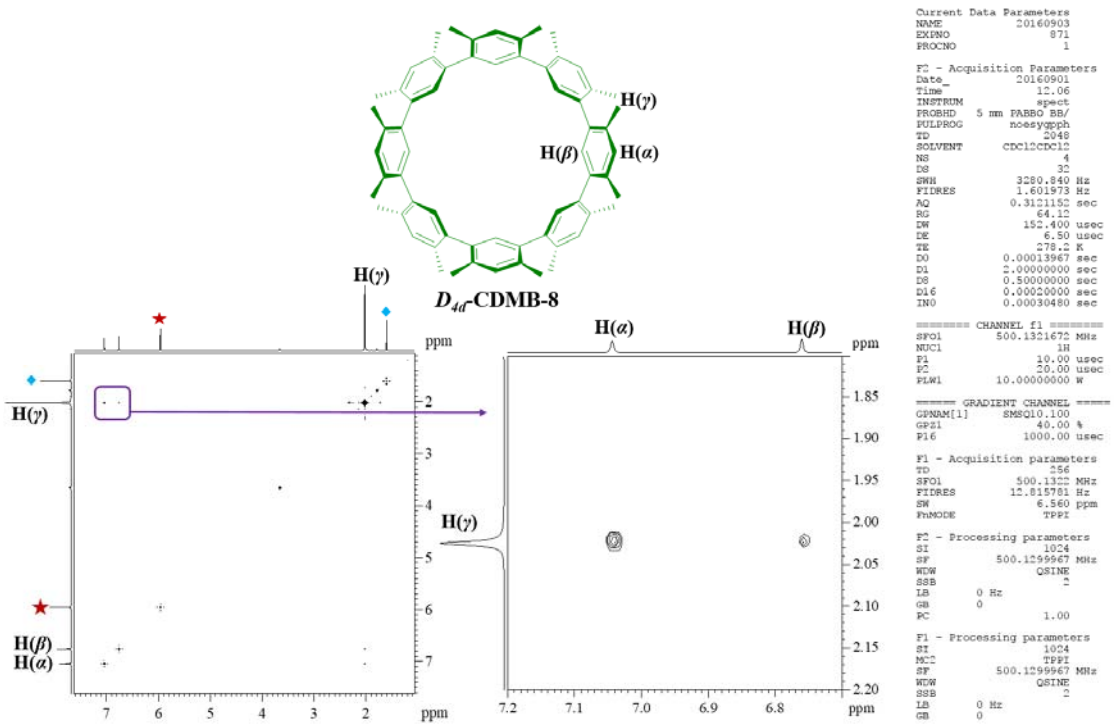

Figure S41. Full view (left) and expanded view (right) of the NOESY spectrum of ***D*$_{4d}$-CDMB-8** (5.00×10^{-3} M) in TCE-d_2 at 278 K (500 MHz) (red "★" represents residual TCE; blue "♦" represents H_2O).

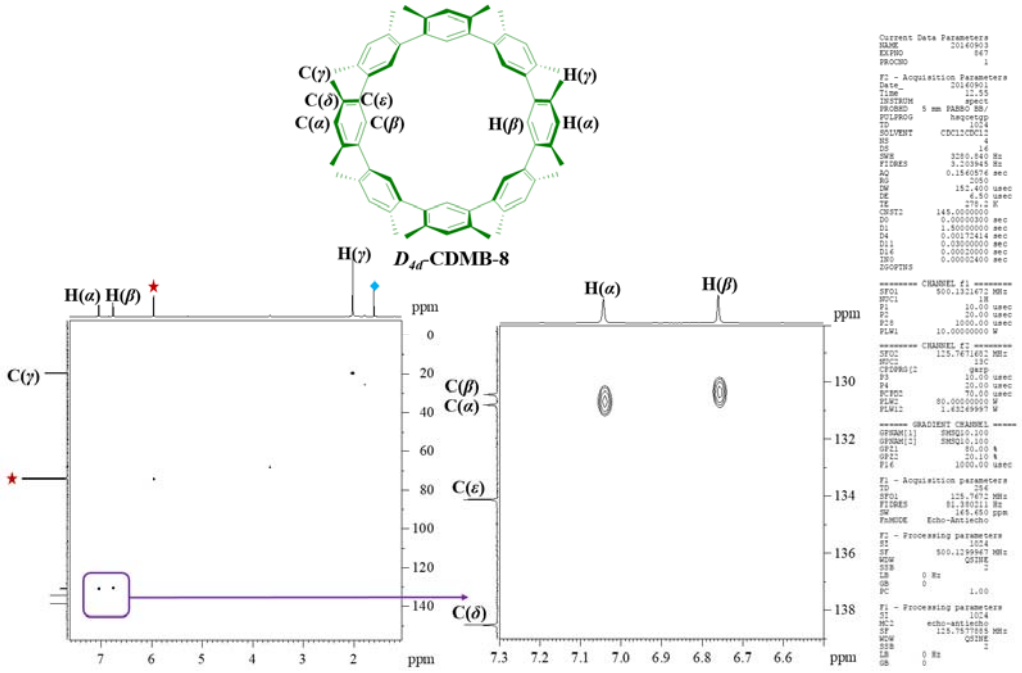

Figure S42. Full view (left) and expanded view (right) of the HSQC spectrum of ***D*$_{4d}$-CDMB-8** (5.00×10^{-3} M) in TCE-d_2 at 278 K (500 MHz) (red "★" represents residual TCE; blue "♦" represents H_2O).

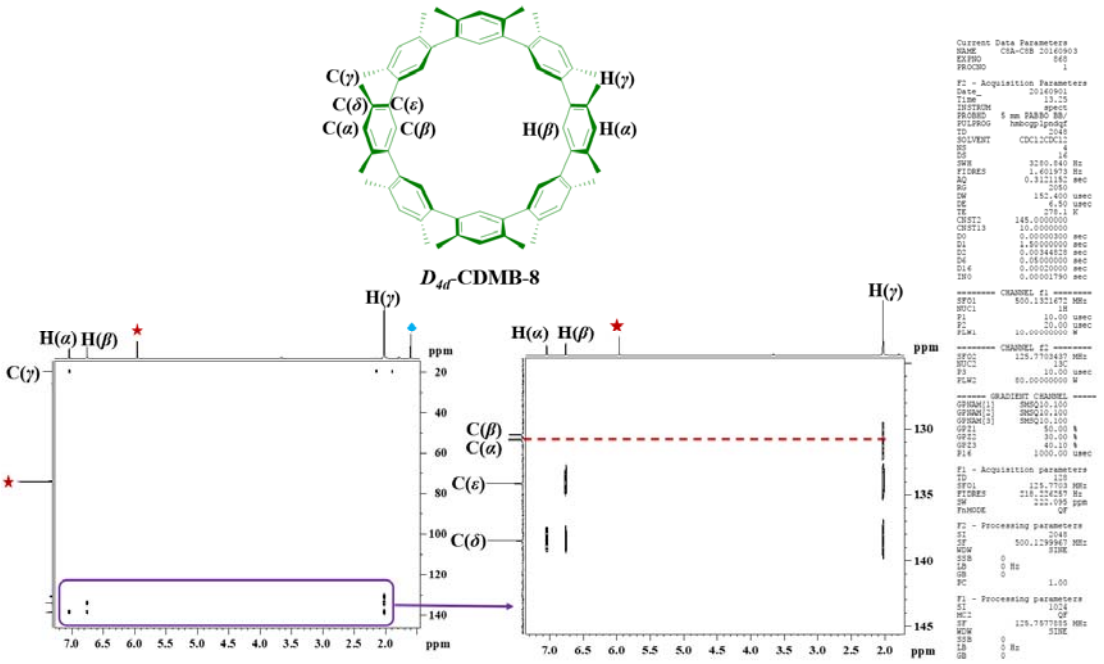

Figure S43. Full view (left) and expanded view (right) of the HMBC NMR spectrum of ***D*$_{4d}$-CDMB-8** (5.00×10^{-3} M) in TCE-d_2 at 278 K (500 MHz) (red "★" represents residual TCE; blue "♦" represents H_2O).

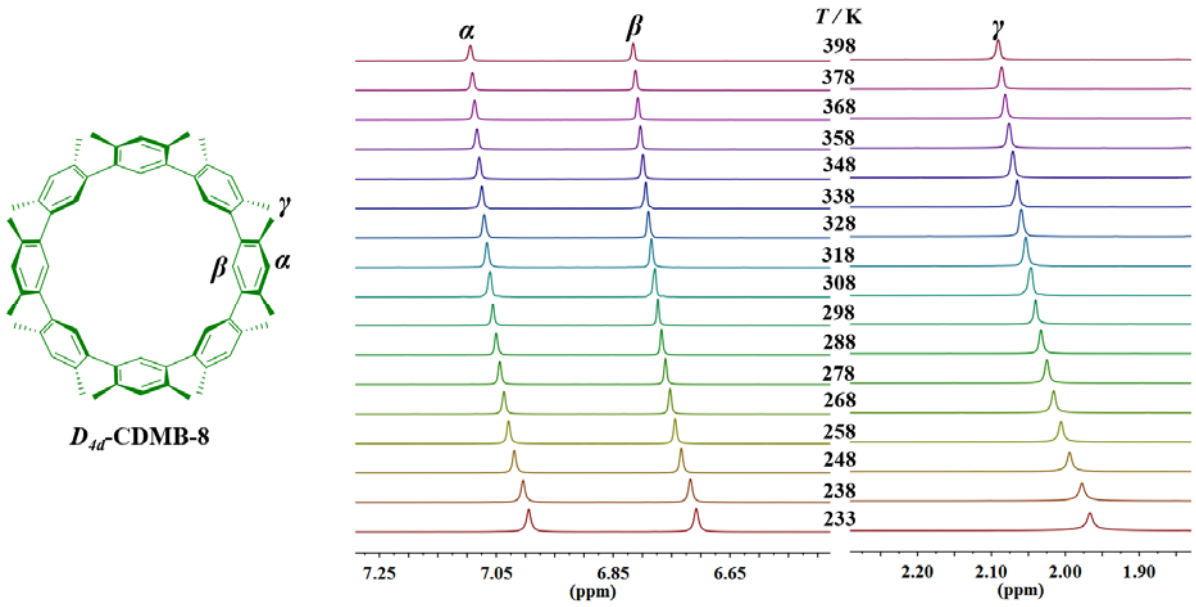

Figure S44. Expansion of the temperature dependent ^{1}H NMR spectra of ***D*$_{4d}$-CDMB-8** (5.00×10^{-3} M) in TCE-d_2 (500 MHz).

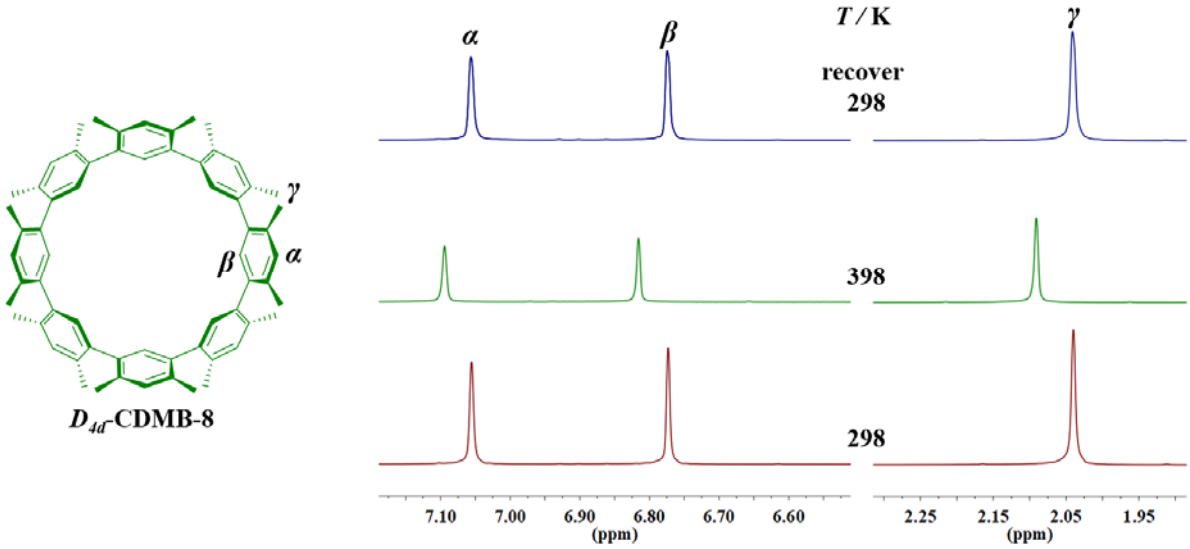

Figure S45. Expansion of ^{1}H NMR spectra of ***D*$_{4d}$-CDMB-8** (5.00×10^{-3} M) which is recorded at 298 K, heating to 398 K and cooling back to 298 K in TCE-*d*$_2$ (500 MHz).

The possible reason of the selective construction of ***C*$_s$-CDMB-8** as main product in original cyclization reaction came from the intermediate calculations. As shown below, the cyclization precursor ***C*$_s$-CDMB-8-im**, which induces ***C*$_s$-CDMB-8** formation, has the lower energy (ΔE = 29.82 kcal•mol^{-1}) than ***D*$_{4d}$-CDMB-8-im**, another cyclization intermediate gave out ***D*$_{4d}$-CDMB-8** (Figure S46).

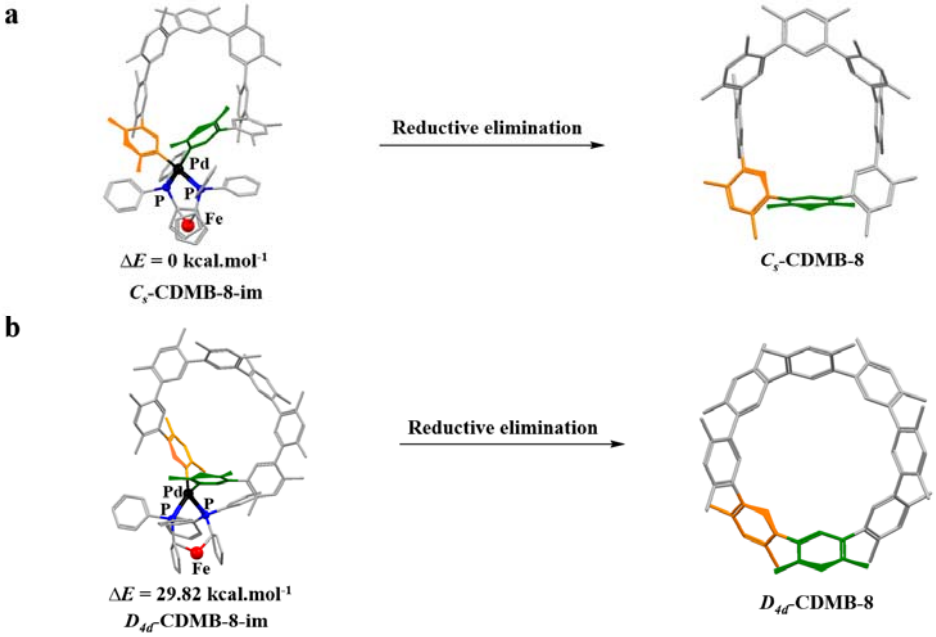

Figure S46. Reductive elimination step of ***C*$_s$-CDMB-8-im** to ***C*$_s$-CDMB-8** (a) and ***D*$_{4d}$-CDMB-8-im** to ***D*$_{4d}$-CDMB-8** (b). Their optimized geometries and relative energy are

obtained by DFT (B3LYP-D3/6-31G(d) basis set for C, H and P atoms, and LanL2DZ basis set for transition metals Pd and Fe). All the hydrogen atoms have been omitted for clarity.

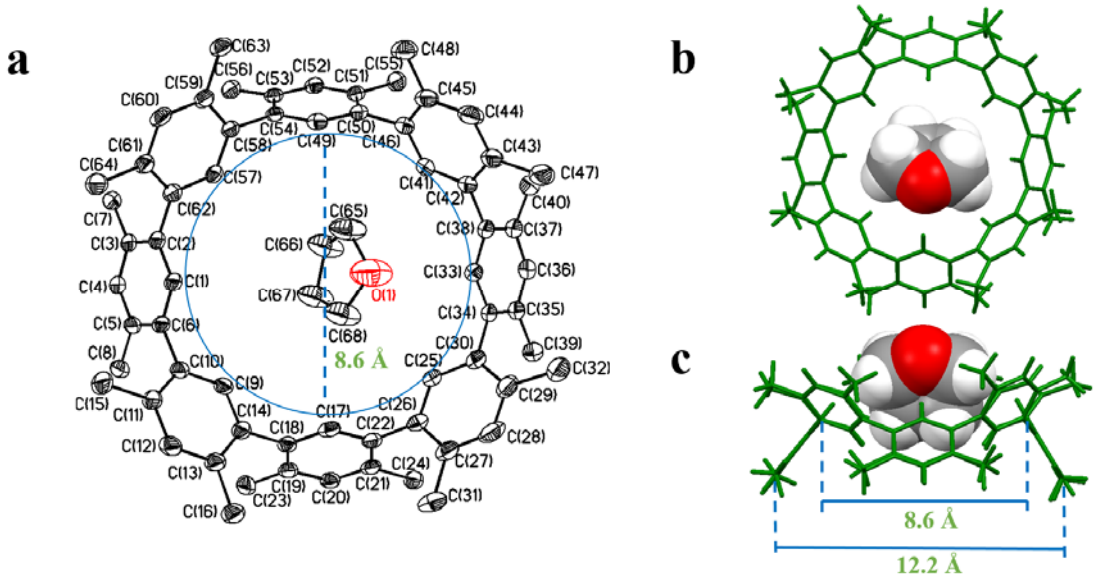

Figure S47. Ellipsoid form (a) showing the ***D*$_{4d}$-CDMB-8**⊃THF in the single crystal structure of [***D*$_{4d}$-CDMB-8**⊃THF•THF]. Also shown as a top view (b) and side view (c) is the structure in stick form. Displacement ellipsoids are scaled to the 50% probability level. All the other molecules and atoms have been omitted for clarity. Possible CH-π interactions are inferred from the following selected distances [Å]: C(65)…C(49) 3.612(8), C(67)…C(9) 3.797(9), C(65)…C(41) 3.84(1), C(66)…C(41) 3.85(1).

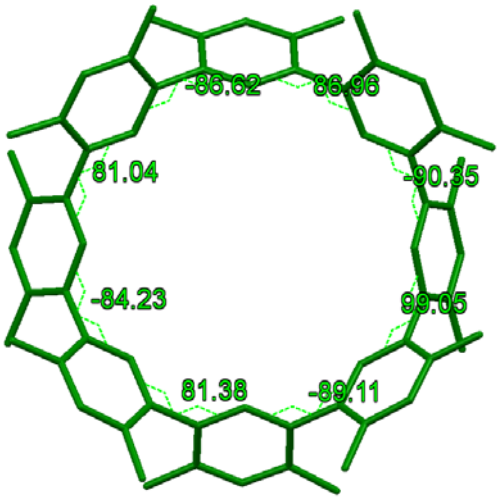

Figure S48. The torsion angles between the neighboring *meso*-dimethyl benzene units range on ***D*$_{4d}$-CDMB-8** in the single crystal structure of [***D*$_{4d}$-CDMB-8**⊃THF•THF].

Table S2. X-ray crystallographic data comparison of [***C*$_s$-CDMB-8**•10.5H_2O] and **[*D*$_{4d}$-CDMB-8⊃**THF•THF**]**.

	[***C*$_s$-CDMB-8**•10.5H_2O]	**[*D*$_{4d}$-CDMB-8⊃**THF•THF**]**
CCDC No.	1820649	1859997
description	prism	block
colour	colourless	colourless
from solution	CH_2Cl_2/CH_3CH_2OH	THF/CH_3CN
empirical formula	$C_{64}H_{85}O_{10.5}$	$C_{72}H_{80}O_2$
Mr	1022.32	977.36
crystal size (mm^3)	0.34 × 0.12 × 0.08	0.16 × 0.13 × 0.11
crystal system	triclinic	monoclinic
space group	P-1	P 21/c
a [Å]	13.224(3)	15.5945(5)
b [Å]	14.975(3)	32.7430(11)
c [Å]	18.393(4)	11.5345(4)
α [deg]	68.87(3)	90.00
β [deg]	72.80(3)	100.066(3)
γ [deg]	64.85(3)	90.00
V / [$Å^3$]	3031.5(10)	5799.0(3)
d / [g/cm^3]	1.120	1.119
Z	2	4
T [K]	173(2)	100.00(10)
R1, wR2 $I > 2ó(I)$	0.0798, 0.1740	0.0960, 0.2126
R1, wR2 (all data)	0.1108, 0.1890	0.1107, 0.2223
quality of fit	1.002	1.020

The UV−vis absorption spectra were recorded for ***C*$_s$-CDMB-8** and ***D*$_{4d}$-CDMB-8** as illustrated in Figure S49. Notably, ***C*$_s$-CDMB-8** shows two peaks at 212 nm and 232 nm. In contrast, only a significant absorption maximum peak at 205 nm of ***D*$_{4d}$-CDMB-8** was observed.

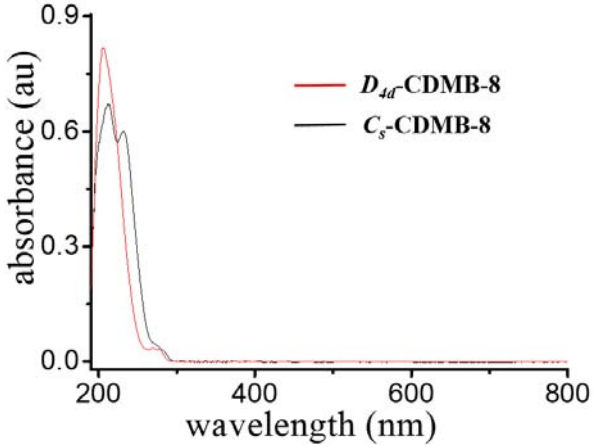

Figure S49. UV-vis spectra of ***C*$_s$-CDMB-8** or ***D*$_{4d}$-CDMB-8** (2.00×10^{-4} M, 1 mm optical path) in *n*-hexane.

Section S3: *Fullerene (C_{60} or C_{70}) receptor property studies of* ***C_s-CDMB-8*** *or* ***D_{4d}-CDMB-8*** *both in solution and solid states*

No change in the ^{1}H NMR spectroscopic of ***C_s-CDMB-8*** was seen upon adding 1 molar equiv. of C_{60} or C_{70} (Figure S50).

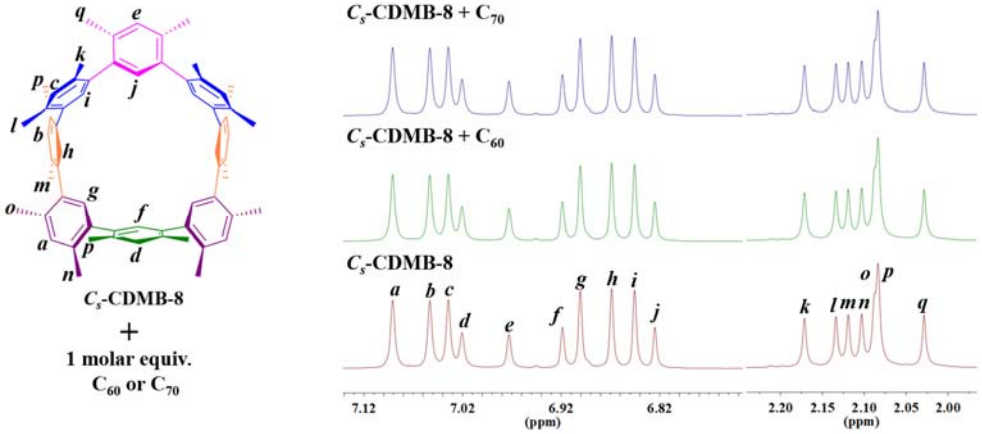

Figure S50. Expansion of the ^{1}H NMR spectra of ***C_s-CDMB-8*** (1.00×10^{-3} M) recorded in the absence and presence of 1 molar equiv. of C_{60} or C_{70} in TCE-d_2 at 298 K (600 MHz).

Additional 1 molar equiv. of C_{60} or C_{70} leads to changes of the proton signals on ***D_{4d}-CDMB-8*** in TCE-d_2 (Figure S51). Furthermore, ^{13}C NMR spectra study showed the carbon signal chemical shift changes on both components after mixing ***D_{4d}-CDMB-8*** and C_{60} in TCE-d_2 (Figure S52). Because of the poor solubility, the ^{13}C NMR detection for the mixture containing ***D_{4d}-CDMB-8*** and C_{70} was unsuccessful.

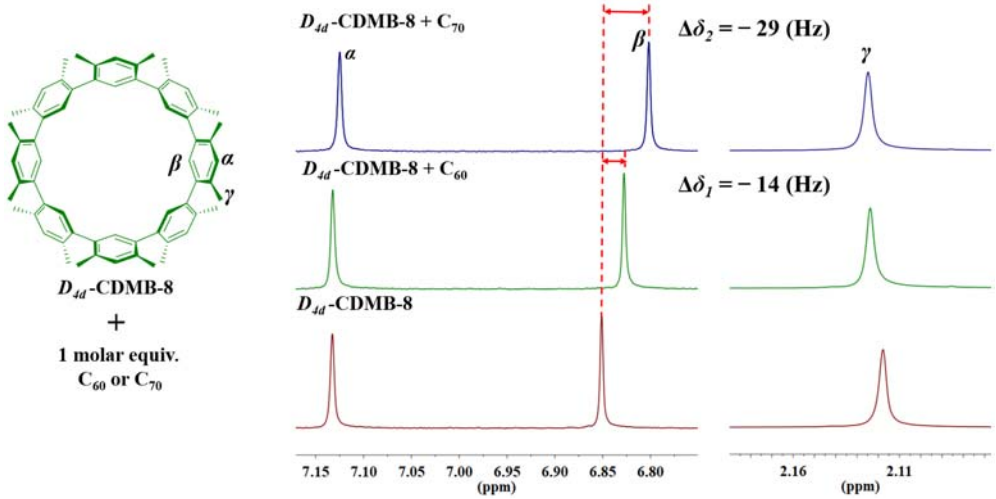

Figure S51. Expansion of the ^{1}H NMR spectra of ***D_{4d}-CDMB-8*** (1.00×10^{-3} M) recorded in the absence and presence of 1 molar equiv. of C_{60} or C_{70} in TCE-d_2 at 298 K (600 MHz).

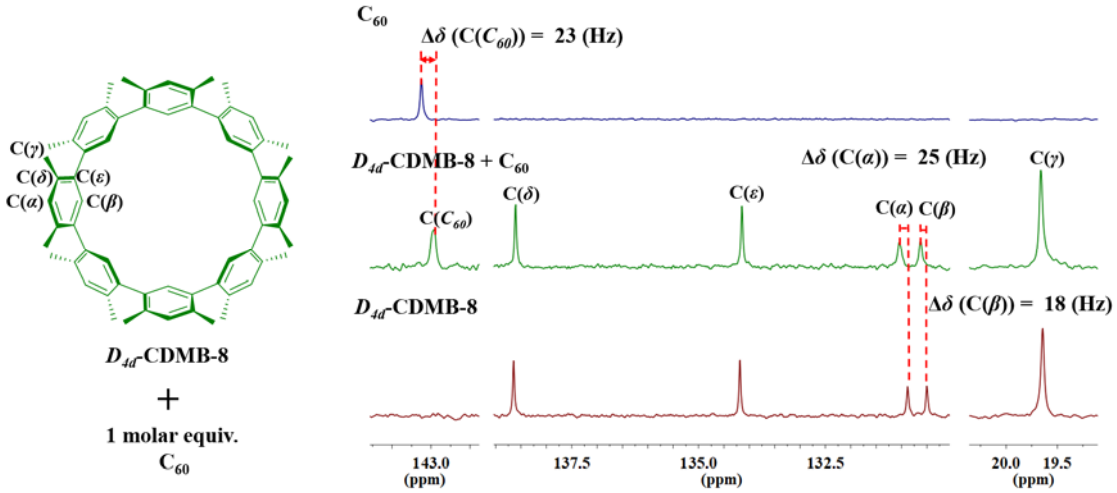

Figure S52. Expansion of the ^{13}C NMR spectra of ***D*$_{4d}$-CDMB-8** (1.00×10^{-3} M) recorded in the absence and presence of 1 molar equiv. of C_{60} in TCE-d_2 at 298 K (600 MHz).

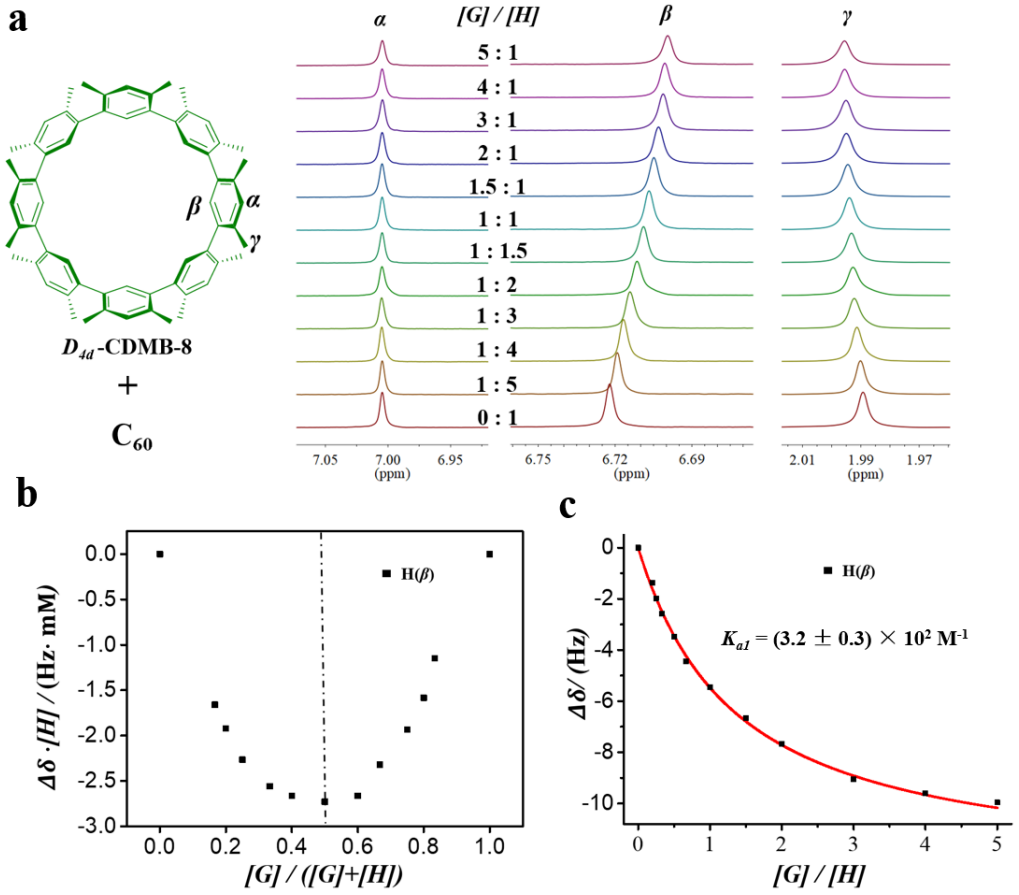

Figure S53. ^{1}H NMR spectroscopic titration of ***D*$_{4d}$-CDMB-8** (host) with C_{60} (guest) ([host] + [guest] = 1.00×10^{-3} M) in TCE-d_2 at 298 K (600 MHz) (a). ^{1}H NMR Job plot corresponding to the interaction between ***D*$_{4d}$-CDMB-8** and C_{60}, as determined by monitoring the chemical shift change of H(β) on ***D*$_{4d}$-CDMB-8**. The maximum value of the plot falls at 0.5, a finding

consistent with the formation of a complex with 1:1 (host/guest) binding stoichiometry[14] (b). ^{1}H NMR binding isotherms corresponding to the interaction between ***D*$_{4d}$-CDMB-8** and C_{60}. The chemical shift change of the H(β) was used to calculate the K_{a1} ((3.2 ± 0.3) × 10^2 M^{-1}) using the Hyperquad 2003 program[15, 16]. The red lines show the non-linear curve fit of the experimental data to the appropriate equation (c).

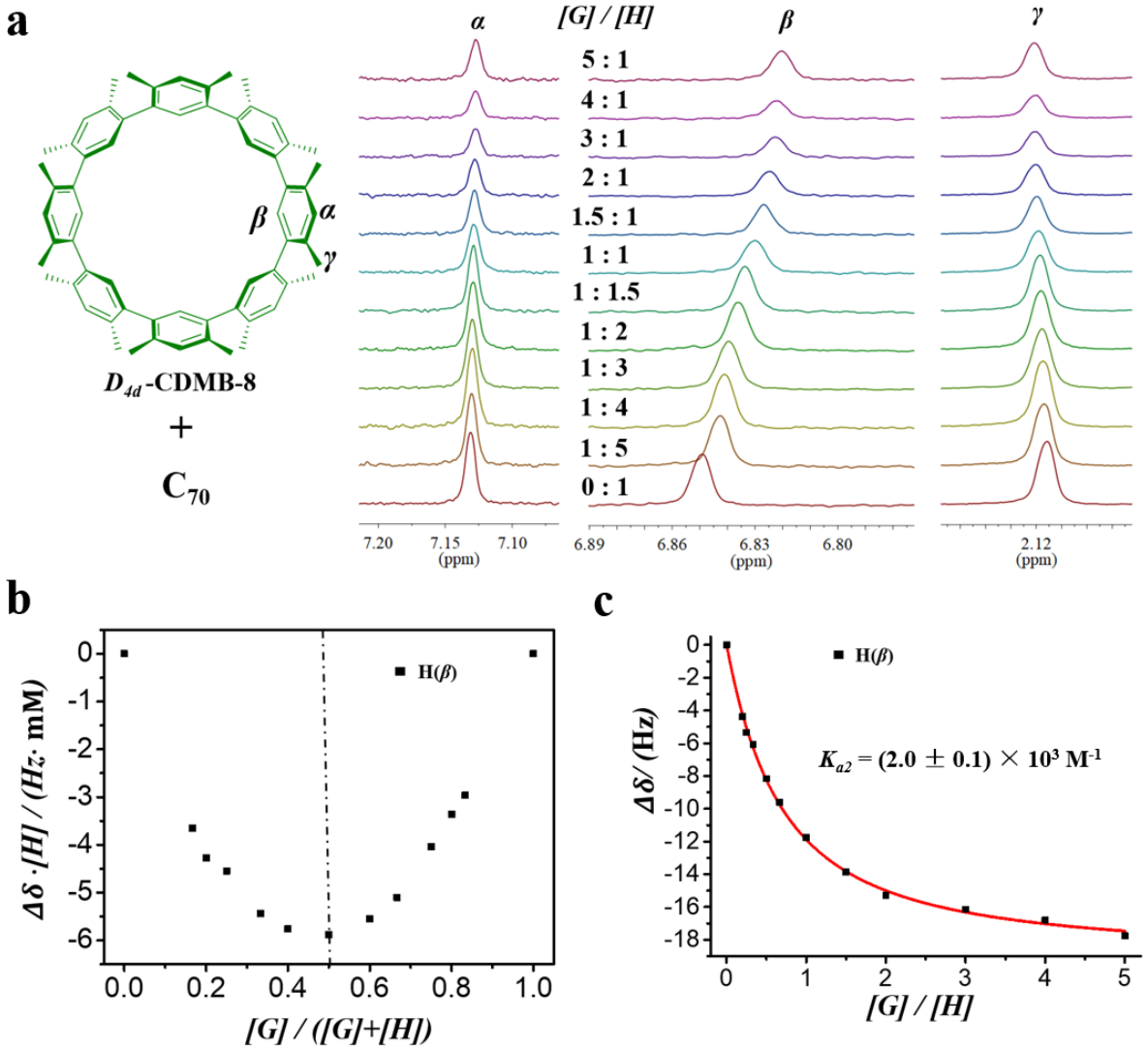

Figure S54. ^{1}H NMR spectroscopic titration of ***D*$_{4d}$-CDMB-8** (host) with C_{70} (guest) ([host] + [guest] = 2.50 × 10^{-4} M) in TCE-d_2 at 298 K (600 MHz) (a). ^{1}H NMR Job plot corresponding to the interaction between ***D*$_{4d}$-CDMB-8** and C_{70}, as determined by monitoring the chemical shift change of H(β) on ***D*$_{4d}$-CDMB-8**. The maximum value of the plot falls at 0.5, a finding consistent with the formation of a complex with 1:1 (host/guest) binding stoichiometry[14] (b). ^{1}H NMR binding isotherms corresponding to the interaction between ***D*$_{4d}$-CDMB-8** and C_{70}. The chemical shift change of the H(β) was used to calculate the K_{a2} ((2.0 ± 0.1) × 10^3 M^{-1}) using the Hyperquad 2003 program[15, 16]. The red lines show the non-linear curve fit of the experimental data to the appropriate equation (c).

In the UV-vis spectroscopic analyses, no change was seen upon adding 20 molar equiv. of ***C*$_s$ -CDMB-8** into C_{60} or C_{70} in TCE. In contrast, additional 20 molar equiv. of ***D*$_{4d}$-CDMB-8** charge transfer (CT) band change in the TCE solution of C_{60} or C_{70} (Figure S55 and S56). Further association constant calculations between ***D*$_{4d}$-CDMB-8** and C_{60} or C_{70} were carried from the UV-vis spectral titration experiment (Figure S57 and S58).

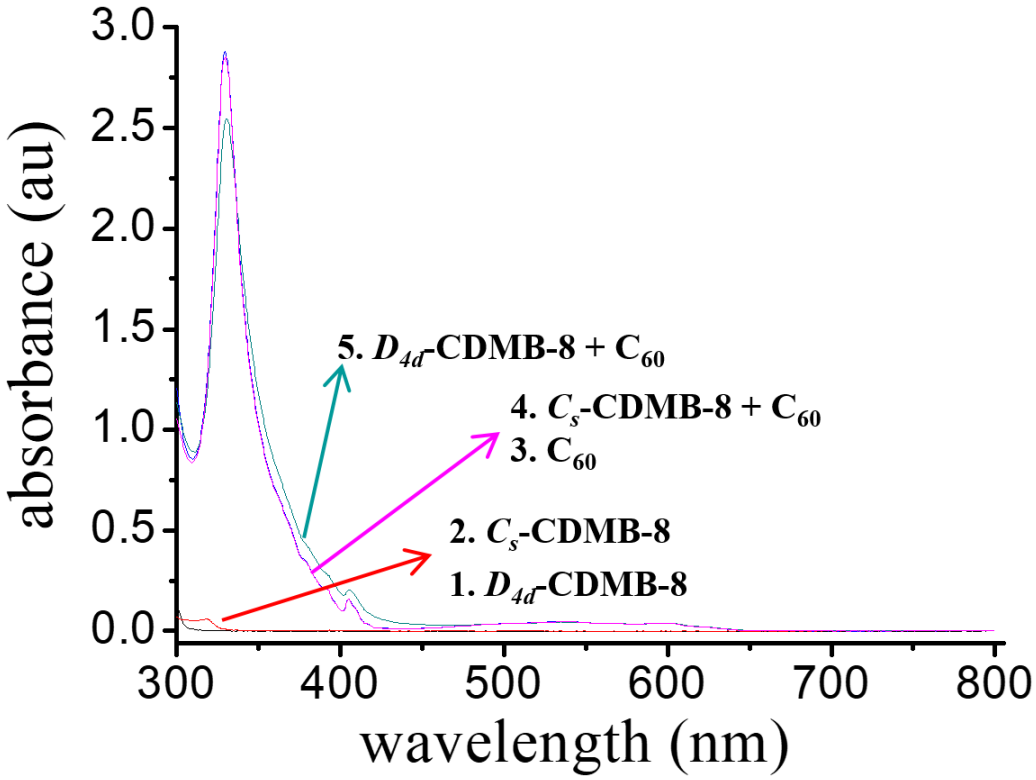

Figure S55. UV-vis spectra of ***D*$_{4d}$-CDMB-8** (black curve, 2.00×10^{-3} M), ***C*$_s$ -CDMB-8** (red curve, 2.00×10^{-3} M), C_{60} (pink curve, 1.00×10^{-4} M), the mixture of C_{60} (1.00×10^{-4} M) and 20 molar equiv. of ***C*$_s$-CDMB-8** (blue curve) and the mixture of C_{60} (1.00×10^{-4} M) and 20 molar equiv. of ***D*$_{4d}$-CDMB-8** (green curve) in TCE (detected in 1 cm optical path).

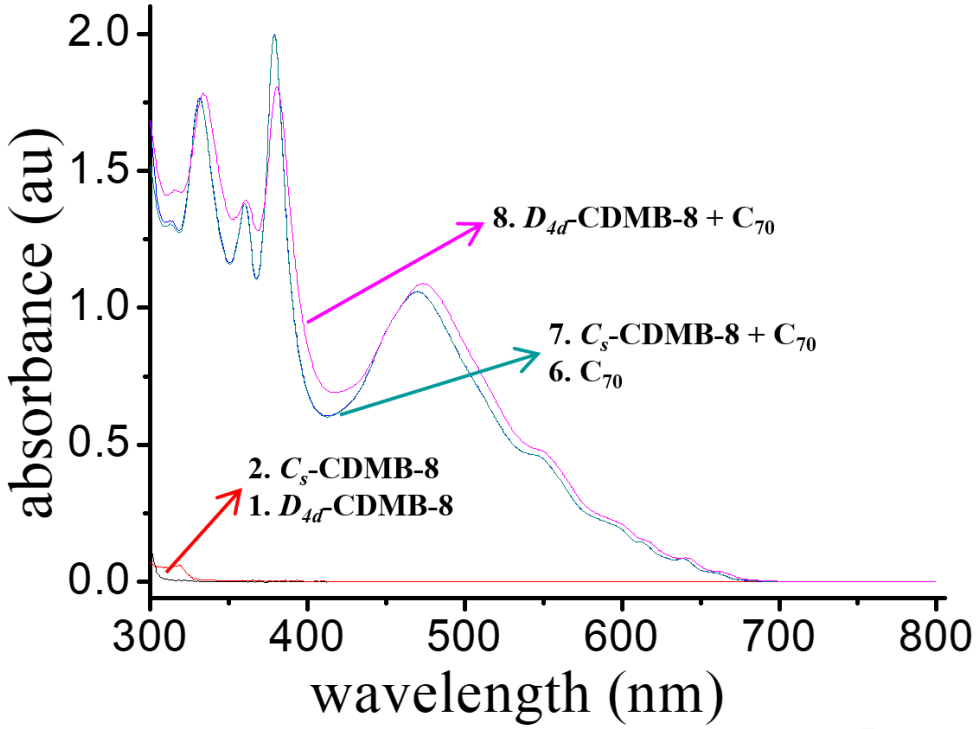

Figure S56. UV-vis spectra of ***D*$_{4d}$-CDMB-8** (black curve, 2.00 × 10^{-3} M), ***C*$_s$-CDMB-8** (red curve, 2.00 × 10^{-3} M), C_{70} (pink curve, 1.00 × 10^{-4} M), the mixture of C_{70} (1.00 × 10^{-4} M) and 20 molar equiv. of ***C*$_s$-CDMB-8** (blue curve) and the mixture of C_{70} (1.00 × 10^{-4} M) and 20 molar equiv. of ***D*$_{4d}$-CDMB-8** (green curve) in TCE (detected in 0.5 cm optical path).

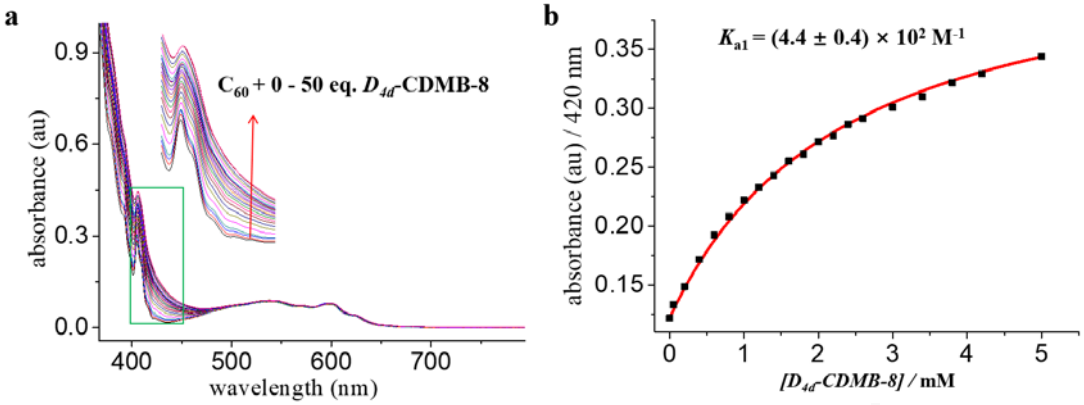

Figure S57. UV-vis spectroscopic titration of C_{60} (1.00 × 10^{-4} M) with the ***D*$_{4d}$-CDMB-8** in TCE (a) (detected in 1 cm optical path). UV-vis binding isotherms corresponding to the interaction between C_{60} and the ***D*$_{4d}$-CDMB-8** in TCE (b). The absorbance change at 420 nm was used to calculate the K_{a1} ((4.4 ± 0.4) × 10^2 M^{-1}) using the Hyperquad 2003 program[15, 16]. The red line shows the non-linear curve fit of the experimental data to the appropriate equation.

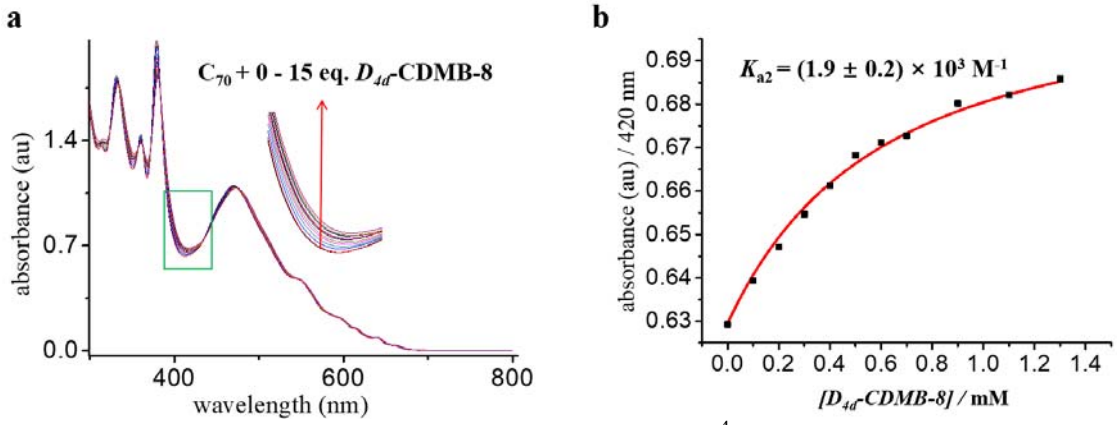

Figure S58. UV-vis spectroscopic titration of C_{70} (1.00×10^{-4} M) with the ***D*$_{4d}$-CDMB-8** in TCE (a) (detected in 0.5 cm optical path). UV-vis binding isotherms corresponding to the interaction between C_{70} and the ***D*$_{4d}$-CDMB-8** in TCE (b). The absorbance change at 420 nm was used to calculate the K_{a1} ($(1.9 \pm 0.2) \times 10^3$ M^{-1}) using the Hyperquad 2003 program[15, 16]. The red line shows the non-linear curve fit of the experimental data to the appropriate equation.

Single crystal X-ray structural studies of the complexes formed from *D*$_{4d}$-CDMB-8 and C_{60} or C_{70}.

Table S3. X-ray crystallographic data comparison of [***D*$_{4d}$-CDMB-8**⊃C_{60}•TCE] and [***D*$_{4d}$-CDMB-8**⊃C_{70}•$(TCE)_7$].

	[***D*$_{4d}$-CDMB-8**•C_{60}•TCE]	[***D*$_{4d}$-CDMB-8**•C_{70}•$(TCE)_7$]
CCDC No.	1820652	1820651
description	prism	prism
colour	red	red
from solution	$C_2H_2Cl_4$	$C_2H_2Cl_4$
empirical formula	$C_{126}H_{66}Cl_4$	$C_{148}H_{78}Cl_{28}$
Mr	1721.58	2848.70
crystal size (mm^3)	0.80 × 0.20 × 0.10	0.30 × 0.04 × 0.03
crystal system	orthorhombic	tetragonal
space group	Pca21	P4/nnc
a [Å]	44.4974(6)	23.643(5)
b [Å]	16.3918(2)	23.643(5)
c [Å]	22.3586(2)	12.250(2)
α [deg]	90.00	90.00(3)
β [deg]	90.00	90.00(3)
γ [deg]	90.00	90.00(3)
V / [Å^3]	16308.2(3)	6847(3)
d / [g/cm^3]	1.402	1.382
Z	8	2
T [K]	100(13)	100(2)
R1, wR2 $I > 2\acute{o}(I)$	0.1493, 0.3413	0.1343, 0.2753
R1, wR2 (all data)	0.1572, 0.3472	0.1851, 0.2881
quality of fit	1.022	1.146

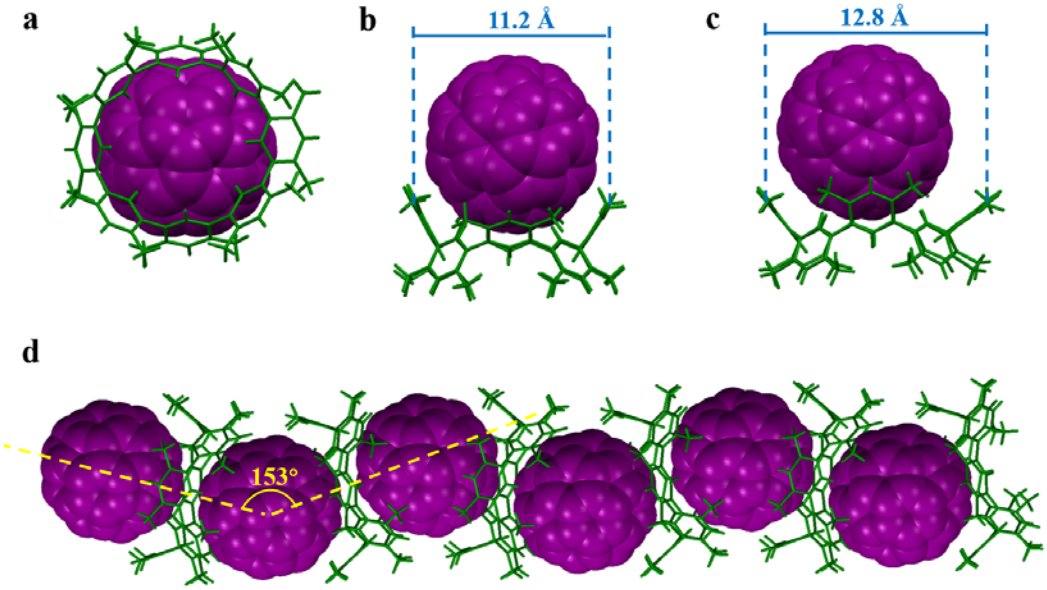

Figure S59. Single crystal X-ray structure of ***D*$_{4d}$-CDMB-8⊃C$_{60}$** which crystalize as [***D*$_{4d}$-CDMB-8**•C$_{60}$•TCE]. All solvent molecules have been omitted for clarity. Top view (a) and side views (b, c) of the monomeric complex of ***D*$_{4d}$-CDMB-8⊃C$_{60}$**. The extended 1D packing linear structure produced *via* self-assembly of monomeric complex of ***D*$_{4d}$-CDMB-8⊃C$_{60}$** (d).

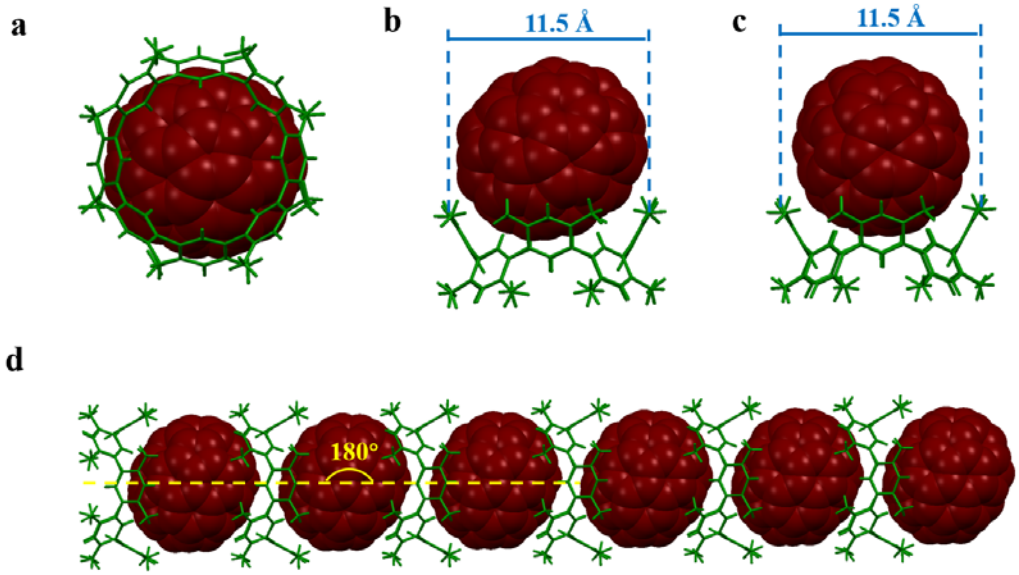

Figure S60. Single crystal X-ray structure of ***D*$_{4d}$-CDMB-8⊃C$_{70}$** which crystalize as [***D*$_{4d}$-CDMB-8**•C$_{70}$•(TCE)$_7$]. All solvent molecules have been omitted for clarity. Top view (a) and side views (b, c) of the monomeric complex of ***D*$_{4d}$-CDMB-8⊃C$_{70}$**. The extended 1D packing linear structure produced *via* self-assembly of monomeric complex of ***D*$_{4d}$-CDMB-8⊃C$_{70}$** (d).

Section S4: *Fullerene (C_{60} and/or C_{70}) purification from mixed C_{60}/C_{70} or carbon soot via adding* ***D_{4d}-CDMB-8***.

The purity of fullerene C_{60} or C_{70} was determined through HPLC analysis with Cosmosil-packed 5PBB analytical column (4.6 × 250 mm; mobile phase, toluene; UV detection, 329 nm; elution rate, 1 mL min^{-1}).

The molar radio between C_{60} and C_{70} [$\boldsymbol{n}(C_{60})/\boldsymbol{n}(C_{70})$] could be calculated from the peak integral area radio between C_{60} and C_{70} [$\boldsymbol{I}(C_{60})/\boldsymbol{I}(C_{70})$] of HPLC analysis by expression (*S-1*).

$$\frac{n(C_{60})}{n(C_{70})} = K\frac{I(C_{60})}{I(C_{70})} \quad \text{---------- } S\text{-}1$$

Where ***I***: peak integrated area radio from HPLC analysis, ***n***: amount of substance, ***K*** *is constant.*

On the basic of the diagram (Scheme S1), $\boldsymbol{L_1}$ ($\boldsymbol{n}(C_{60})/\boldsymbol{n}(C_{70})$ = 1:1) was detected as standard for further fullerene mixture determination (Figure S57). ***K*** was calculated as 0.75 from the HPLC analysis of $\boldsymbol{L_1}$.

The molar purity show in below was defined as expressions *S-2* and *S-3*.

$$C_{60}\% = \frac{n(C_{60})}{n(C_{60})+n(C_{70})}\times 100\% \quad \text{---------- } S\text{-}2$$

$$C_{70}\% = \frac{n(C_{70})}{n(C_{60})+n(C_{70})}\times 100\% \quad \text{---------- } S\text{-}3$$

The separation of the mixture of C_{60}/C_{70} (1:1 molar ratio) by ***D_{4d}*-CDMB-8** was show in Scheme S1. ***D_{4d}*-CDMB-8**, C_{60}, and C_{70} were dissolved in TCE to give a final solution that was 0.5 mM in each. The resulting mixture was allowed to sit on the bench for 48 h. This led to the formation of red-brown prismatic crystals. HPLC analysis of the crystals revealed a C_{60}/C_{70} molar ratio of roughly 9:92 (12:88 area%, Figure S64). When this precipitate was recrystallized in *o*-dichlorobenzene (*o*-DCB)/*n*-hexane (1:5, *v*/*v*), a corresponding HPLC analysis revealed the purified product with a C_{60}/C_{70} molar ratio of < 1:99 (Figure S65). Dissolving this purified complex, ***D_{4d}*-CDMB-8⊃C_{70}**, in a mixture of CS_2 and toluene containing excess S_8 yielded C_{70} •$2S_8$[17], which could be converted to pure C_{70} (purity > 99%, molar yield = 43%) (Figure S66) *via* sublimation at 423 K for 3 hours under vacuum (2.0 kPa). Moreover, the solution remaining after

the precipitation step, which is enriched in C_{60}, may be treated with additional ***D*$_{4d}$-CDMB-8** to remove additional C_{70}. In this way, C_{60} with a purity exceeding 99% (Figure S67) could be obtained in approximately 39% molar yield after removing the solvent and further purification in *o*-DCB/THF (1:5, *v*/*v*). The receptor itself was obtained in high purity following decomplexation, allowing it to be recycled and reused if so desired.

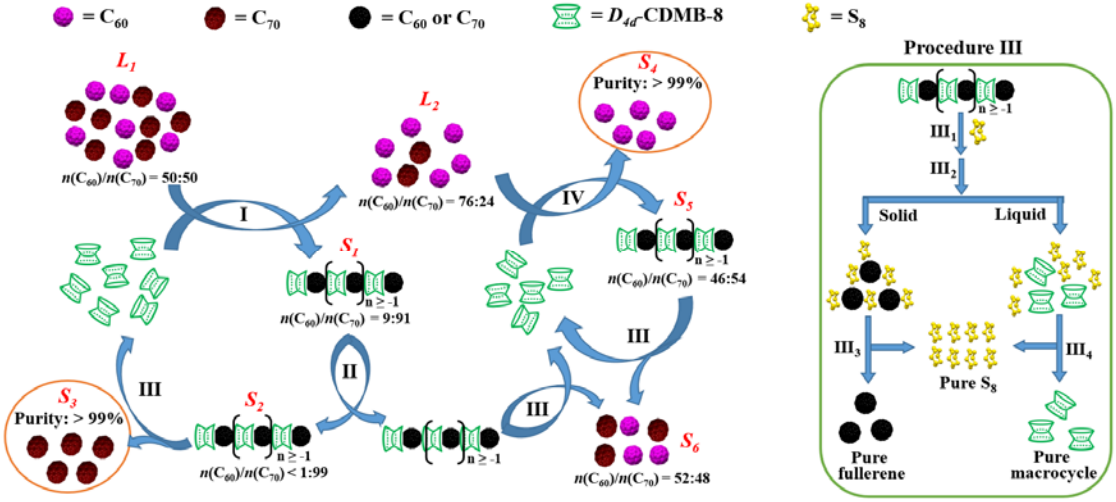

Scheme S1. Separation of C_{60} and C_{70} from their mixture (***n***(C_{60})/***n***(C_{70}) = 1:1) using macrocycle ***D*$_{4d}$-CDMB-8**. Procedure: **I**, C_{60}, C_{70} (1.0 molar equiv.), ***D*$_{4d}$-CDMB-8** (1.0 molar equiv.), TCE, rt, 48 h, solid-liquid separation; **II**, recrystallization from *o*-dichlorobenzene (*o*-DCB)/*n*-hexane (1:5, *v*/*v*); **III**, the decomposition of the complexes between ***D*$_{4d}$-CDMB-8** and fullerene(s) (**III$_1$,** complexes (***D*$_{4d}$-CDMB-8**⊃C_{60} and/or ***D*$_{4d}$-CDMB-8**⊃C_{70}), CS_2, S_8 (excess); **III$_2$,** toluene, CS_2 removement, solid-liquid separation; **III$_3$,** sublimation; **III$_4$,** toluene removement, sublimation.); **IV**, ***D*$_{4d}$-CDMB-8** (0.5 molar equiv.) was added in the supernatant after Step **I**, rt, 48 h, solid-liquid separation, remove TCE, and further purification in *o*-DCB/THF (1:5, *v*/*v*).

L*$_1$**: C_{60} (72 mg, 0.10 mmol) and C_{70} (84 mg, 0.10 mmol) were dissolved in 200 mL TCE, with ***I(C_{60})/***I***(C_{70}) = 57:43 in HPLC analysis (Figure S57).

L*$_1$**→(S*$_1$** and ***L*$_2$**): ***D*$_{4d}$-CDMB-8** (83 mg, 0.10 mmol) was added into solution ***L*$_1$** for standing at room temperature. After 48 h, red-brown prismatic crystals ***S*$_1$** were cultivated. Filter, the residue was washed with 5 mL THF to obtain ***S*$_1$** (154 mg), with ***n***(C_{60})/***n***(C_{70}) = 9:91 (***I***(C_{60})/***I***(C_{70}) = 12:88, Figure S60). The filtrate ***L*$_2$** with ***n***(C_{60})/***n***(C_{70}) = 76:24 (***I***(C_{60})/***I***(C_{70}) = 81:19, Figure S58).

S₁*→*S₂: 154 mg ***S₁*** was dissolved in 30 mL *o*-DCB and pour into 150 ml *n*-hexane, red-brown prismatic crystals were obtained immediately. Filter, the residue was washed with 5 mL THF to obtain ***S₂*** (72 mg), with ***n***(C_{60})/***n***(C_{70}) < 1:99 (***I***(C_{60})/***I***(C_{70}) = 1:99, Figure S61). The filtrate containing C_{60}, C_{70} and ***D₄d*-CDMB-8** was collected together for further recycle of fullerenes and macrocycle.

S₂*→*S₃: 72 mg ***S₂*** was dissolved in 30 mL CS_2. Then 360 mg S_8 was added into the solution. Pour this mixture into 30 mL toluene to produce a red-brown solution. After remove CS_2 *via* rotary evaporation, bulk of red-brown crystals C_{70}•$2S_8$ were observed with the colour change of the solution (from red-brown to light yellow). Collected the solid, removed S_8 *via* sublimation at 423 K for 3 hours under vacuum (2.0 kPa) to obtain ***S₃*** as a dark solid (C_{70}, 36 mg, 43%), with ***n***(C_{60})/***n***(C_{70}) < 1:99 (***I***(C_{60})/***I***(C_{70}) = 1:99, Figure S62). ^{1}H NMR and X-ray photoelectron spectroscopy (XPS) analysis revealed that no ***D₄d*-CDMB-8** and S_8 were detected in ***S₃*** (Figure S79), ^{13}C NMR revealed C_{70} (***S₃***) with high purity (Figure S77). The filtrate was collected for further recycle of ***D₄d*-CDMB-8** and S_8.

L₂*→(*S₄* and *S₅*)**: ***D₄d*-CDMB-8** (42 mg, 0.05 mmol) was added into ***L₂ and then standing at room temperature for 48 h, red-brown prismatic crystals ***S₅*** were created. Filter, the solid was washed with 5 mL THF to give out ***S₅*** (83 mg), with ***n***(C_{60})/***n***(C_{70}) = 46:54 (***I***(C_{60})/***I***(C_{70}) = 53:47, Figure S64). The filtrate ***L₃***, with ***n***(C_{60})/***n***(C_{70}) = 96:4 (***I***(C_{60})/***I***(C_{70}) = 97:3, Figure S59). Removed the solvent of ***L₃*** *via* rotary evaporation, the resulting residue dissolved in 20 mL *o*-DCB and pour into 100 mL THF to obtain a red-brown solution. Stewing this solution at room temperature for 12 h, bulk of red-brown crystals were observed with the colour change of the solution (from red-brown to purple). Filter, and collected the solid for further recycle of C_{60}, C_{70} and ***D₄d*-CDMB-8**. Removed the solution of the filtrate *via* rotary evaporation to obtain ***S₄*** as a dark solid (28 mg, 39%), with ***n***(C_{60})/***n***(C_{70}) > 99:1 (***I***(C_{60})/***I***(C_{70}) > 99:1, Figure S63). ^{1}H NMR and X-ray photoelectron spectroscopy (XPS) analysis revealed that no ***D₄d*-CDMB-8** and S_8 were detected in ***S₄*** (Figure S80). ^{13}C NMR revealed C_{60} (***S₄***) with high purity (Figure S78).

The recycle of mix solid C_{60} and C_{70} (*S₆*): All the mix compounds between C_{60}, C_{70} and ***D₄d*-CDMB-8** were combined and then treated with same procedure of ***S₂*→*S₃***. This afforded 81

mg ***S6***, as a dark solid, with ***n***(C_{60})/***n***(C_{70}) = 52:48 (***I***(C_{60})/***I***(C_{70}) = 59:41, Figure S65), recycle yield: C_{60} (54%), C_{70} (50%).

The recycle of *D_{4d}*-CDMB-8: Collecting all the mixture solution of ***D_{4d}*-CDMB-8** and S_8, remove the solvent *via* rotary evaporation, and S_8 was separated *via* sublimation at 423 K for 3 hours under vacuum (2.0 kPa). The residue solid was recrystallization in CH_2Cl_2/CH_3CN (1:1, *v*/*v*) to afford pure ***D_{4d}*-CDMB-8** (115 mg, recycle yield: 92%).

Further C_{60} purification and higher fullerenes extraction from carbon soot were achieved *via* using ***D_{4d}*-CDMB-8** (Scheme S2).

The peak intergrade area purity (area%) of C_{60} show in below was defined as expression *S-4*.

$$C_{60}\ \text{area\%} = \frac{I(C_{60})}{I(C_{60})+I(C_{70})} \times 100\ \text{area\%} \quad \text{---------- } S\text{-}4$$

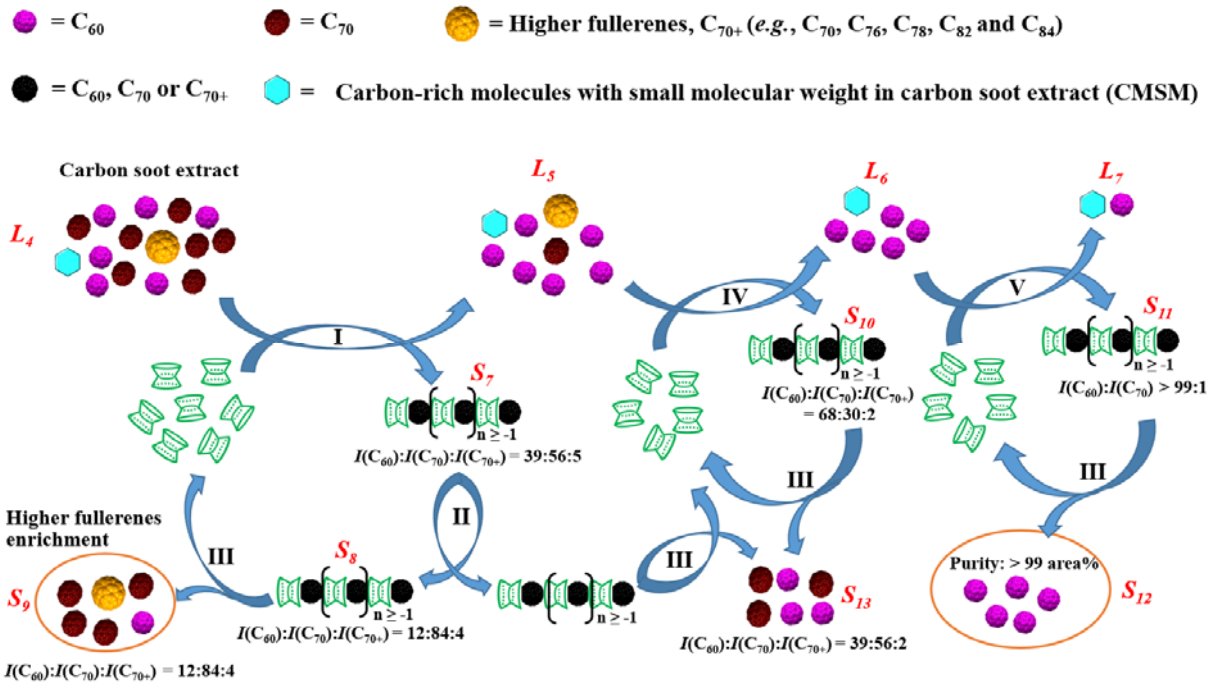

Scheme S2. Separation of C_{60} and higher fullerenes extraction from carbon soot using macrocycle ***D_{4d}*-CDMB-8.** Procedure: **I**, Carbon soot extract (200 mg), ***D_{4d}*-CDMB-8** (42 mg,

0.05 mmol), TCE, rt, 48 h, solid-liquid separation; **II**, recrystallization from *o*-DCB/*n*-hexane (1:5, *v*/*v*); **III**, the decomposition of the complexes between ***D*$_{4d}$-CDMB-8** and fullerene(s) as step **III** in Scheme S1; **IV**, ***D*$_{4d}$-CDMB-8** (42 mg, 0.05 mmol) was added in the supernatant (***L*$_5$**) after Step **I**, rt, 48 h, solid-liquid separation; **V**, ***D*$_{4d}$-CDMB-8** (62 mg, 0.07mmol) was added in the supernatant (***L*$_6$**) after Step **IV**, remove half of TCE, rt, 48 h, solid-liquid separation.

The preparation of carbon soot extract: 5.0 g carbon soot was added in Soxhlet extractor, and 200 mL toluene was used for its extraction. After reflux for 12 hours, remove toluene to obtain carbon soot extract as a dark solid (0.65 g, 13 wt%).

L*$_4$**: 200 mg carbon soot extract was dissolved in 50 mL TCE, the purity revealed as ***I(CMSM):***I***(C_{60}):***I***(C_{70}):***I***(C_{70+}) = 13:70:16:1 (Figure S66).

L*$_4$**→(S*$_7$** and ***L*$_5$**): ***D*$_{4d}$-CDMB-8** (42 mg, 0.05 mmol) was added into ***L*$_3$** to sit on the bench at room temperature. After 48 h, red-brown prismatic crystals ***S*$_7$** were created. Filter, wash with 5 mL THF, ***S*$_7$** (84 mg) was collected with ***I***(C_{60}):***I***(C_{70}):***I***(C_{70+}) = 39:56:5 (Figure S70). The filtrate ***L*$_5$** was characterized as ***I***(CMSM):***I***(C_{60}):***I***(C_{70}):***I***(C_{70+}) = 17:76:5:2 (Figure S67).

S*$_7$**→S*$_8$**: Similar with the procedure from ***S*$_1$**→***S*$_2$**, 84 mg ***S*$_7$** was recrystallization from *o*-DCB/*n*-hexane (1:5, *v*/*v*) to obtain ***S*$_8$** as a red-brown prismatic crystals (40 mg), with ***I***(C_{60}):***I***(C_{70}):***I***(C_{70+}) = 12:84:4 (Figure S71).

S*$_8$**→S*$_9$**: Analogue procedure as ***S*$_2$**→***S*$_3$** was carried out. 40 mg ***S*$_2$** was breakup by adding 200 mg S_8 to obtained ***S*$_9$** as a dark solid (19 mg, 9.5 wt%) with ***I***(C_{60}):***I***(C_{70}):***I***(C_{70+}) = 12:84:4 (Figure S72).

L*$_5$**→(S*$_{10}$** and ***L*$_6$**): Dissolve ***D*$_{4d}$-CDMB-8** (42 mg, 0.05 mmol) into ***L*$_5$**, and then to sit on the bench at room temperature for 48 h. Red-brown prismatic crystals ***S*$_{10}$** (74 mg) were collected after filtered and washed with 5 mL THF, which components include ***I***(C_{60}):***I***(C_{70}):***I***(C_{70+}) = 68:30:2 (Figure S73). The filtrate ***L*$_6$** was analyzed with ***I***(CMSM):***I***(C_{60}):***I***(C_{70}) = 19:80:1 (Figure S68)

L*$_6$→(*S*$_{11}$ and *L*$_7$)**: ***D*$_{4d}$-CDMB-8** (62 mg, 0.07 mmol) was added into ***L*$_6$**. Remove half of TCE, and keep the solution standing at room temperature. After 48 h, red-brown prismatic crystals ***S*$_{11}$** (161 mg) were obtained after filtered and washed with 5 mL THF, with ***I(C_{60}):***I***(C_{70}) > 99:1 (Figure S74). The filtrate ***L*$_7$** was detected with ***I***(CMSM):***I***(C_{60}) = 70:30 (Figure S69).

S*$_{11}$→*S*$_{12}$**: As the procedure of ***S*$_2$→*S*$_3$**, 161 mg ***S*$_{11}$** was breakup by adding 800 mg S_8 to obtain ***S*$_{12}$** as a dark solid (70 mg, 35 wt%), with ***I(C_{60}):***I***(C_{70}) > 99:1 (Figure S75). ^{1}H NMR and X-ray photoelectron spectroscopy (XPS) analysis revealed that no ***D*$_{4d}$-CDMB-8** and S_8 were detected in ***S*$_{12}$** (Figure S78). ^{13}C NMR revealed C_{60} (***S*$_{12}$**) with high purity (Figure S81).

The recycle of fullerenes (***S*$_{13}$**): All the mix compounds containing fullerenes and ***D*$_{4d}$-CDMB-8** were treated with same procedure of ***S*$_2$→*S*$_3$**. This afforded 50 mg ***S*$_{13}$** as a dark solid, with ***I***(C_{60}):***I***(C_{70}):***I***(C_{70+}) = 77:21:2 (Figure S76), recycle yield: 25 wt%.

The recycle of *D*$_{4d}$-CDMB-8: Collecting all the mixture solution of containing ***D*$_{4d}$-CDMB-8** and S_8, remove the solvent *via* rotary evaporation, and pure S_8 could be recycled *via* sublimation at 423 K for 3 hours under vacuum (2.0 kPa). Meanwhile the residue solid was recrystallization in CH_2Cl_2/CH_3CN (1:1, *v*/*v*) to afford pure ***D*$_{4d}$-CDMB-8** (136 mg, recycle yield: 93%).

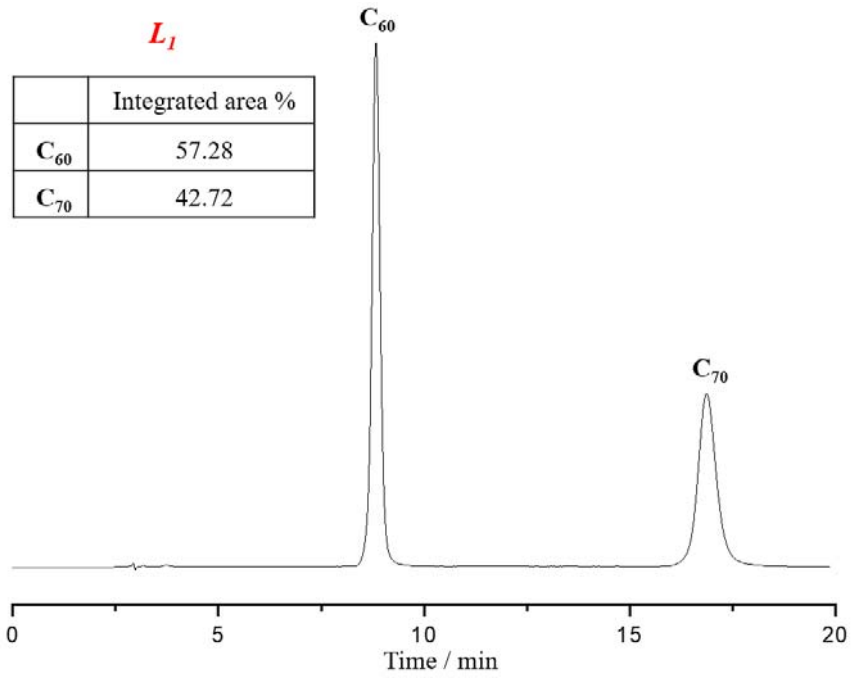

Figure S61. HPLC analysis of ***L*$_1$**.

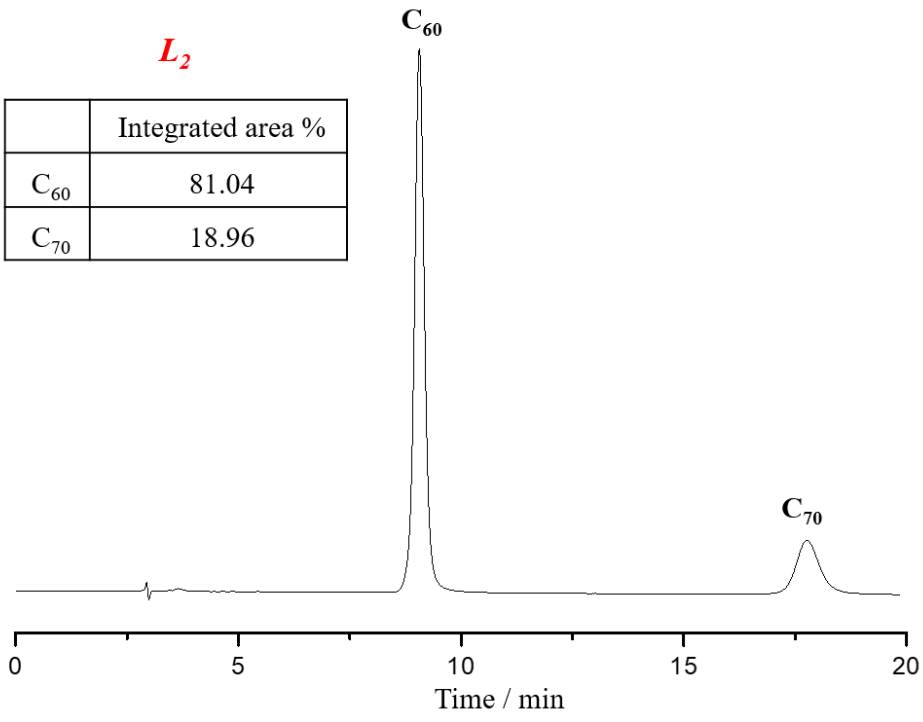

Figure S62. HPLC analysis of ***L*$_2$**.

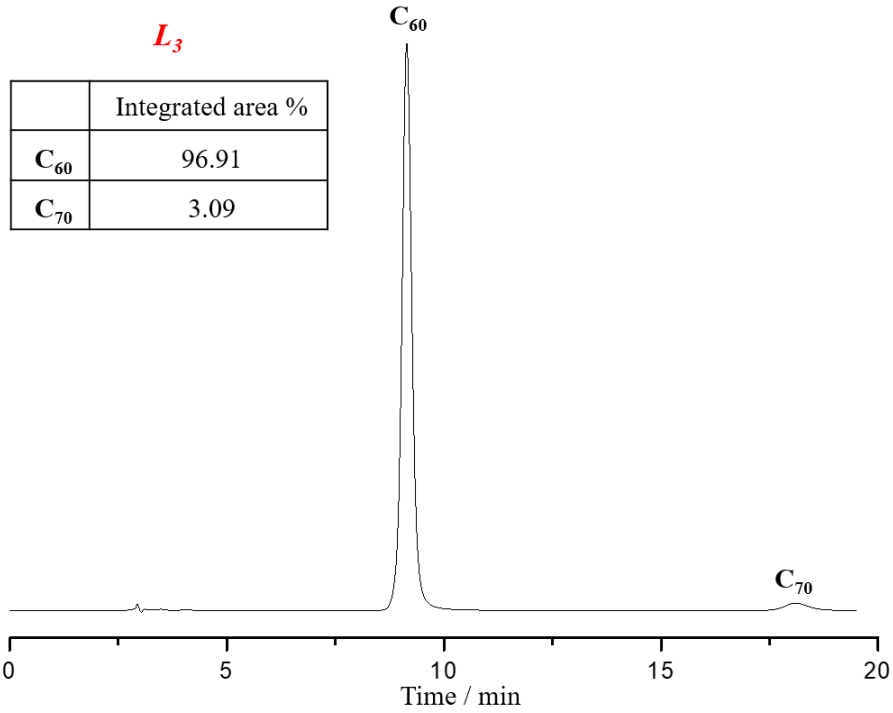

Figure S63. HPLC analysis of ***L*$_3$**.

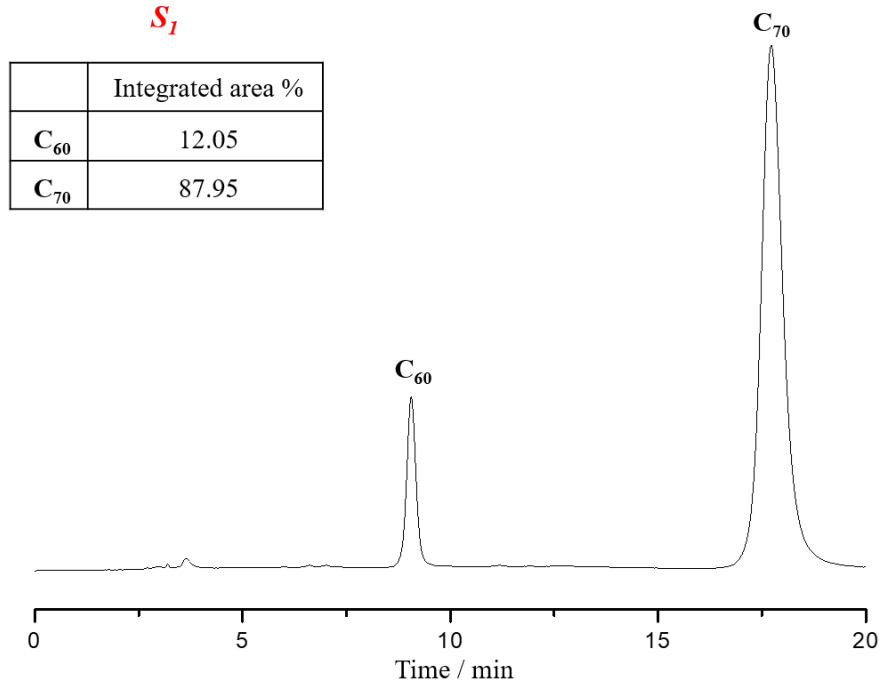

Figure S64. HPLC analysis of ***S*$_1$**.

***S*$_2$**

	Integrated area %
C_{60}	1.35
C_{70}	98.65

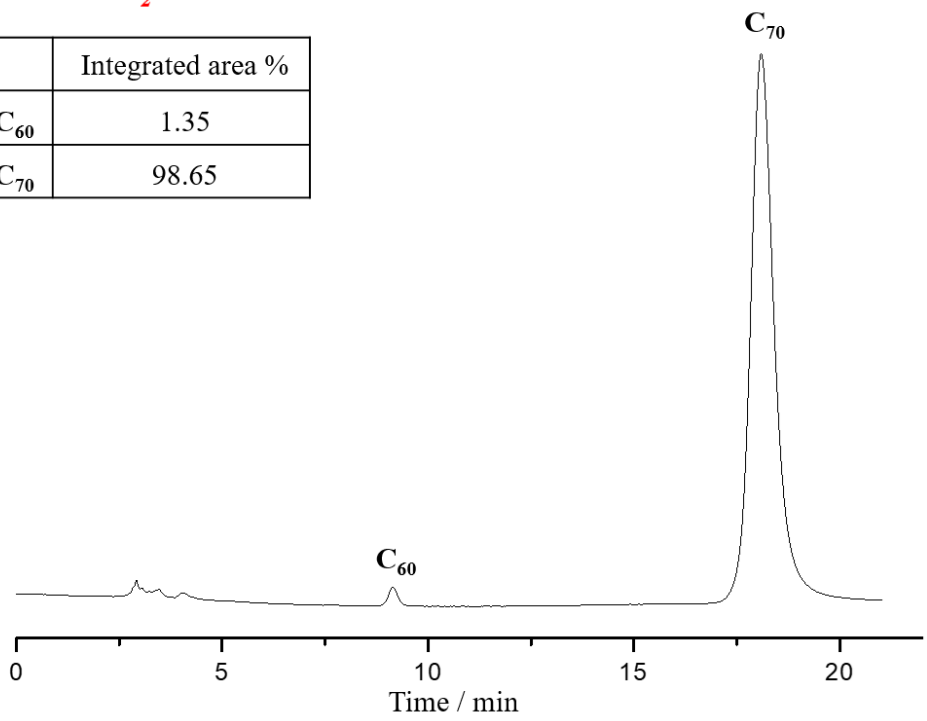

Figure S65. HPLC analysis of ***S*$_2$**.

***S*$_3$**

	Integrated area %
C_{60}	1.19
C_{70}	98.81

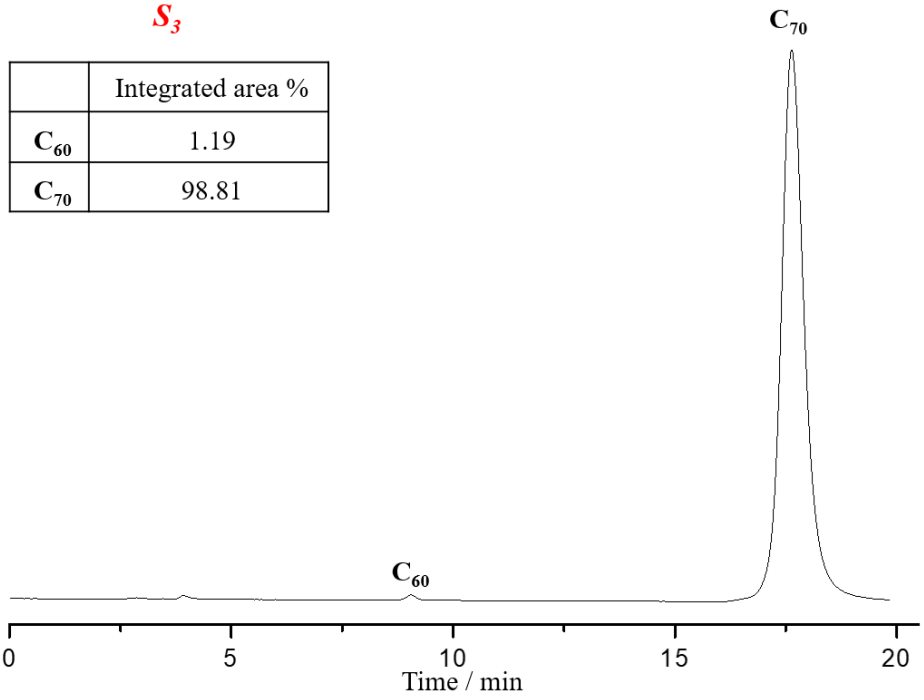

Figure S66. HPLC analysis of ***S*$_3$**.

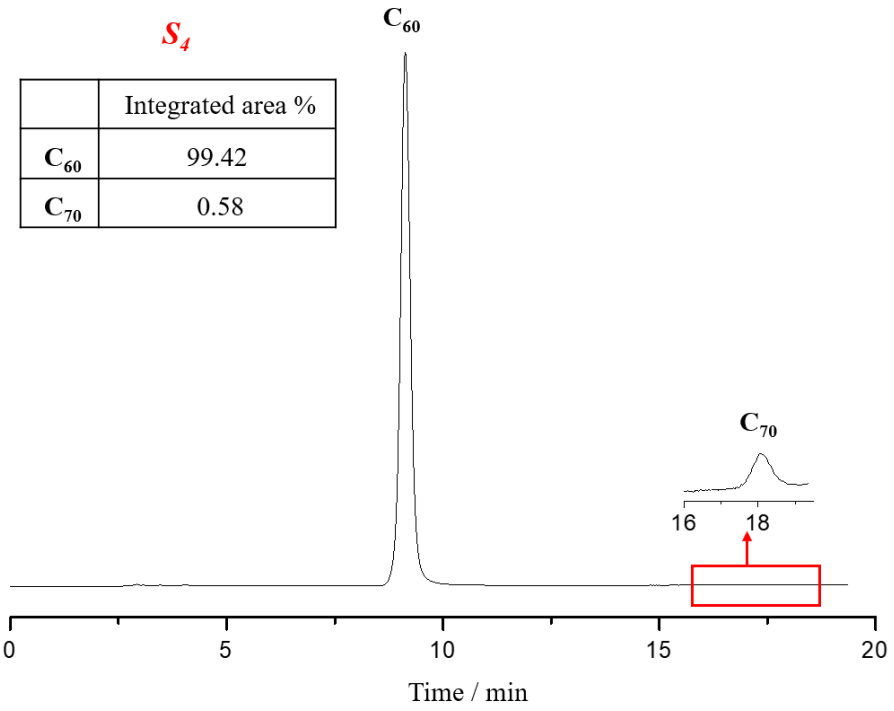

Figure S67. HPLC analysis of ***S*$_4$**.

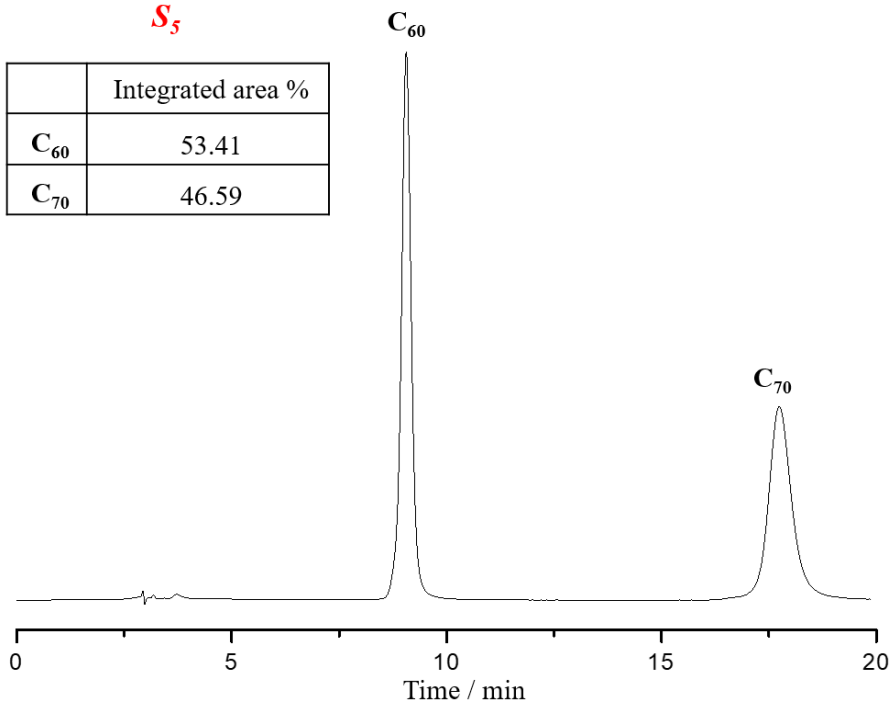

Figure S68. HPLC analysis of ***S*$_5$**.

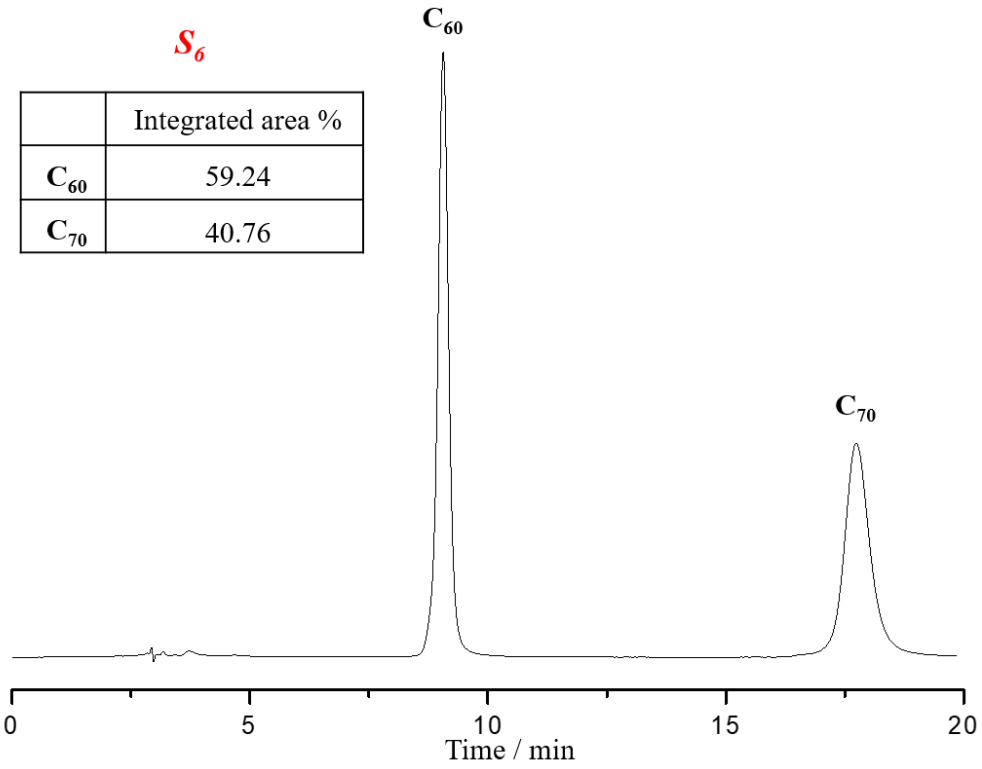

	Integrated area %
C_{60}	59.24
C_{70}	40.76

Figure S69. HPLC analysis of ***S*$_6$**.

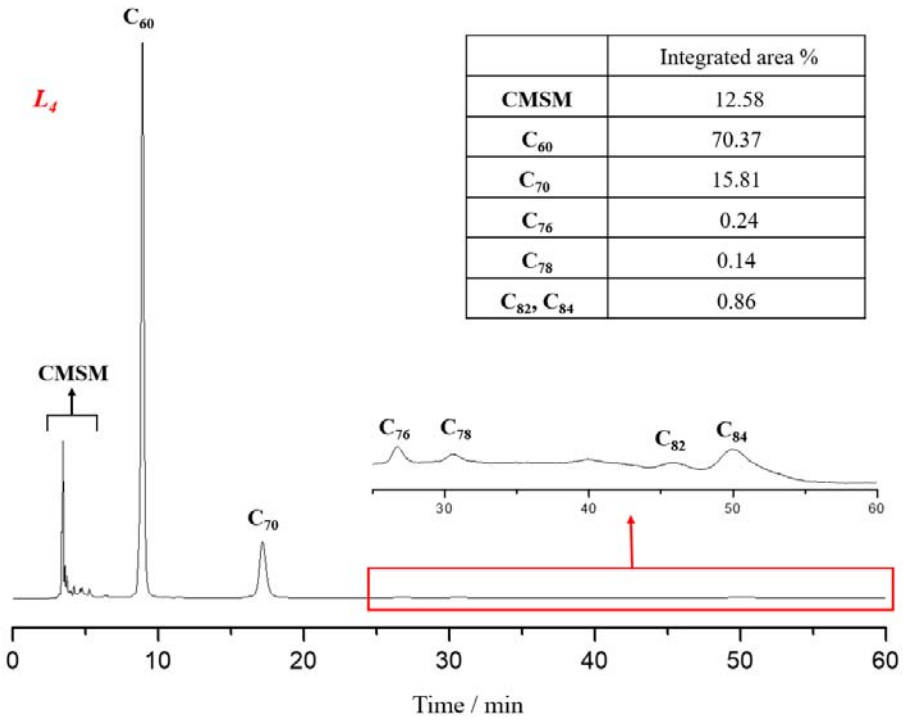

	Integrated area %
CMSM	12.58
C_{60}	70.37
C_{70}	15.81
C_{76}	0.24
C_{78}	0.14
C_{82}, C_{84}	0.86

Figure S70. HPLC analysis of ***L*$_4$**[19-20].

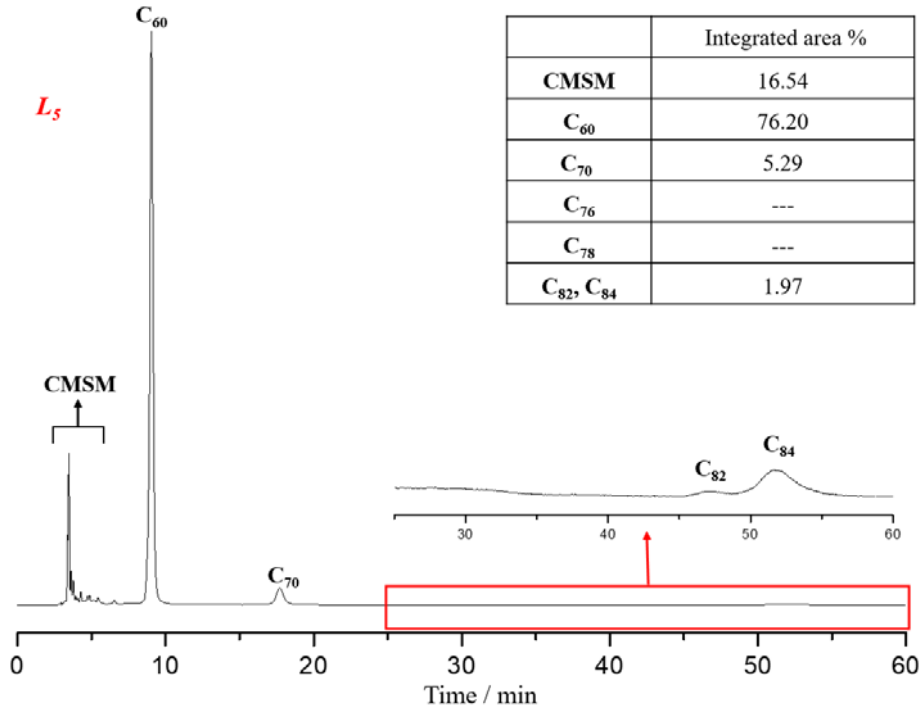

	Integrated area %
CMSM	16.54
C_{60}	76.20
C_{70}	5.29
C_{76}	---
C_{78}	---
C_{82}, C_{84}	1.97

Figure S71. HPLC analysis of ***L*$_5$**.

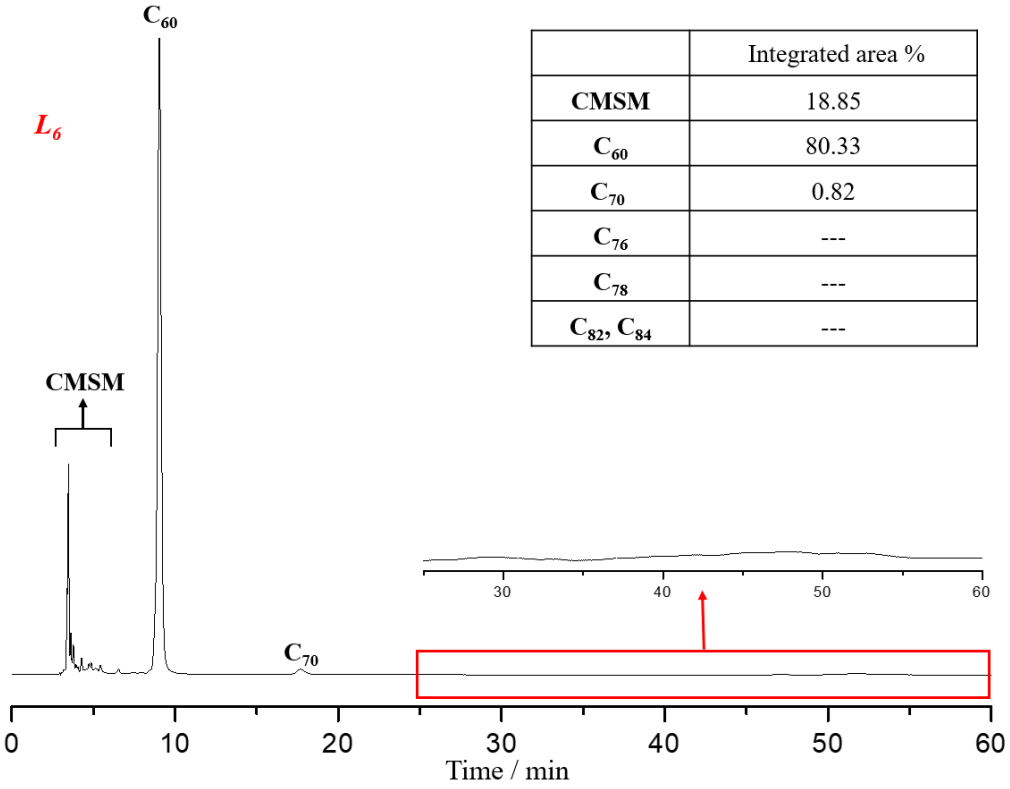

	Integrated area %
CMSM	18.85
C_{60}	80.33
C_{70}	0.82
C_{76}	---
C_{78}	---
C_{82}, C_{84}	---

Figure S72. HPLC analysis of ***L*$_6$**.

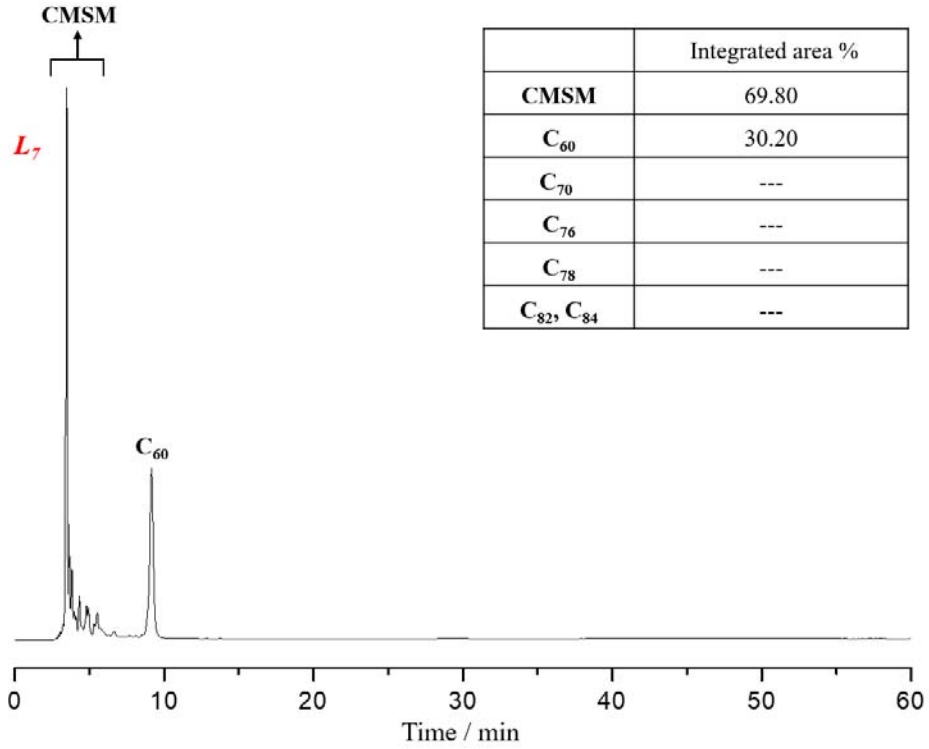

	Integrated area %
CMSM	69.80
C_{60}	30.20
C_{70}	---
C_{76}	---
C_{78}	---
C_{82}, C_{84}	---

Figure S73. HPLC analysis of ***L*$_7$**.

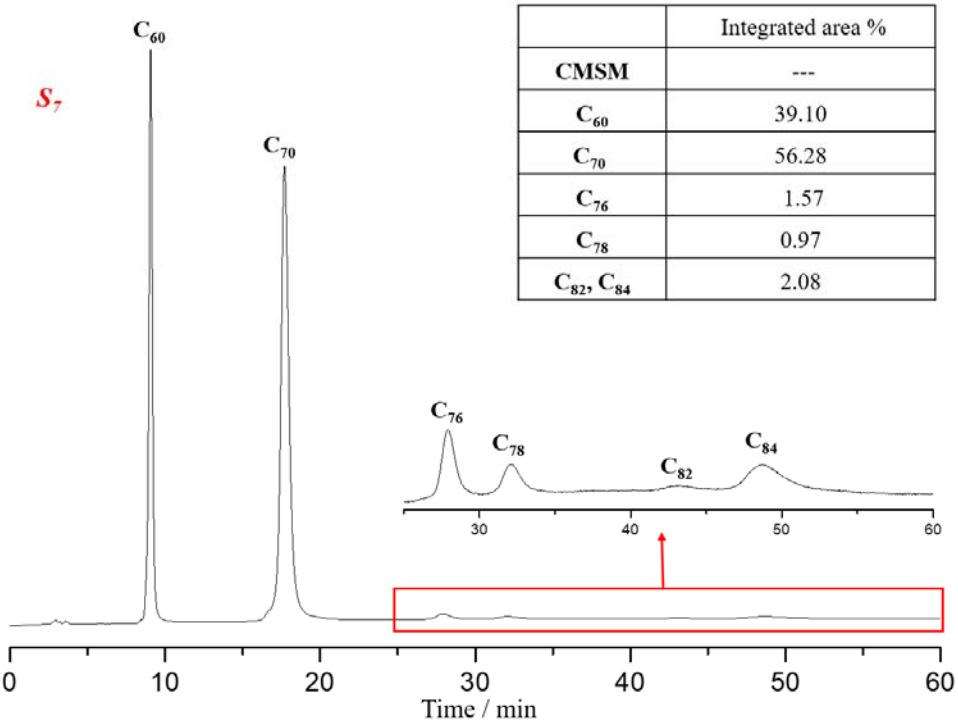

	Integrated area %
CMSM	---
C_{60}	39.10
C_{70}	56.28
C_{76}	1.57
C_{78}	0.97
C_{82}, C_{84}	2.08

Figure S74. HPLC analysis of ***S*$_7$**.

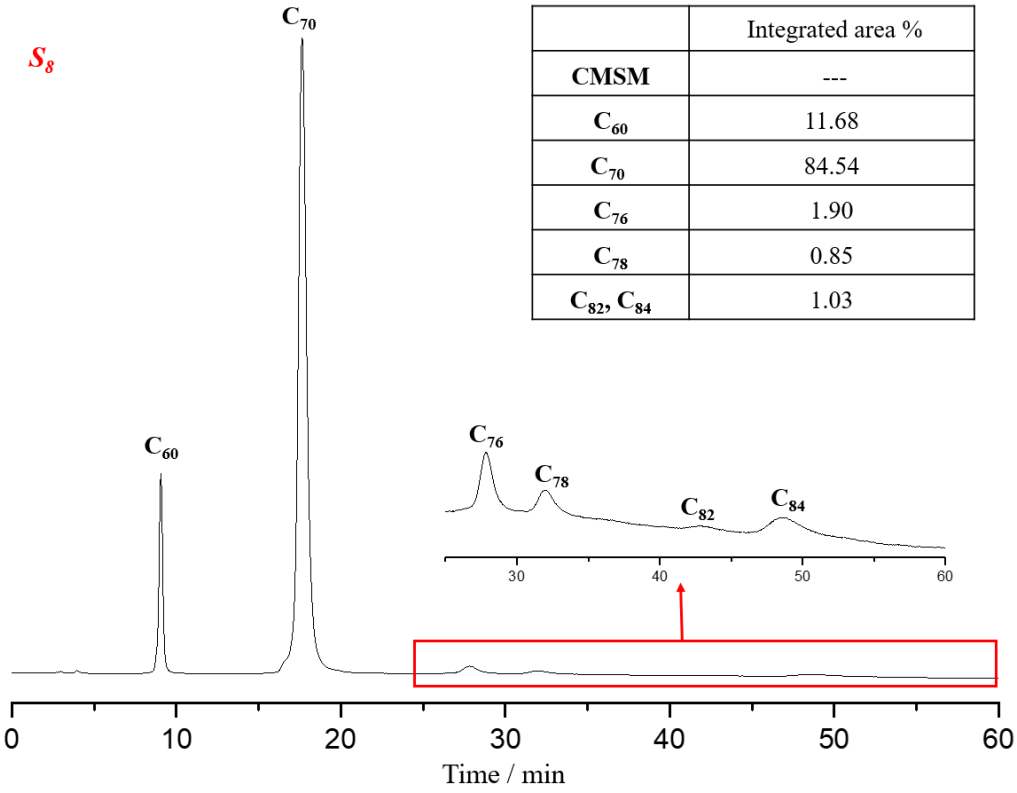

	Integrated area %
CMSM	---
C_{60}	11.68
C_{70}	84.54
C_{76}	1.90
C_{78}	0.85
C_{82}, C_{84}	1.03

Figure S75. HPLC analysis of ***S8***.

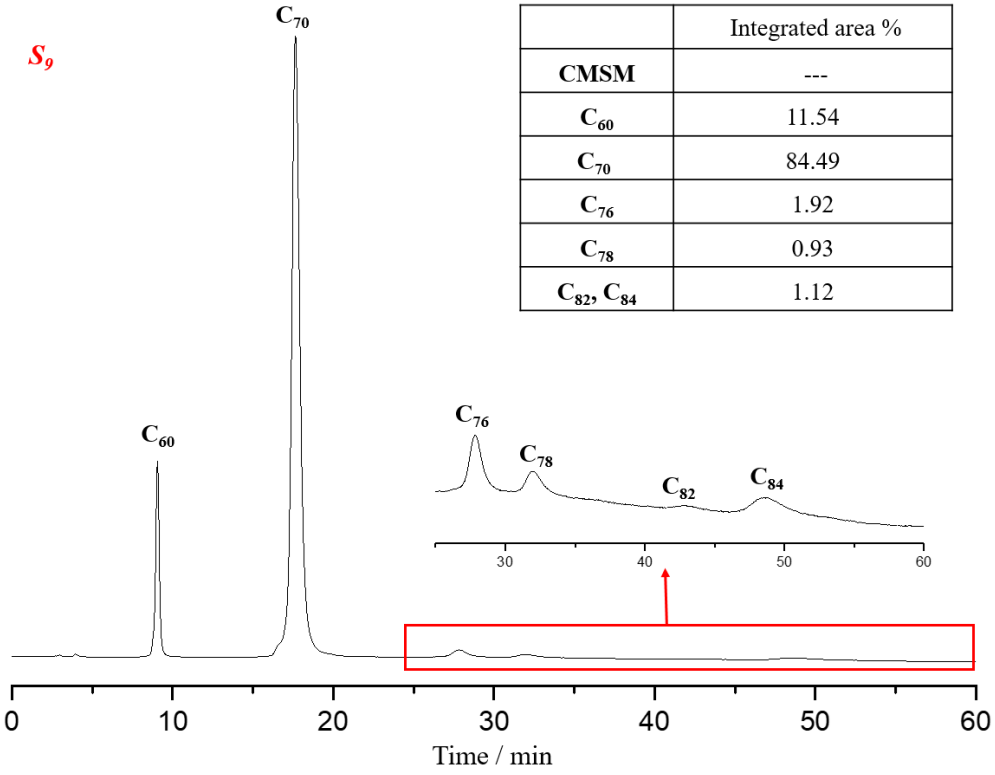

	Integrated area %
CMSM	---
C_{60}	11.54
C_{70}	84.49
C_{76}	1.92
C_{78}	0.93
C_{82}, C_{84}	1.12

Figure S76. HPLC analysis of ***S*$_9$**.

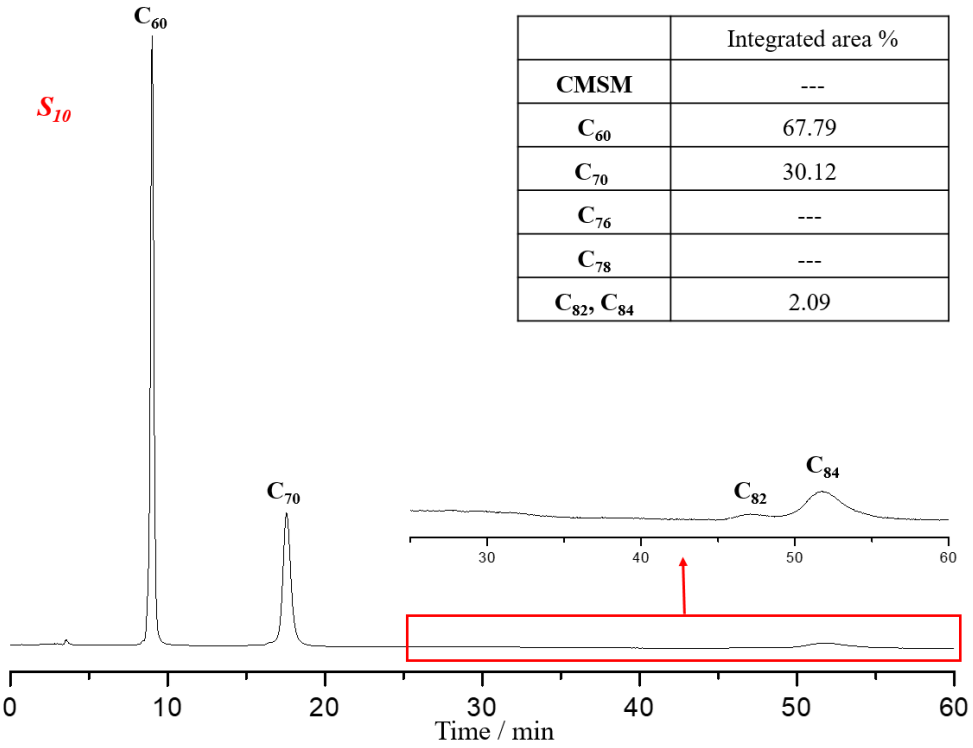

	Integrated area %
CMSM	---
C_{60}	67.79
C_{70}	30.12
C_{76}	---
C_{78}	---
C_{82}, C_{84}	2.09

Figure S77. HPLC analysis of ***S*$_{10}$**.

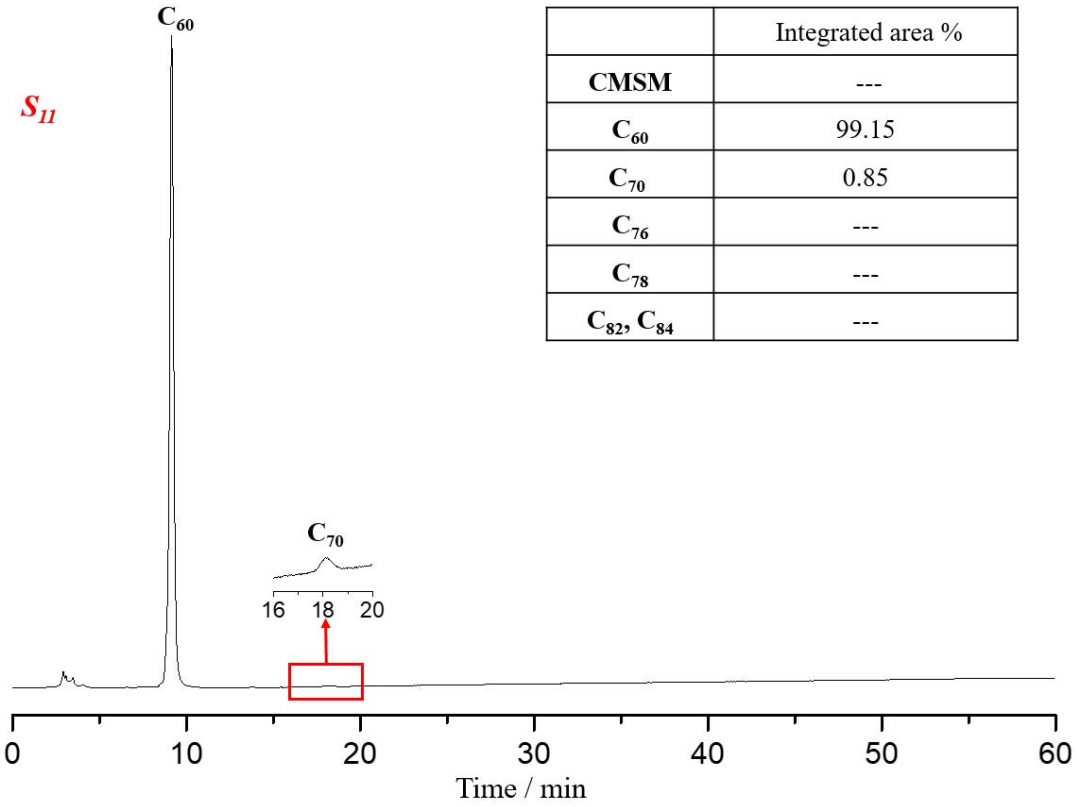

	Integrated area %
CMSM	---
C_{60}	99.15
C_{70}	0.85
C_{76}	---
C_{78}	---
C_{82}, C_{84}	---

Figure S78. HPLC analysis of ***S*$_{11}$**.

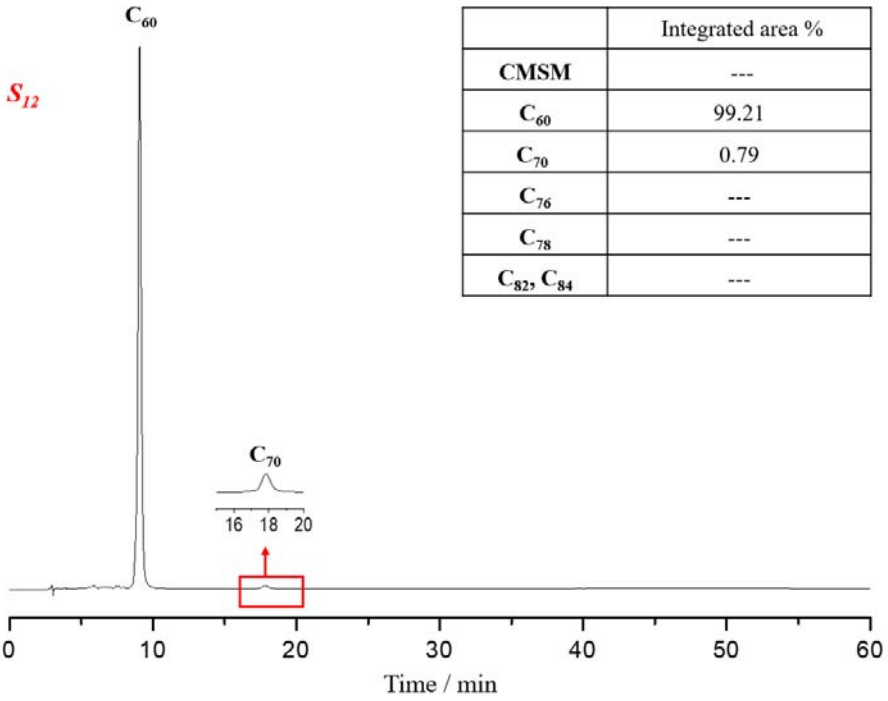

	Integrated area %
CMSM	---
C_{60}	99.21
C_{70}	0.79
C_{76}	---
C_{78}	---
C_{82}, C_{84}	---

Figure S79. HPLC analysis of ***S*$_{12}$**.

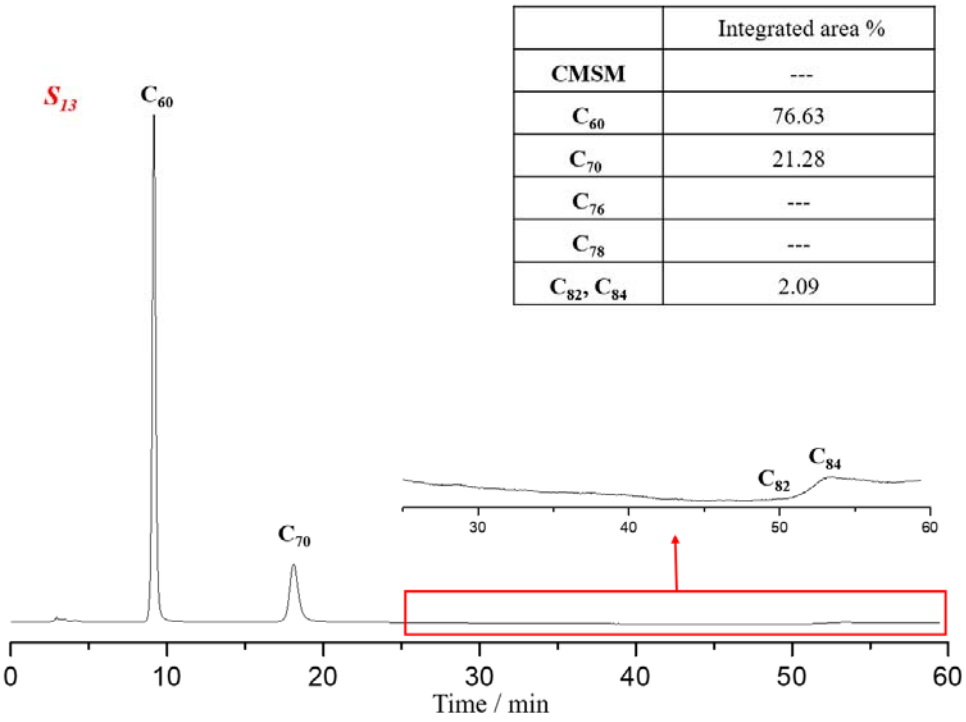

	Integrated area %
CMSM	---
C_{60}	76.63
C_{70}	21.28
C_{76}	---
C_{78}	---
C_{82}, C_{84}	2.09

Figure S80. HPLC analysis of ***S*$_{13}$**.

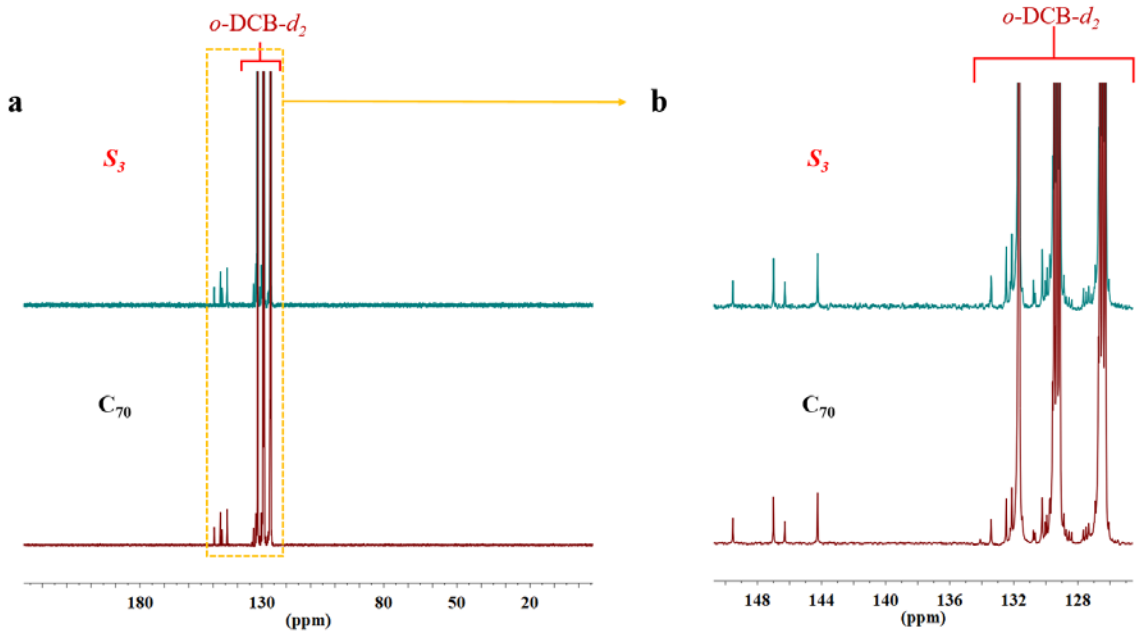

Figure S81. Full view (a) and expanded view (b) ^{13}C NMR spectra of C_{70} and ***S*$_4$** (5.00 mg/mL) in *o*-DCB-d_2 at 298 K (150 MHz).

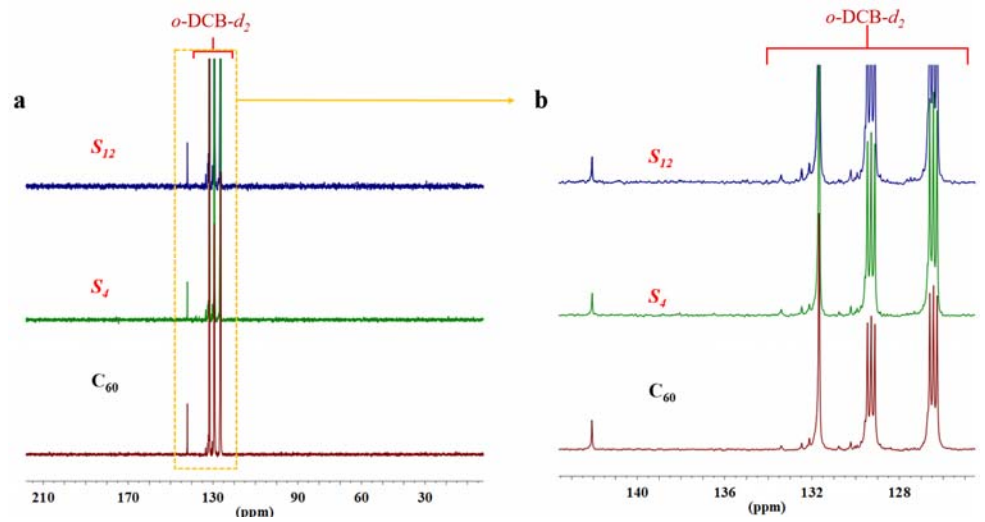

Figure S82. Full view (a) and expanded view (b) of ^{13}C NMR spectra of C_{60}, ***S4*** and ***S12*** (5.00 mg/mL) in *o*-DCB-d_2 at 298 K (150 MHz).

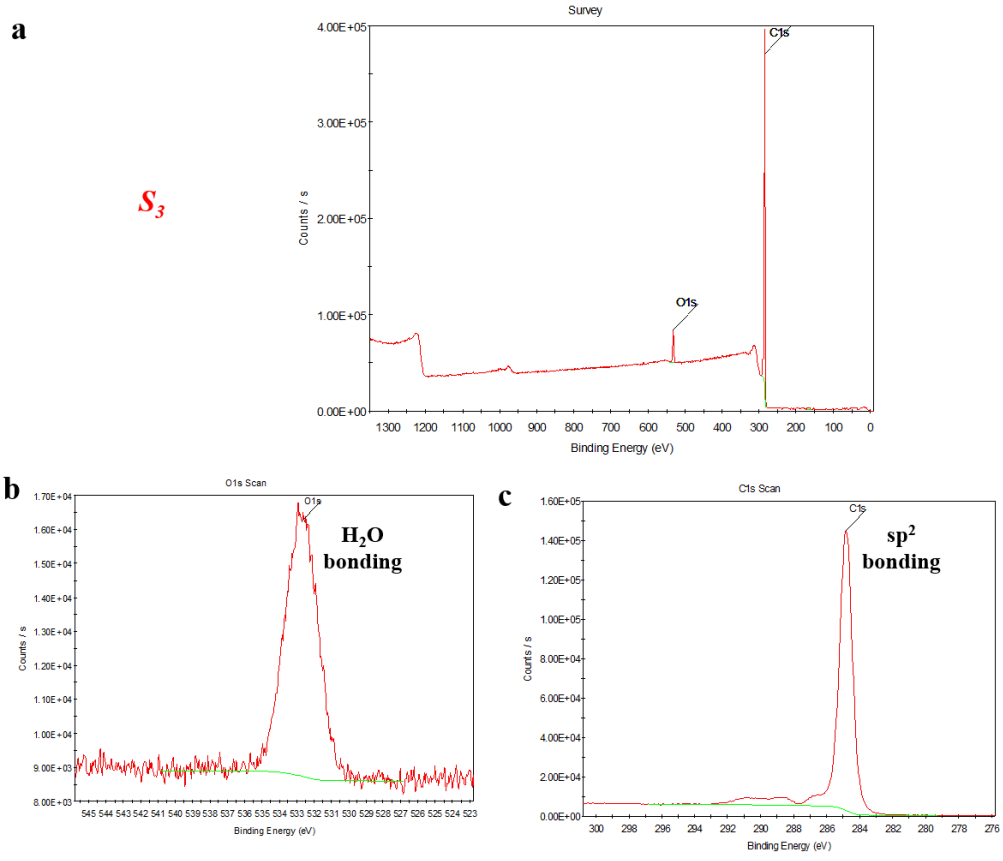

Figure S83. Full view (a) and expanded views (b, c) of XPS spectrum of ***S3***.

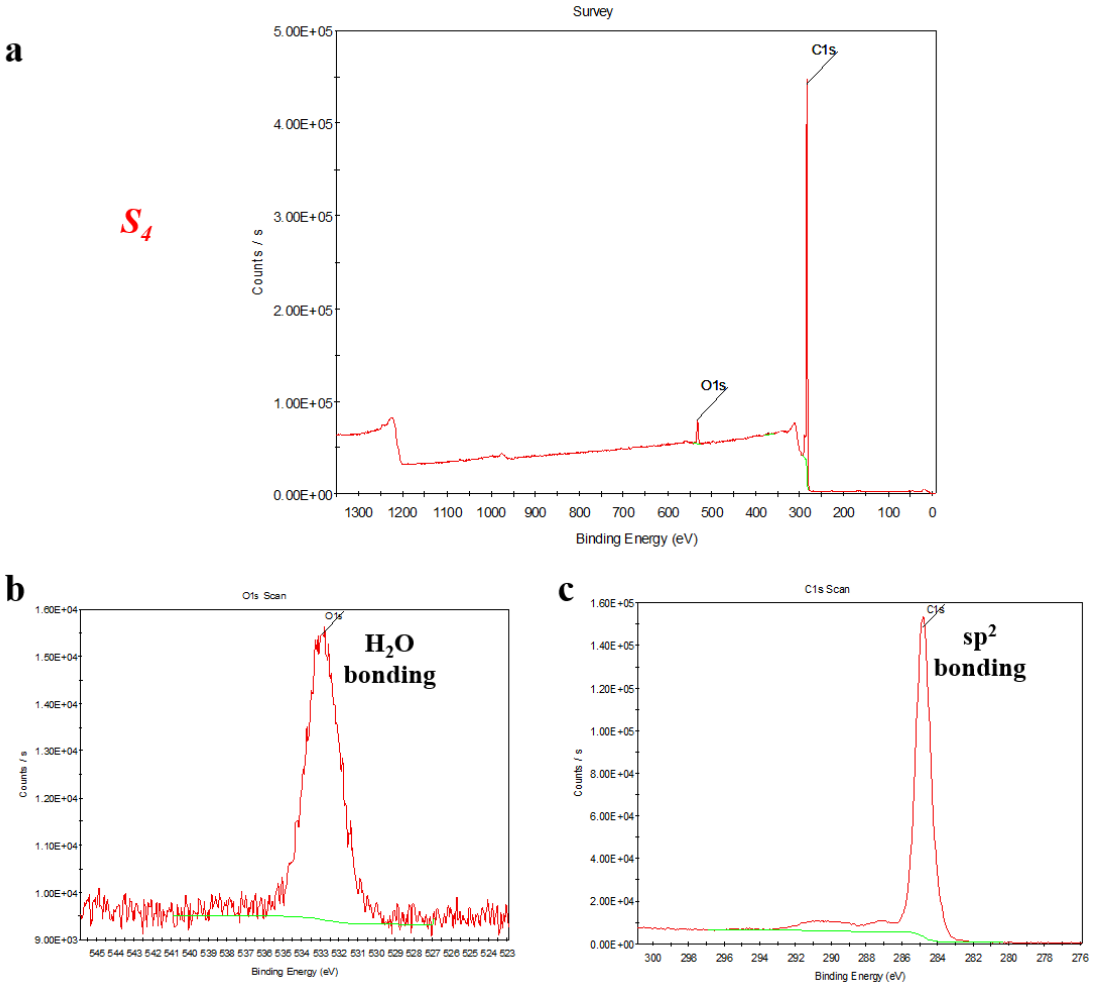

Figure S84. Full view (a) and expanded views (b, c) of XPS spectrum of ***S*****4**.

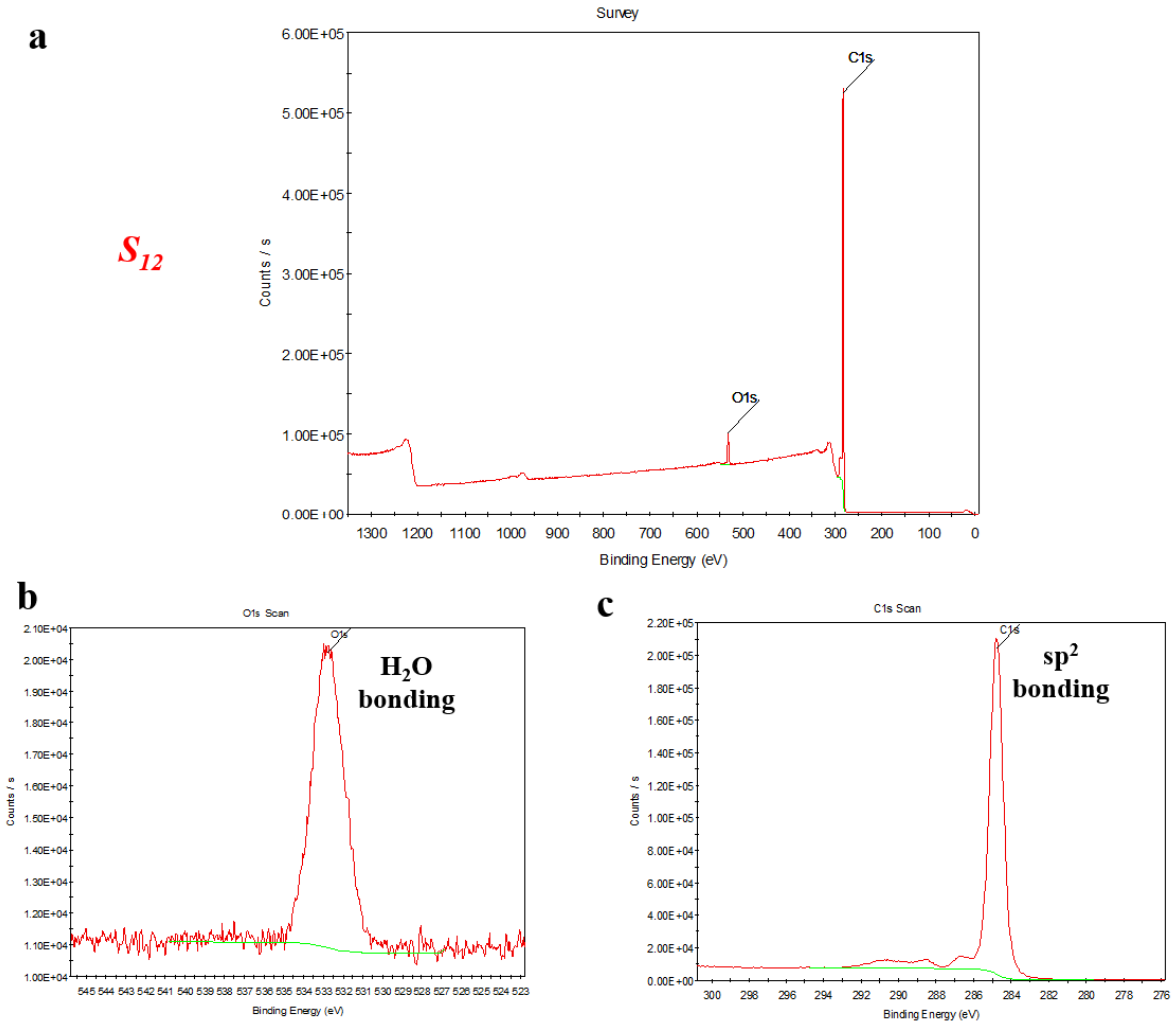

Figure S85. Full view (a) and expanded views (b, c) of XPS spectrum of S_{12}.

Reference

(1) G. M. Sheldrick, *SHELXL97. Program for the Refinement of Crystal Structures*, University of Gottingen, Gottingen, 1994.

(2) O. V. Dolomanov, L. J. Bourhis, R. J. Gildea and J. A. K. Howard, *J. Appl. Cryst.*, 2009**, 42**, 339-341.

(3) G. M. Sheldrick, *Acta Cryst. A*., 2015, **71**, 3-8.

(4) $R_W(F^2) = \{w(|F_o|^2 - |F_c|^2)^2/w(|F_o|)^4\}^{1/2}$ where w is the weight given each reflection. $R(F) = (|F_o| - |F_c|)/ |F_o|\}$ for reflections with $F_o > 4((F_o))$. $S = [w(|F_o|^2 - |F_c|^2)^2/(n - p)]^{1/2}$, where n is the number of reflections and p is the number of refined parameters.

(5) A. J. C. Wilson, *International Tables for X-ray Crystallography. Vol. C, Tables 4.2.6.8 and 6.1.1.4*. Kluwer Academic Press, 1992.

(6) G. M. Sheldrick, *SHELXTL/PC (Version 5.03)*. Siemens Analytical X-ray Instruments, Inc., Wisconsin, 1994.
(7) M. J. Frisch, *et al*, *Gaussian 09, Revision A.1*. Gaussian, Inc., Wallingford, Connecticut, 2009.
(8) A. D. Becke, *J. Chem. Phys.*, 1993, **98**, 5648-5652.
(9) S. Grimme, J. Antony, S. Ehrlich and H. Krieg, *J. Chem. Phys.*, 2010, **132**, 154104.
(10) P. J. Hay and W. R. Wadt, *J. Chem. Phys.*, 1985, **82**, 299-310.
(11) A. W. Ehlers, M. Böhme, S. Dapprich, A. Gobbi and G. Frenking, *et al*, *Chem. Phys. Lett.*, 1993, **208**, 111-114.
(12) P. J. Hay and W. R. Wadt, *J. Chem. Phys.*, 1985, **82**, 284-298.
(13) L. E. Roy and P. J. Hay, *J. Chem. Theory Comput.*, 2008, **4**, 1029-1031.
(14) P. Job, *Ann. Chim*., 1928, **9**, 113-203.
(15) K. A. Connors, *Binding Constants*. John Wiley and Sons, New York, 1987.
(16) P. Gans and A. Sabatini, A. *Talanta*, 1996, **43**, 1739-1753.
(17) H. Takahashi, E. Matsubara, R. V. Belosludov, S. Matsubara, N. Sato, A. Muramatsu, Y. Kawazoe, K. Tohji, *Materials Transactions*, 2002, **43**, 1530−1532.
(18) D. Canevet, E. M. Pérez, N. Martín, *Angew. Chem. Int. Ed.* 2011, **50**, 9248–9259.
(19) K. Tashiro, T. Aida, *Chem. Soc. Rev.* 2007, **36**, 189–197.
(20) M.-J. Li, C.-H. Huang, C.-C. Lai, S.-H. Chiu, *Org. Lett.* 2012, **14**, 6146–6149.